2000

Flexible reinforced pavement structure-sensitivity analysis.

Jianbin. Yu
University of Windsor

Follow this and additional works at: http://scholar.uwindsor.ca/etd

INFORMATION TO USERS

This manuscript has been reproduced from the microfilm master. UMI films the text directly from the original or copy submitted. Thus, some thesis and dissertation copies are in typewriter face, while others may be from any type of computer printer.

The quality of this reproduction is dependent upon the quality of the copy submitted. Broken or indistinct print, colored or poor quality illustrations and photographs, print bleedthrough, substandard margins, and improper alignment can adversely affect reproduction.

In the unlikely event that the author did not send UMI a complete manuscript and there are missing pages, these will be noted. Also, if unauthorized copyright material had to be removed, a note will indicate the deletion.

Oversize materials (e.g., maps, drawings, charts) are reproduced by sectioning the original, beginning at the upper left-hand corner and continuing from left to right in equal sections with small overlaps.

Photographs included in the original manuscript have been reproduced xerographically in this copy. Higher quality 6" x 9" black and white photographic prints are available for any photographs or illustrations appearing in this copy for an additional charge. Contact UMI directly to order.

FLEXIBLE REINFORCED PAVEMENT STRUCTURE
– SENSITIVITY ANALYSIS

By

Jianbin Yu

A Thesis

Submitted to the College of Graduate Studies and Research

Through Civil and Environmental Engineering

in Partial Fulfillment of the Requirements for the

Degree of Master of Applied Science at the

University of Windsor

Windsor, Ontario, Canada

2000

The author has granted a non-exclusive licence allowing the National Library of Canada to reproduce, loan, distribute or sell copies of this thesis in microform, paper or electronic formats.

L'auteur a accordé une licence non exclusive permettant à la Bibliothèque nationale du Canada de reproduire, prêter, distribuer ou vendre des copies de cette thèse sous la forme de microfiche/film, de reproduction sur papier ou sur format électronique.

The author retains ownership of the copyright in this thesis. Neither the thesis nor substantial extracts from it may be printed or otherwise reproduced without the author's permission.

L'auteur conserve la propriété du droit d'auteur qui protège cette thèse. Ni la thèse ni des extraits substantiels de celle-ci ne doivent être imprimés ou autrement reproduits sans son autorisation.

0-612-52682-8

Canada

ABSTRACT

As a natural occurrence, rutting develops during the using stage of flexible pavement. When the rutting becomes worse, users will experience an uncomfortable feeling. Moreover, this may eventually influence the life span of the pavement. It is .of researcher's interest to find out an effective way to mitigate this phenomenon. The application of geotextile/geogrid is a good method.

The objective of this research is to study the function of geotextile/geogrid during gradual stiffening stage. In doing so, this research was processed in two steps. The first step was triaxial tests on the soil sample (base material) reinforced by different layers of geotextiles under different confining pressure. One-dimensional analysis was performed upon the test results. The second step was numerical analysis on the published data dealing with the permanent deformation. Finite Element Analysis and Sensitivity Analysis were exercised. The FEA was undertaken to identify the permanent resilient modulus (PRM) by assuming that the inclusion of geogrid influenced the PRM of all the layers, while the sensitivity analysis was done by assuming that the inclusion of geogrid merely affected the properties of base material.

From the experiments, it was observed that the effect of adding more layers of geotextiles was more pronounced than the increase of confining pressure. From the numerical analysis, the conclusion can be drawn that the variation of permanent deformation was very sensitive to the variation of thickness coupled with permanent resilient modulus (PRM) of base layer.

ACKNOWLEDGEMENTS

TABLE OF CONTENTS

LIST OF FIGURES

viii

LIST OF TABLES

Chapter I

INTRODUCTION

1.1 Pavements and Design

There are three major types of pavements nowadays used in North America, namely, flexible pavement, rigid pavement, and composite pavement.

Flexible pavement is constructed of bituminous and granular materials, also called asphalt pavement. Three types of constructions have been used: conventional flexible pavement, which consists of mainly seal coat, surface course, tack coat, binder course, prime coat, base course, subbase course, compacted subgrade, and natural subgrade, full-depth asphalt pavement, which is constructed by placing one or more layers of hot mixed asphalt (HMA) directly on the subgrade or improved subgrade, and contained rock asphalt mats (CRAM), which is composed of dense-graded hot mixed asphalt (HMA) wearing course, dense-graded aggregate, open-graded aggregate, and prepared subgrade, from the top to the bottom.

These three types of pavements are illustrated with Figure 1.1 to 1.3.

The construction of rigid pavement involves portland cement concrete (PCC), and this gives rigid pavement another name as concrete pavement. It can be classified into four types: jointed plain concrete pavement (JPCP), jointed reinforced concrete pavement (JRCP), continuous reinforced concrete pavement (CRCP), and prestressed concrete pavement (PCP).

Composite pavement consists of both hot mixed asphalt (HMA) and portland cement concrete (PCC), with HMA being top layer and PCC as bottom layer. This is the ideal choice of pavement from the functional point of view since it provides a strong base and

a smooth, non-reflective surface. However, the construction expense for such type of pavement is very high, which limits its popular use.

The research was carried out exclusively on flexible pavement, more exactly, the conventional flexible pavement.

When designing the flexible pavement, there are five categories, namely, empirical method with or without a soil strength test, limiting shear failure method, limiting deflection method, regression method based on pavement performance or road test, and mechanistic-empirical method. Some other concepts such as serviceability, reliability, and dynamic loading are also incorporated in American Association of State Highway and Transportation Officials (AASHTO) (1). All the design methods have their advantages and disadvantages, which limit their application under certain circumstances.

1.2   Rutting and Geosynthetics

In the mechanistic-empirical method, rutting, "as indicated by the permanent deformation or rut depth along the wheelpaths", is a very important criterion. As a natural occurrence on the flexible pavement subjected to repetitive traffic, rutting influences the performance of the pavement, the comfortable extent of users, and then determine the service life span of the flexible pavement. Two methods have been used to control rutting: one is to limit the vertical compressive strain on the top of subgrade and the other is to limit the rutting to a tolerable amount.

In practice, mankind has tried a number of ways to mitigate the rutting of flexible pavement, one of them being that geosynthetics are included into the base material as reinforcement like what steels do for concrete. In the meanwhile, numerous researches have studied the mechanism of geosynthetics as reinforcement. The mechanisms that have been proposed include:

- Membrane action by the displaced geosynthetics,
- Restraint of the granular fill through shear stresses acting on the geosynthetics,
- Improved load distribution, and
- Interlocking of the fill particles with the geogrid.

1.3   Previous Works

Giroud (9,11) , who first coined the term "geotextile" and "geomembrane" in 1977, and Noiray (9) studied the mechanisms of geotextile reinforced pavement under monotonic traffic load and provided the early design methods for geotextile reinforced unpaved roads. It was pointed out that the thickness of aggregate layer could be reduced 30% to 50% after the inclusion of geotextile compared with unreinforced road. Nevertheless, it was indicated that the width of base of pyramid stress distribution is larger and this width increases with the increase of modulus of geotextile when the pavement was reinforced with geotextile. However, the distribution of strain under geotextile is far from uniform.

Likewise, Giroud et al (10,11) studied the mechanisms of geogrid reinforced pavement subject to monotonic traffic loading and then provided the design method for geogrid reinforced unpaved roads. It was concluded that approximately half of the thickness reduction was due to subgrade confinement and the other half is contributed from improved load distribution.

Hass , Walls and Carrol (12) studied the low deformation system and the high deformation system as well. They concluded that interlocking and confining action are required for low deformation system, while tension membrane action is more effective for the high deformation system. Suggestion was made that grids should be placed at the base-subgrade interface of thin base sections and in the middle of thicker base layers.

Miura, Sakai and Taesiri (19) studied a pavement on a soft clay subgrade and concluded that the improved performance was mainly due to interlocking effect. Their calculations

3

showed, however, that a reinforcement in a pavement is comparable to that of base material about 100 mm thick.

Chan, Barksdale, and Brown (7) carried out large-scale experiments in order to investigate the aggregate base reinforcement potential of geogrids and geotextiles in surface pavements. Their experimental results showed geogrid performed better than geotextile in term of mitigating the permanent deformation, while geotextile was more effective than geogrid as separator. They even observed that the overall resilient behavior of the pavement was not significantly influenced by the geosynthetics.

Nejad and Small (21) conducted a series of tests on the one-quarter scale laboratory models to study the reinforcing effect applied by geogrids. Furthermore, it was aimed to determine which position is more effective when geogrids was placed in the middle of base layer or at the base-subgrade interface. By recording and comparing the permanent deformations, it was concluded that "the geogrid at the middle of base layer was most effective in reducing pavement settlement".

1.4   Objective and Methodology

The major objective of this research is to evaluate the function of geogrid/geotextile in flexible pavement during gradual stiffening by introducing the permanent resilient modulus. Nonetheless, the equivalent thickness is to be evaluated to count the effectiveness of geogrids.

In order to identify the function of geosynthetics in flexible pavement, a series of triaxial tests were performed. Two parameters were being studied, namely, permanent deformation and elastic modulus. The confining pressure varied from 10 psi (69 kPa) to 20 psi (138 kPa), while the layers included in the sample increased from non-reinforced to 3-layer reinforced. The data was recorded by the program Test Control Software (TCS) and numerical analysis was rendered in accordance with one-dimensional assumption.

4

To numerically analyze the data presented Nejed et al (21), FEM package ABAQUS (2) was utilized to identify the permanent resilient modulus. The term "permanent resilient modulus" (PRM) was introduced because the elastic analysis was employed to analyze the permanent deformation, and the analysis of the consequent deformation was based on the geometry of previous deformation. To verify the correctness of PRM, a multi-layer analysis package KENLAYER, was utilized by substituting the PRM obtained by ABAQUS and then calculating the corresponding deformation. Regression analysis was done, however, to generate the function of PRM with respect to the number of passes.

As the next stage of analysis, sensitivity analysis was performed to study the variation of permanent deformation respectively the variation of resilient modulus of base layer. It was assumed that the PRM of wearing course as well as subgrade kept constant as the tire passed, whereas that of base layer would be altered with respect to the number of passes. As the result of derivation in Chapter 5, Section 5.3.3, Equation

$$\delta E * \delta H = \frac{\delta v_{ji}^{1} * E}{2\pi \int_{r} (\bar{\sigma}_{z} \varepsilon_{z} + \bar{\sigma}_{r} \varepsilon_{r} + \bar{\sigma}_{\theta} \varepsilon_{\theta} + \bar{\tau}_{rz} \gamma_{rz}) r dr}$$

(1.1)

in which δE: the variation of permanent resilient modulus

δH: the variation of thickness of base layer

δv_{ji}^{1}:   the variation of permanent deformation

E: the modulus of base layer

$\overline{\sigma_{z}, \sigma_{r}, \sigma_{\theta}}$:   the normal stresses generated in adjoint structures

$\overline{\tau_{rz}}$:   the shear stress generated in adjoint structures

$\varepsilon_{z}, \varepsilon_{r}, \varepsilon_{\theta}$:   the direct strains generated in primary structures

γ_{rz}:   the shear strain generated in primary structures

was used to evaluate the sensitivity of how the change of thickness and PRM affects the change of permanent deformation.

The equation indicates that the variation of resilient modulus and the variation of thickness of base layer are coupled. To study the sensitivity of one parameter with respect to another, decoupling is needed. The decoupling is implemented by assuming one of these two variables is constant.

Chapter II

GEOTEXTILE AND GEOGRID

2.1　General

Geotextile and geogrid are two individual members of geosynthetics family. Geosynthetics is defined as "a variety of synthetic polymer materials that are specially fabricated to geotechnical applications". The constituent polymers used in the manufacture of geosynthetics are high-density polyethylene, polypropylene or polyster.

As illustrated in Figure 2.1, geosynthetics can be classified into several categories, based on structure and function:

- Geotextiles
- Geogrids
- Geonets
- Geocomposites
- Geocells
- Geomembranes

The standard terminology can be found in ASTM D4439 (16) and draft CGSB (Canadian General Standards Board) (16).

The primary functions of geosynthetics include:

- Separation
- Filtration
- Drainage
- Reinforcement

- Fluid/Gas containment

In terms of geosynthetic properties, variation in the procedures for testing of geosynthetics and inherent variation in the true properties of geosynthetics can be recorded due to the manufacturing process. "Minimum Roll Value" or "Maximum Roll Value" depending on the application need to be reported to ensure a common basis.

Among the five functions specified above, reinforcement of geotextile and geogrid is of primary interest in this research. It was commonly agreed that the geosynthetic "reinforced" the road structure by such mechanisms as:

- Membrane action by the displaced geosynthetic: when the pavement is subject to loading, the geosynthetic becomes stretched and exhibits a curved shape. Hence, the pressure against its concave face is higher than pressure against its convex face. This is also known as "tensioned membrane effect".
- Restraint of the granular fill through shear stresses acting on the geosynthetics: when the subgrade is confined, deformations caused by local shear failure do not become large enough to result in general shear failure and the subgrade can support a vertical stress close to plastic limit which is higher than elastic limit. Geotextiles provide restraint because they have small openings, while geogrids' opening can prevent the soil from escaping to cause the heave of the base layer. In addition, they are continuous materials.
- Improved load distribution along the depth: Load distribution is basically due to the mechanical properties and thickness of base layer. The inclusion of geosynthetics mitigates either the degradation of soil, which keeps the mechanical properties of soil, or prevents the lateral displacement of soil particles, which keeps the thickness of base layer, and
- For geogrids, interlocking of the fill particles with the geogrid: The interlocking can be optimized when the geogrids are placed around aggregates whose size is more or less the same as that of the openings of geogrids. As the number of passages

increases, the layer of aggregates around the geogrids becomes stiffer, thus improving the behavior of pavement.

2.2 Geotextiles

Geotextiles are one of the largest groups of geosynthetic family, the other being geomembrane. Their growth during last decade has been nothing short of awesome. In the traditional sense, they are indeed textiles, but consist of synthetic fibers rather than natural fibers which give them the ability to resist erosion. The synthetic fibers are assembled into a flexible, porous fabric by standard weaving machinery or are matted together in a random manner. The most pronounced feature for geotextile is that it must be ensured that they are permeable to water flow across their manufactured plane and within their plane, to a widely varying degree.

The manufacture, functions, properties and testing methods of geotextiles are briefly described in the following:

2.2.1 Manufacture of Geotextiles

As far as manufacturing is concerned, three points are important: the type of polymer, the type of fiber, and the fabric texture.

The polymers used in geotextiles are made of polymeric materials which comprise polypropylene, polyester, polyethylene, and polyamide, with different percentages. The fibers are made of the basic polymers by melting them and forcing them through a spinneret, and the resulting fiber filaments are then hardened or solidified by one of three methods: wet, dry or melt process. Most geotextile fibers are fabricated by the melt process.

With regard to fabric texture, there are three basic types of fabrics:

- Woven materials, consisting of two series of perpendicular threads combined systematically (threads made either of extruded filaments with a circular section or of ribbons produced by splitting a plastic film),
- Knitted materials, consisting of a single strand systematically intertwined with itself,
- Nonwoven materials, consisting of fibers arranged randomly.

Compound fabrics are also available in market by combining two or more types of fabrics.

2.2.2   Functions of Geotextiles

With the wider application of geotextiles in geotechnical engineering, in so far sixteen functions have been identified as listed below:

- Drain: The geotextile is used to gather and convoy the water towards the outlet when being placed in a soil of low permeability through which water is seeping slowly,
- Waterproof membrane: The geotextile is used to stop liquid and gas when impregnated or/and coated with an impermeable material,
- Solid filter: The geotextile is utilized to allow water going through the fine soil and coarse soil but to prevent the soil particles from movement,
- Liquid filter: The geotextile is employed to stop the fine particles and allow the water to go through when placed across a flow of liquid carrying fine soils,
- Support: The geotextile is manipulated to prevent bursting of the membrane over the voids,
- Separator: The geotextile is used to keep apart two different types of soils which tend to mix when they are squeezed together,
- Surfacing: The geotextile is exercised to provide a flat and clean surface for traffic,
- Curtain: The geotextile is applied to prevent the passage in one way of light and/or in the other way of falling rocks when hung alongside an earth or rock mass,

- Membrane (or mechanical membrane): The geotextile is employed to contain the material having the higher pressure when placed between two materials having different pressures,

- Tie: The geotextile is utilized to keep together two earth, rock or concrete masses which have a tendency to move apart,

- Binder: The geotextile is used to keep together the soil which tends to move when subject to mechanical actions,

- Reinforcement: The geotextile is exercised to carry the tensile not able to be carried by the soil,

- Absorber: The geotextile is manipulated to reduce the intensity of shocks and vibrations from outside,

- Crack barrier: The geotextile is applied to prevent cracks in one material to extend to the other one,

- Bond: The geotextile is included to increase the interlocking between two materials,

- Lubricator: The geotextile is incorporated to reduce the interlocking between two materials which tend to move along each other.

Though up to sixteen functions have been identified, the major points fall into four categories: drain, filter, separator and reinforcement.

2.2.3   Properties and Test Methods

The properties of geotextiles include physical, mechanical, hydraulic, endurance, and degradation properties.

Physical properties

These include specific gravity, mass per unit area, thickness, and stiffness. In the scope of ASTM, D792 (16) is designated to determine specific gravity, D1910 or D3776 (16) to mass per unit area, D1777 (16) to thickness, while D1388 (16) is applied to test the stiffness, which is a measure of interaction between fabric weight and fabric stiffness.

The stiffness is indicative of the fabric's capability of providing a suitable working surface for installation.

Mechanical properties

- Compressibility

For most geotextiles the compressibility is relatively low. However, it is of great interest for nonwoven needle-punched material when used to convey the liquid.

- Tensile strength

To measure the tensile strength, the geotextile is placed within a set of clamps or jaws, stretched under the testing machine until failure occurs. Four values, namely, maximum tensile stress, strain at failure, toughness, and modulus of elasticity, are measured.

- Seam strength

Seam strength refers to the strength of the ends which are joined together by sewing. Insofar there is no adopted standard regarding this subject, but ASTM provided some preliminary recommendations.

- Fatigue strength

Fatigue is defined as the ability of the fabric to withstand repetitive loading before failure happens. After a number of loading and unloading, the cyclic modulus can be measured according to the stress-strain relationship.

Hydraulic properties

When geotextiles are used to perform the functions of drainage and filter, certain hydraulic requirements need to be met. These hydraulic properties include:

- Porosity,
- Percent Open Area (POA),
- Apparent Opening Size (AOS) or Equivalent Opening Size (EOS),
- Permittivity (cross-plane permeability),
- Permittivity under load,
- Transmissivity (in-plane permeability), and
- Soil retention.

Endurance properties

The tests in assessing endurance properties of geotextiles encompass:

- Creep (sustained loading) tests,
- Confined creep tests,
- Abrasion tests,
- Long-term flow (clogging) test, and
- Gradient ratio (clogging) test.

Degradation properties

Several factors influence the degradation properties:

- Installation damage,
- Temperature degradation,
- Chemical degradation,

13

- Hydrolysis degradation,
- Biological degradation, and
- Sunlight degradation.

2.3   Geogrids

Geogrid is defined as "a geosynthetic used for reinforcement which is formed by a regular network of tensile elements with apertures of sufficient size to allow strike-through of surrounding soil, rock or other geotechnical materials". At present, geogrids represent a rapidly growing segment within geosynthetic family and have extended their use in geotechnical area more and more. Rather than being a tightly woven, nonwoven, or knit textile, as geotextiles do, geogrids are plastics formed into a very open, gridlike configuration. By unique methods, geogrids are either stretched for improved physical properties or made on weaving machinery .

2.3.1   Manufacture of Geogrids

Geogrids are classified into two categories in term of configuration: uniaxial geogrid and biaxial geogrid (See Figure 2.2). The polymer materials used in the manufacture of oriented geogrids are high-density polyethylene, or polypropylene. Holes are punched into the sheeting on a regular pattern, and the sheet is then drawn uniaxially or biaxially. The key variable in the process is the draw ratio. However, other variables, such as molecular weight, molecular weight distribution, and degree of branching or cross-linking, are also the controlling factors.

After the manufacturing process, the creep sensitivity of the ribs and modulus as well as strength have been greatly increased.

2.3.2 Functions of Geogrids

Compared with those of geotextiles, the functions of geogrids are much simple. As indicated clearly from its definitions, geogrid is designed primarily for the purpose of reinforcement, which is materialized by the function of interlocking, thus providing the tensile stress for the soil. On the other hand, the geogrids are exercised as separators as well, to a less extent.

2.3.3 Properties and Test Methods

The properties of geogrids include physical, mechanical, endurance, and degradation properties.

Physical properties

These include the type of structure, junction type, aperture size, thickness, mass per unit area, and percent open area. What is of direct construction interest is its stiffness, which can be measured by ASTM's D1388 (16), a test for flexural rigidity, and therefore separate the geogrids into two groups, namely, stiff geogrids and flexible geogrids.

Mechanical properties

• Single rib and junction (node) strength

By pulling a single rib in tension until failure, the geogrid's tensile strength can be assessed, or by pulling a longitudinal rib away from its transverse rib's junction, the in-isolation junction strength can be evaluated.

15

- Wide-width tensile strength

Wide-width tensile strength is the most important property which will directly determine the performance of geogrids on-site. The values are given in units of force per unit width, and can be tested by ASTM's D4595 (16).

- Shear strength

A set of tests like the direct shear test in geotechnical engineering is conducted subject to normal stress to get a series of maximum shear stress. This can result in a failure envelope, from which the shear strength can be determined. In ASTM, D5321 (16) gives the indication of how to conduct large-scale test.

- Anchorage strength from soil pullout

A soil pull-out box is employed to evaluate the anchorage strength which results from three mechanisms: shear strength along the top and bottom of the longitudinal ribs of the geogrid, shear strength along the top and bottom of the transverse rib, and passive resistance against the front of the transverse ribs.

- Anchorage strength from wall pullout

When subject to a normal stress, the geogrid is tensioned until failure by using modular concrete blocks. The mode of failure and the ultimate strength of the entire anchorage system can be accordingly identified.

Endurance properties

As geogrids are used in soil to serve a long lifetime, endurance properties as well as degradation properties need to be tested and certain requirement needs to be met. As a matter of convenience, only index of these properties will be mentioned herein.

- Installation damage: this is to test the strength-loss due to improper operation.

- Creep behavior: In ASTM, D5262 (16) describes the method of testing the unconfined tension creep of geosynthetics.

Degradation properties

These contain the following:

- Temperature degradation,
- Oxidation degradation,
- Hydrolysis degradation,
- Chemical degradation,
- Radioactive degradation,
- Biological degradation,
- Sunlight (UV) degradation, and
- Stress cracking

17

Chapter III

TRIAXIAL TEST ON SOIL REINFORCED BY GEOTEXTILES

3.1   General

Triaxial test is initially designed to measure the shear strength of natural soil. However, the behavior of soil reinforced with geotextile was also studied by triaxial tests by some researchers. The elastic and frictional parameters were investigated.

In this research, a series of triaxial tests were conducted to study the relationship between applied force and generated strain on the reinforced soil. The purpose was to study the change of yield stresses and elastic modulus of the soil sample after reinforced with layers of geotextiles..

The soil sample employed in the tests were simulating the base material described in Nejad and Small's (21). In the tests conducted by the authors, geogrids were used to serve as reinforcement. However, this would not be applicable for the triaxial tests due to the small size of the samples (diameter 4 in (100 mm) , height 8 in (200 mm)). Instead, geotextile took the place of geogrid , and was shaped by being cut into small, round pieces to fit the shape of sample.

Nevertheless, the conventional triaxial-test machine had been modified by adding some new features. These included some new equipment and a computer software to record the experimental data.

3.2   Laboratory Set-up

3.2.1   Compression Test Machine

The compression test machine Model WF10040 was used, and has been slightly modified to be able to perform automatic recording. The principal components include:

- An adjustable fixed cross beam,
- Rigid steel strain rods,
- Cast metal pedestal,
- Bottom platen,
- Loading jack,
- Hand wheel,
- Black knobs,
- Air-cylinder,
- Clutch.

3.2.2   Air Regulator

Air rather than water was used from the tube to fill the space within the Lucite pressure cell and outside the sample to provide the confining pressure σ_3 . According to the standard experimental procedure, σ_3 is supposed to be kept constant throughout the experimental process, which requires the space between Lucite pressure cell and the sample to be air-tight. However, this air-tightness could not be achieved by fastening the pressure cell to the bottom platen with the six tie rods and nuts, therefore, air leakage always took place. To prevent that from happening, air-regulator renders a good quality to serve this requirement. The smallest capacity for the air-regulator available in the market was 50 psi (345 kPa). One such air-regulator was installed between the air cylinder and the Lucite pressure cell.

3.2.3 Load Cell

A 5000 lbs (22.5 kN) capacity load cell was used in determining the load applied to the soil sample. The load cell was calibrated with the universal test machine and the load was recorded by the TCS (Test Control Software) program. Between two iron columns was the iron beam underneath which the load cell was mounted.

3.2.4 Displacement Transducer

One displacement transducer rather than proving ring was mounted on the beam to measure the displacement. The data of displacement was transferred to MEGADAC, the data-acquisition system.

3.2.5 MEGADAC

The data-acquisition system, MEGADAC, was used to connect the load cell as well as displacement transducer with the computer which was equipped with TCS (Test Control Software). The load and displacement taking place were converted into electronic symbols which would be recorded and saved in MEGADAC and then transferred to TCS.

3.2.6 TCS (Test Control Software)

TCS is a software that is capable of acquiring the data from MEGADAC and then saving the data in various format, or plotting by means of graphs, bar-graph or strip chart simulation. For the sake of convenience of further analysis, the data was being converted into ASCII format and exported. Further analysis was implemented with more powerful package as EXCEL.

The lab set-up is illustrated as Figure 3.1.

3.3   Material Preparation

3.3.1   Soil Preparation

In the Nejad and Small's paper (21) , the base material used in their tests was described as "crushed aggregate of basaltic origin consisting of mainly subangular particles of .5 mm nominal size", and "the D_{10} and D_{60} sizes were approximately 2.0 mm and 4.0 mm, respectively, giving a uniformity coefficient of 2.0, therefore, the road base can be classified as a uniform fine gravel with less than 1% of particles finer than 75 μm".

Mechanical method was employed to carry out the grain-size classification. A set of sieves, the numbers (ASTM designations) of which include 3/8 in (9.52 mm, coarse series), No.4 (4.76 mm), No.8 (2.38 mm), No.10 (2.00 mm), No.20 (0.84 mm), and No.200 (0.074 mm), were chosen. After the soils were sieved by the mechanical shaker for 5 to 10 min, certain amounts of soil for each level were picked and made such that D_{10} and D_{60} were approximately 2.0 mm and 4.0 mm, respectively, and 1.0% of particles was finer than 75 μm.

The gradation of soil is illustrated in Figure 3.2 and Table 3.1.

3.3.2   Geotextile Preparation

As mentioned previously, geotextile rather than geogrid was used to serve as reinforcement. The geotextiles included in the experiments were the products of AMOCO Fabrics and Fibers Company, the type was 2006. The properties of this type of geotextile is listed in Table 3.2. The geotextile was cut with scissors into round shape with diameter being 4 in (100 mm). Care should be practiced to ensure that geotextile was still in good shape after cutting.

21

3.4   Test Procedure

The tests were conducted under different conditions. The confining conditions could be altered from 10 psi (69 kPa) to 20 psi (138 kPa), the increment being 5 psi (35 kPa), whereas the sample conditions could be changed from un-reinforced to 3-layer-reinforced, the increment being 1 layer each time.

At the beginning of test, computer should be turned on and the TCS program should be called upon to the current window. When connecting the MEGADAC with load cell as well as displacement transducer, caution should be taken that:

- For the load cell, "+" is connected with white wire, while "-" with green wire, "V" with red wire, and "R" with the black wire,
- For the displacement transducer, the same principle as above should be applied, whereas "R" and "-" need to be connected by a separate wire.

For one single test, the test procedure was arranged in the following order:

- Calibrate the machine,
- Fasten the sample membrane to the bottom platen with 2~3 o-rings,
- Place one filter paper on the bottom platen. The filter paper should fit the shape of bottom platen and the rubber membrane,
- Erect the three pieces of sample molds around the rubber membrane and fold the top portion of the membrane down over the mold. Connect the vacuum pump and vacuum inlet on the body of mold with a plastic tube and turn the vacuum pump on so that the membrane can be tightly attached to the mold,
- Adjust the level of molds until they are completely vertical. Hold the pieces of molds together using the fastener. Check the membrane by listening to the sound of vacuum or picking the membrane up and then releasing it to see if there is any leakage happening. It should be guaranteed that no hole is on the membrane. If this happens, the membrane must be discarded and use a brand new one,

- Connect the vacuum and the vacuum inlet on the bottom platen with another plastic tube, and turn the vacuum on,

- Scoop the prepared soil into the membrane by layers. The thickness of each layer could be 2 in (50 mm). (note: The thickness can be adapted according to the different conditions. For instance, it could be 1/6 of the height of the sample membrane if there are two layers of geotextiles included in the sample). Compact each layer with an iron bar (about 2.5 kg) for 25 blows per layer. During the process of compaction, much care should be exercised in case that the membrane would be broken by the careless operation. When geotextiles were involved, compaction should be finished before placing the geotextile on the soil and the surface of soil must be kept level,

- Place the geotextile on the surface of soil. Compact the geotextile with a wooden bar to ensure the surfaces were contacting well enough,

- When the soil sample reached the height of membrane, place a new filter paper on the soil,

- Place the sample cap on the filter paper in the center. Make sure that the meniscus is in the center of soil and use the level ruler to check if the surface of cap is level,

- Stretch the membrane upward to wrap the top platen. Use the o-rings to fasten the membrane with the cap,

- Turn off the vacuum pump on the mold and then remove the mold. Check the membrane if there is any holes,

- Move the triaxial cell onto the platform of test machine. Cover it with the Lucite pressure cell. Make sure that loading piston is exactly lying in the center of the meniscus of sample cap to prevent the eccentric loading from taking place. Should it not be the case, remove it from the platform and adjust the sample by putting back the mold around the sample until the requirement has been met,

- Fasten the Lucite pressure cell with 6 nuts as tightly as possible. This could be critical to control the air-tightness within the Lucite pressure cell,

- Connect the air-inlet on the bottom platen with the air cylinder, where the air regulator is lying. Set the air pressure to a certain reading and open the valve. The loading piston can be observed to move upward and not to touch the meniscus anymore,

- Turn off the vacuum on the bottom platen,
- Set the button to "coarse", pull the black knob and move the cell upward manually by the hand wheel until the meniscus touches the loading piston gently again.
- Set the computer program to the recording window, get the computer ready to record,
- Set the button to "fine", push the black knob in,
- Turn the engine on, and the loading begins,
- After the load begins to decrease, which means that the yield stress has been reached, stop the test,
- Check the data being recorded, plot the graphs with load or displacement vs time. Transfer the data into ASCII format and save the file.

After a full process, the sample was made as illustrated in Figure 3.3.

3.5   Test Results

After the geotextiles were included in the test soil, it was observed that the stress for the soil to reach the yield point had been significantly increased. On the other hand, the shapes of deformed sample were different under different reinforced conditions, but of no big difference under different confining pressures. These are illustrated by Figure 3.4~Figure 3.8.

When the soil sample was not subject to reinforcement of geotextiles, the most-deformed part lay in the middle of sample which showed bulging behaviors. After inclusion of layers of geotextiles, the upper and lower parts around the geotextiles almost kept their original sizes. There may be two types of mechanisms involved:

- Interlocking
- Confinement

Meanwhile, geotextiles were serving as separators in the physical sense, which divided the sample into several layers. It was recognized that the deformed shape of each layer was like that of unreinforced sample, the most-deformed part taking place in the middle.

Calculation can be implemented under one-dimensional assumption.

The strain of the soil sample was:

$$\varepsilon = \Delta l / l \tag{3.1}$$

where: ε: the current strain of the soil sample,

     Δl: the variation of length of sample,

     l: the original length of sample.

The corresponding stress was calculated by taking into account the current strain which influenced the current area:

$$\sigma = \frac{F(1-\varepsilon)}{\pi r^2} \tag{3.2}$$

where σ: the current stress of the soil sample,

     F: the external load applied by the load cell,

     r: radius of sample = 4 in.

Hence, the elastic modulus was

$$E = \frac{\sigma}{\varepsilon} \tag{3.3}$$

where E: the elastic modulus.

In terms of yield stress, it is observed in Table 3.3 that :

- Under the same confining pressure, the yield stress increases with the increase of the geotextile layers. For example, the yield stress increases approximately 40%, 80%, 260% for the cases of 1 layer, 2 layers, 3 layers respectively, compared with the non-reinforced case when confining pressure equals to 10 psi (69 kPa), the yield stress increases approximately 70%, 120%, 185% for the case of 1 layer, 2 layers, 3 layers respectively, compared with the non-reinforced case when the confining pressure equals to 15 psi(104 kPa), however, the yield stress increases approximately 110%, 170%, 225% for the case of 1 layer, 2 layers, 3 layers respectively, compared with the non-reinforced case when the confining pressure equals to 20 psi (140 kPa).

- Under the same reinforcement condition, the yield stress increases with the increase of confining pressure, but no as significant as the above observation. For example, when the sample was unreinforced, yield stress increases 40 % for the case of confining pressure equal to15 psi (104 kPa), 20 psi (140 kPa) in comparison to the case of confining pressure equal to 10 psi (69 kPa).

The detailed comparisons are also illustrated in Figure 3.9~Figure 3.15.

In term of elastic modulus, it is observed that:

- Elastic modulus reaches its peak at very small displacement, and falls very rapidly, then goes downward smoothly until the sample fails.

- Under the same confining pressure, more layers of reinforcement will definitely increase the elastic modulus, especially the peak elastic modulus.

- Under the same reinforcement condition, higher confining pressure will increase the elastic modulus throughout the loading process.

The detailed comparisons are illustrated in Figure 3.16~Figure 3.22.

Chapter IV

PROBLEM FORMULATION

4.1 General

In the experiments described in Chapter III, it was aimed to study the reinforcement effect exerted by the geotextiles in term of yielding stress together with elastic modulus. Comparatively, in order to determine the position where the geogrids should be placed to achieve the most ideal effect of mitigating the rutting, Nejad and Small (21) conducted a series of tests.

In their experiment, a model test facility consisting of " a laboratory scale driven wheel that is guided around an oval-shaped track by an overhead guided-rail system", was utilized. Load was applied by the moving tire, the movement of which was generated and controlled by the pre-determined computer program. The magnitude of load was 210 kPa (30 psi), while the contact area was suggested to be circular and the magnitude was 24.5 cm^2.

The pavement was constructed at one-quarter scale and was composed of three layers: the wearing course (20 mm), which was constructed from "a proprietary cold-mix bituminous material", the road base (20 mm), which was "a crushed aggregate of basaltic origin", and the sand subgrade (2000 mm), which was made up of Sydney sand. Hence the system is identified as conventional flexible pavement.

Biaxially oriented polymer geogrids were placed in the middle of base layer and at the base-subgrade interface. Linear voltage displacement transducers (LVDT) were employed and located at the surface, at the course-base interface, and at the base-subgrade interface, respectively.

The permanent deformation (rutting) occurred at those three points under three different reinforcement conditions were recorded by the computer with respect to number of passes.

As the results of experiments, several graphs were presented which showed that the permanent deformations at the surface, at the base-course interface and at the base-subgrade interface have been significantly mitigated with the inclusion of geogrids either in the middle of base layer or at the base-subgrade interface.

Moreover, it was pointed out that "the plot suggests that the main mechanism of the reinforcement is interlocking with the granular material and confinement of the base material preventing lateral displacement of the base layer, which accumulates with an increasing number of passes".

Thus one problem arises: How can the interlocking and confinement play their roles in improving the performance of the soils? Is it through the change of resilient modulus, or permanent resilient modulus? And by what extent has the resilient modulus been increased?

4.2 Permanent Resilient Modulus

Resilient modulus is the elastic modulus based on the recoverable strain under repeated load. It is a very important concept in the design of flexible pavement.

Figure 4.1 shows the straining of a specimen under a repeated load test.

When the base material is subject to the repeated load at the initial stage, it shows considerable permanent deformation as indicated by the plastic strain in Figure 4.1. As the number of repetitions increased, the plastic deformation decreases. On the other hand, the elastic deformation as indicated as recoverable deformation becomes stable. Thus

28

resilient modulus is defined as the quotient of deviator stress with respect to recoverable strain.

$$M_r = \frac{\sigma_d}{\varepsilon_r} \qquad (4.1)$$

The determination of resilient modulus was standardized in 1994 after being tested for more than 10 years in AASHTO (1). Historically, AASHTO T274-82, T292-91I, T292-92I, and T294-94 (27) had been proposed. Difference had been detected due to certain factors in different test procedures. These factors comprise: (i) sample conditioning prior to test, (ii) applied stress sequence, (iii) number of loading cycles, (iv) waveform of cyclic loading, and (v) location of LVDT's.

In this research, permanent deformation rather than recoverable elastic deformation was studied at the surface, at the course-base interface and at the base-subgrade interface in the flexible pavement. Hence permanent resilient modulus was introduced and incorporated into the Finite Element Method (FEM) analysis.

4.3   Polynomial Regression of Test Data

To study the behavior of soil, the test data obtained in the tests of Nejad et al (21) needs to be re-acquired and modeled to find the theoretical formulas to formulate the problem.

The initial stage of re-acquiring the test data is to scan and copy the graphs presented in the paper. Some key data were determined by measurement and made into tables. As the statistical analysis stage, polynomial regression, one method of nonlinear regressions, had been employed to interpret the data and build the corresponding formulas.

Suppose the curve can be expressed by the polynomials of order m:

$$P(x) = a_m x^m + a_{m-1} x^{m-1} + \cdots + a_1 x + a_0 \qquad (4.2)$$

29

where the $m+1$ coefficients a_m, $a_{m-1},...,a_1$, and a_0 define a polynomial of order m. Equation (4.2) may also be written as

$$P(x) = \sum_{j=0}^{m} a_j x^j$$

(4.3)

Polynomial regression consists of fitting a set of n data points (x_i, y_i) to a polynomial model. The sum E of the squared distances between data points and fitted points is set as the standard of evaluating the accuracy of the fit between data points and fitted points.

$$E = \sum_{i=1}^{n} [P(x_i) - y_i]^2$$

(4.4)

The fit can be evaluated as best when E is minimum, namely, when E being differentiated with respected to the coefficients a_i $(i=0,1,...,m)$ equals to 0. This means, however, the following $m+1$ equations are satisfied:

$$\frac{\partial E}{\partial a_j} = 0 \qquad \text{for } j=0,1,2,...,m$$

(4.5)

This implies that

$$\sum_{i=1}^{n} [P(x_i) - y_i] \frac{\partial P(x_i)}{\partial a_j} = 0 \qquad \text{for } j=0,1,2,...,m$$

(4.6)

After some algebraic manipulations, the above equation becomes:

$$\sum_{k=0}^{m} \sum_{i=1}^{n} x^{k+j} a_k = \sum_{i=1}^{n} y_i x_i^j \qquad \text{for } j=0,1,2,...,m$$

(4.7)

30

Equation (4.7) can also be written as:

$$\sum_{k=0}^{m} G_{jk} a_k = H_j \qquad \text{for } j=0,1,2,\dots,m \qquad (4.8)$$

where

$$G_{jk} = \sum_{i=1}^{n} x_i^{j+k} \qquad (4.9)$$

and

$$H_j = \sum_{i=1}^{n} y_i x_i^{j} \qquad (4.10)$$

The coefficients vector is denoted as:

$$A = a_k \qquad \text{for } k=0,1,\dots,m \qquad (4.11)$$

Employing the matrix notation, Equation (4.11) can be summarized as:

$$GA = H \qquad (4.12)$$

Hence the polynomial coefficients can be found:

$$A = G^{-1} H \qquad (4.13)$$

Where G^{-1} is the inverse matrix of G.

For instance the quadratic polynomial is

$$A = \begin{pmatrix} a_0 \\ a_1 \\ a_2 \end{pmatrix}, \qquad G = \begin{bmatrix} n & \sum_{i=1}^{n} x_i & \sum_{i=1}^{n} x_i^2 \\ \sum_{i=1}^{n} x_i & \sum_{i=1}^{n} x_i^2 & \sum_{i=1}^{n} x_i^3 \\ \sum_{i=1}^{n} x_i^2 & \sum_{i=1}^{n} x_i^3 & \sum_{i=1}^{n} x_i^4 \end{bmatrix}, \text{ and } H = \begin{pmatrix} \sum_{i=1}^{n} y_i \\ \sum_{i=1}^{n} x_i y_j \\ \sum_{i=1}^{n} x_i^2 y_i \end{pmatrix} \qquad (4.14)$$

and the cubic polynomial is

$$A = \begin{pmatrix} a_0 \\ a_1 \\ a_2 \\ a_3 \end{pmatrix}, \qquad G = \begin{bmatrix} n & \sum_{i=1}^{n} x_i & \sum_{i=1}^{n} x_i^2 & \sum_{i=1}^{n} x_i^3 \\ \sum_{i=1}^{n} x_i & \sum_{i=1}^{n} x_i^2 & \sum_{i=1}^{n} x_i^3 & \sum_{i=1}^{n} x_i^4 \\ \sum_{i=1}^{n} x_i^2 & \sum_{i=1}^{n} x_i^3 & \sum_{i=1}^{n} x_i^4 & \sum_{i=1}^{n} x_i^5 \\ \sum_{i=1}^{n} x_i^3 & \sum_{i=1}^{n} x_i^4 & \sum_{i=1}^{n} x_i^5 & \sum_{i=1}^{n} x_i^6 \end{bmatrix},$$

$$\text{and } H = \begin{pmatrix} \sum_{i=1}^{n} y_i \\ \sum_{i=1}^{n} x_i y_j \\ \sum_{i=1}^{n} x_i^2 y_i \\ \sum_{i=1}^{n} x_i^3 y_i \end{pmatrix} \qquad (4.15)$$

The same approach can be applied to acquire the polynomial of higher order.

With the advent of computer and a lot of powerful application software, the process of ι. ιding the coefficient polynomial can be easily accomplished by such software as EXCEL.

In applying EXCEL, several trials have to be done to get the exact solution, depending on what accuracy should be satisfied. Regarding to the present problem, cubic polynomial is always the first attempt.

In using EXCEL to obtain the matrix *G, A, H*, the following commands will be used to implement the certain tasks:

- COUNT(X): to get the value of *n*,
- SUM(X): to get the summation of variable *x*: Σx_i,
- SUMPRODUCT(X): to get the summation of multiplication of variables *x* and *y*. The multiplication could be of different orders,
- MINVERSE: to get the inverse matrix of *G*,
- MMULT: to get the coefficient matrix *A* by multiplying the inverse matrix, G^I, with matrix, *H*.

By this means, the polynomials for the three curves of permanent deformations under three different conditions, namely, un-reinforced section, geogrids at base-subgrade interface and geogrids in the middle of base, as the function of the number of passes *n*, have been obtained:

Case 1: unreinforced section

- Formula (permanent deformation as a function of number of passes *n*) for the point at the top of surface:

$$F(n) = 0.0109 - 0.5376 * \log_{10}(n) - 1.6435 * \log_{10}^2(n) + 0.0741 * \log_{10}^3(n) \qquad (4.16)$$

- Formula (permanent deformation as a function of number of passes *n*) for the point at the base-wearing course interface:

33

$$F(n) = 0.0007 + 0.7529 * \log_{10}(n) - 1.7378 * \log_{10}^{2}(n) + 0.1316 * \log_{10}^{3}(n) \qquad (4.17)$$

- Formula (permanent deformation as a function of number of passes n) for the point at the base-subgrade interface:

$$F(n) = 0.0048 + 1.398 * \log_{10}(n) - 1.5101 * \log_{10}^{2}(n) + 0.1803 * \log_{10}^{3}(n) \qquad (4.18)$$

The corresponding curves are illustrated as Figure 4.2.

Case 2: geogrids in the middle of base layer

- Formula (permanent deformation as a function of number of passes n) for the point at the top of surface:

$$F(n) = 0.003 - 0.135 * \log_{10}(n) - 0.3518 * \log_{10}^{2}(n) - 0.0139 * \log_{10}^{3}(n) \qquad (4.19)$$

- Formula (permanent deformation as a function of number of passes n) for the point at the base-wearing course interface:

$$F(n) = 0.0038 + 0.6986 * \log_{10}(n) - 0.8495_{10}^{2} * \log(n) + 0.1183 * \log_{10}^{3}(n) \qquad (4.20)$$

- Formula (permanent deformation as a function of number of passes n) for the point at the base-subgrade interface:

$$F(n) = 0.0099 + 0.3933 * \log_{10}(n) - 0.3879 * \log_{10}^{2}(n) + 0.0376 * \log_{10}^{3}(n) \qquad (4.21)$$

The corresponding curves are illustrated as Figure 4.3.

Case 3: Geogrids at the base-subgrade interface:

34

- Formula (permanent deformation as a function of number of passes n) for the point at the top of surface:

$$F(n) = 0.0237 + 0.1626 * \log_{10}(n) - 1.1642 * \log_{10}^2(n) + 0.0444 * \log_{10}^3(n) \qquad (4.22)$$

- Formula (permanent deformation as a function of number of passes n) for the point at the base-wearing course interface :

$$F(n) = 0.0015 + 0.4348 * \log_{10}(n) - 0.6063 * \log_{10}^2(n) + 0.0187 * \log_{10}^3(n) \qquad (4.23)$$

- Formula (permanent deformation as a function of number of passes n) for the point at the base-subgrade interface:

$$F(n) = 0.0147 + 0.7707 * \log_{10}(n) - 0.5491 * \log_{10}^2(n) + 0.0693 * \log_{10}^3(n) \qquad (4.24)$$

The corresponding curves are illustrated as Figure 4.4.

Chapter V

RESILIENT MODULUS IDENTIFICATION - SENSITIVITY ANALYSIS

5.1   General Discussion

As stated previously, the pavement system that Nejad et al (21) had been testing on could be identified as conventional flexible pavement, with asphalt layer paved at the top, and then the base layer, followed by the subgrade at the bottom. The geometry of the system is shown as Figure 5.1.

To perform the numerical analysis, the following assumptions have been made:

- This is a 3-layer system,

- Each layer is homogeneous, isotropic, and linearly elastic,

- The properties of each layer are characterized by a permanent resilient modulus E and a Poisson ratio v. The reason why the permanent resilient modulus rather than the elastic modulus or resilient modulus has been applied herein is that the parameter (displacement) recorded is the permanent deformation, which is unrecoverable,

- The Poisson ratio v for each layer is 0.4, 0.3, 0.45, respectively. They would not change throughout the loading and unloading process,

- The material is weightless and infinite in areal extent,

- Each layer has a finite thickness h, but the lowest layer, subgrade, is infinite in thickness,

- A uniform pressure q=210 kPa is applied on the surface over a circular area of radius a=0.025 m. This pressure was generated by the passing tire. The loading waveform, which might be triangular, rectangular or haversine shaped, was not taken into account. Nonetheless, th. loading duration was not being considered,

36

- Continuity conditions are satisfied at the layer interfaces, as indicated by the same vertical displacement, and radial displacement.

With the processing of tire loading, the system is stiffened, and as the result of the stiffening effect, the permanent deformation generated by each pass of tire becomes less and less. This was summarized in Figure 5.2~Figure 5.4.

The consequent numerical analysis was divided into two stages. The first was to identify the permanent resilient modulus of every layer as the function of number of passes. The second was to identify the properties of new layer around the geogrids in the base layer. These properties comprise the thickness and the permanent resilient modulus.

For the first stage, it was assumed that the inclusion of geogrids influenced the permanent resilient modulus of every layer. The finite element method (FEM) package ABAQUS was employed to identify the permanent resilient modulus (PRM) as the function of passes. Then another program, KENLAYER, the software developed by Huang (16) based on the multi-layer elastic theory was used to verify the correctness of PRM.

As the second stage, it was presumed that a new layer whose resilient modulus is higher than the surrounding layers had been developed around the geogrids, while the properties of the remaining layers are the same as those of unreinforced section. As far as the methodology is concerned, sensitivity analysis was performed.

5.2 Identification of Permanent Resilient Modulus

As the first stage of analysis, the process consists of two steps. The first is the identification of PRM by the means of ABAQUS (2), the finite element analysis package. The consequent step is the verification by means of KENLAYER, a multi-layer elastic software.

37

5.2.1 Identification of Permanent Resilient Modulus by ABAQUS

ABAQUS (2) is such a general-purpose FEA package that it requires two parts of data to build up its source code. The first part is model data, which consists of geometry and material properties, and the second part is history data, which consists of the type of simulation (static, dynamic, etc), the loads and boundary conditions, as well as the output required. The geometry data comprises nodal coordinates, element connectivity, and element properties.

5.2.1.1 Model Set-up

Though the tests were conducted in the tank, the boundary of which was restricted to a certain range, it is possible and reasonable to assume the boundary as infinite considering the trivial displacement on the boundary, the stress as well as strain are so small as negligible. Nevertheless, the system was subjected to the circular tire load, as mentioned in the assumption in Section 5.1.

Because of the axisymmetric feature of geometry and load, it was proper to simulate the system by half. Furthermore, the initial 3-D problem could be simplified into 2-D problem. The area of interest can be restricted within 0.48 x 0.48 m. Inside this area, axisymmetric elements were employed. On the other hand, ABAQUS (2) provides the infinite element which could be incorporated to simulate the half-space property involved into analysis by assuming that "the material is ...infinite in areal extent". The elastic model has been incorporated into finite permanent deformation associated with each application of tire pressure during single passage through the elastic half-space which deformed in unrecoverable fashion. Thus, model was set-up as shown in Figure 5.5.

5.2.1.2 History Description

The system was subjected to the repetitive tire loading. In the process of simulation, only one pass would be considered for once. This enables the use of static loading. When

38

simulating the system by means of axisymmetric elements, the axis, which is the boundary at the same time, was constrained from all the directions except the vertical direction, whereas the infinite elements surrounding the axisymmetric elements provided another kind of boundary conditions, on the other hand.

5.2.1.3 Methodology

The methodology of FEM analysis was to analyze the permanent deformation by the concept of permanent resilient modulus (PRM) introduced in Chapter 4.

Taking into account the fact that 6000 passes are involved in the tests, the discrete approach with respect to the number of passes suggests more possible and realistic analysis. Moreover, considering the fact that the slope of the curve of deflection becomes smaller as the number of passes increases, one could assume that the change of deflection within certain passes (for instance, 100 passes, or larger with the increase of passes) was linear, which in turn provides the feasibility of changing the geometry manually.

In the procedure, one trial of analysis was accomplished when the permanent deformations at the three points obtained in the program agreed with those of the tests. The corresponding PRM for each layer was recorded, followed by the change of geometry. And the new trial of analysis would be based on the updated geometry.

5.2.1.4 Analysis Results and Regression Analysis of Results

The extensive numerical simulations provided results of PRM under three conditions. These are illustrated with Table 5.1 ~ Table 5.3 and Figure 5.6 ~ Figure 5.9.

In addition, Figures 5.10 ~ Figure 5.19 bring some ideas of the response of system (contour of strain and stress) for certain pass.

39

Regression analysis was employed to derive the equations of PRM as the functions of number of passes. It was interesting to discover that all the PRM could be expressed as quadratic equations respectively passes except those of base and subgrade when reinforcing in the middle of base layer, which should be expressed by the cubic equations. Thus, for

- Unreinforced section

  ❖ Wearing course

  $$PRM(n) = 0.6887 + 0.0217 * n - (1.1885e - 6) * n^2 \qquad (5.1)$$

  ❖ Base layer

  $$PRM(n) = 1.5296 + 0.02 * n - (1.2989e - 6) * n^2 \qquad (5.2)$$

  ❖ Subgrade

  $$PRM(n) = 0.9127 + 0.0283 * n + (2.3959e - 6) * n^2 \qquad (5.3)$$

- Geogrids reinforced in the middle of the base layer

  ❖ Wearing course

  $$PRM(n) = 8.5737 + 0.0318 * n - (4.2836e - 6) * n^2 \qquad (5.4)$$

  ❖ Base layer

  $$PRM(n) = 31.625 + 0.3462 * n - 0.0003 * n^2 + (2.5855e - 7) * n^3 \qquad (5.5)$$

❖ Subgrade

$$PRM(n) = 2.0858 + 0.0706 * n + (9.1059e - 6) * n^2 - (7.8083e - 9) * n^3 \qquad (5.6)$$

• Geogrids at the interface between base layer and subgrade

❖ Wearing course

$$PRM(n) = 0.592 + 0.0158 * n - (3.7688e - 7) * n^2 \qquad (5.7)$$

❖ Base layer

$$PRM(n) = 5.4032 + 0.0333 * n - (1.6605e - 6) * n^2 \qquad (5.8)$$

❖ Subgrade

$$PRM(n) = 4.2064 + 0.1233 * n + (1.9935e - 5) * n^2 \qquad (5.9)$$

Comparison in terms of the PRM of each layer under different conditions has been done, and results are illustrated by the Figure 5.20 ~ Figure 5.22.

Based on these figures, it is manifested that the materials have been significantly improved in term of PRM, which directly results in the decrease of permanent deformation.

5.2.2 Verification of PRM by KENLAYER

KENLAYER is a program developed by Huang (14), under DOS platform written with FORTRAN77. The backbone of the program is Burmister's multi-layer theory dealing

with the multi-layer system under a circular loading area and the theory of elasticity. The governing differential equation can be written as:

$$\nabla^4 \phi = 0$$ (5.10)

where ϕ is the stress function.

For a system with axisymmetric stresses distribution, the operator ∇^4 has the following form:

$$\nabla^4 = (\frac{\partial^2}{\partial r^2} + \frac{1}{r}\frac{\partial}{\partial r} + \frac{\partial^2}{\partial z^2})(\frac{\partial^2}{\partial r^2} + \frac{1}{r}\frac{\partial}{\partial r} + \frac{\partial^2}{\partial z^2})$$ (5.11)

The four constants involved in this fourth-order differential equation will be determined employing the boundary and continuity conditions, and thus result in the determination of stresses and displacements.

For an axisymmetric case, the stresses can be expressed as follows:

$$\sigma_z = \frac{\partial}{\partial z}[(2-v)\nabla^2\phi - \frac{\partial^2\phi}{\partial z^2}]$$ (5.12.a)

$$\sigma_r = \frac{\partial}{\partial z}[v\nabla^2\phi - \frac{\partial^2\phi}{\partial r^2}]$$ (5.12.b)

$$\sigma_t = \frac{\partial}{\partial z}[v\nabla^2\phi - \frac{1}{r}\frac{\partial\phi}{\partial r}]$$ (5.12.c)

$$\tau_{rz} = \frac{\partial}{\partial r}[(1-v)\nabla^2\phi - \frac{\partial^2\phi}{\partial z^2}]$$ (5.12.d)

where r: radial coordinate

z: vertical coordinate

σ_z: vertical stress

σ_r: radial stress

42

σ_t: tangential stress

τ_{rz}:   shear stress

In order to verify the permanent resilient modulus yielded by means of ABAQUS (2), the PRM was incorporated in KENLAYER, and the resulting displacements are listed in Table 5.4 ~ Table 5.5.

From these Tables, it is self-evident that the displacements obtained from two sources are agreeing with each other very well, which can be regarded as the proof of the correctness of calculation of PRM by ABAQUS (2).

5.3   Sensitivity Analysis

As the second stage of analysis, the purpose of sensitivity analysis is to study how the variation of thickness and PRM of base layer have affected the variation of permanent deformations on specified points.

In this method, it was assumed that a new layer has been formed around the geogrids within the base layer after the structure had been reinforced by the geogrids in the middle of base layer or at the interface between base layer and subgrade. The formation of the new layers is mainly due to the interlocking taking place between geogrids and the surrounding soil. As the result, the properties, mainly permanent resilient modulus, of this new layer were varied from the initial base layer, while those of the initial structure kept unchanged.

5.3.1   Introduction of Interlocking

Interlocking is a concept first introduced and widely incorporated in the design of concrete block pavement (CBP) which is basically composed of an aggregate/unbound granular/cement- treated/asphalt-treated base, bedding sand , and concrete paver. This kind of pavements is commonly practiced for both pedestrian and vehicular use.

43

As stated in Shackel's (23): "block pavements develop interlocking under traffic... once interlocking has been achieved the response of the pavement becomes independent of the magnitude of the wheel loads (within the range from 24 to 70 kN) and the number of load repetitions".

Marvin (18) designed pull-out testing to pull out one single block out of pavement and carried out a series of tests in lab and on-site. His works answered the pertinent questions as:

- Why does interlocking occur, and what factors play a part?
- When, in term of trafficking/time, does interlocking occur?
- Does interlocking occur in the wheel path first/only?

Nishizawa et al (26) studied the mechanism of interlocking in concrete block pavement by means of finite element method (FEM) in view of the stresses due to traffic load. In the study, the concrete block was treated as plate element, bedding sand as joint element which was modeled as a set of springs, while the sub-base was assumed to be liquid foundation or "Winkler foundation".

Similarly, Houben et al (13) formulated the concrete blocks as non-deformable 'rigid bodies', while the bedding sand was schematized as two horizontal springs together with two vertical springs and the base was modeled as non-deformable base, when the finite element method package ICES STRUDL was applied.

Furthermore, Houben et al (13) carried out a series of on-site experiments, the resulting data being analyzed by means of two types of analyzing packages, one being FEM package, and the other being linear-elastic multi-layer program CIRCLY. Three of them came to good agreement.

In sum, Rada et al (24) stated: "the performance of CBP pavements depends on the interlocking of the individual units and, to a lesser degree, on the shape and thickness of the blocks. The interlocking of the paver blocks is, in turn, influenced by the laying pattern and thickness of the bedding sand."

When the conception of interlocking was introduced into geosynthetics-reinforced structures, different approaches towards the problem simulation or design have been adopted.

Cividini et al (8) employed two schemes to simulate the "interlocking" behavior of geotextile in reinforced sand after a series of triaxial tests. The first one was called "non-homogeneous scheme", while the second was called "non-isotropic scheme". In the first one, the reinforcement and the sand layers were discretized and considered seperatedly. On the contrary, the second one treated the non homogeneous medium as equivalent to a continuous, non isotropic, non linear composite material characterized by the constitutive law.

Giroud et al (10) proposed the design method for unpaved road and trafficked area reinforced with geogrids. In his method, interlocking was considered as the combination influence of three mechanisms, namely, confinement, load distribution and tensioned membrane effect. Every mechanism influenced the performance of pavement in different manner and contributed in different percentage. Confinement improves the ultimate bearing capacity to plastic limit. Load distribution was resulted from the larger distribution angle. And membrane effect decreased the vertical stress when the geogrids deformed.

When performing the sensitivity analysis, interlocking was taken into account by discretizing the layer developed around the geogrids and the remaining base material. During the theoretical formula derivation, the virtual displacement theorem and the conception o· primary structure as well as adjoint structure (4,5,17,28,29,30) were incorporated.

45

5.3.1 Formula Derivation

According to the virtual displacement theorem, the displacement at the certain point can be determined with the involvement of primary structure and adjoint structure described in Budkowska (4,5). The primary is subject to the original loading, while the adjoint structure is subject to the virtual unit loading at the point of interest, i.e., where the generated displacement is calculated. For the sake of convenience, let's denote the point at the surface as point #1, the point at the course-base interface as point #2, and the point at the base-subgrade interface as point #3.

Thus the primary structure is illustrated as Figure 5.1, and the adjoint structures for the displacement at point #1, point #2, point #3 are shown in Figure 5.23, Figure 5.24, and Figure 5.25, respectively.

Suppose that FEM is employed in determination of the state of deformation and stresses. For a point of interest, the displacement can be determined with the involvement of primary structure and adjoint structure. As described previously, the primary structure is subject to the given load condition, while the unit load associated with the type of displacement is applied to the adjoint structure. The mathematical form of the virtual work theorem gives:

$$\bar{1}v = \int_v (\varepsilon_{ij} \bar{\sigma}_{ij})dV$$

(5.13)

where $\bar{1}$:   the unit virtual force applied upon the calculated point, which will be point #1, point #2, and point #3, respectively

v: the displacement (permanent deformation) caused by the force exerted on the primary structure at the point where the virtual force is applied on

46

ε_{ij}: the strain at the integration points in the primary structure

$\bar{\sigma}_{ij}$: the stress at the integration points in the adjoint structure

For the axisymmetric problem, the strain vector for one finite element can be defined in matrix form as:

$$\{\varepsilon\} = \begin{Bmatrix} \varepsilon_z \\ \varepsilon_r \\ \varepsilon_\theta \\ \gamma_{rz} \end{Bmatrix} = \begin{Bmatrix} \dfrac{\partial v}{\partial z} \\ \dfrac{\partial u}{\partial r} \\ \dfrac{u}{r} \\ \dfrac{\partial u}{\partial z} + \dfrac{\partial v}{\partial r} \end{Bmatrix} \tag{5.14}$$

where v: the displacement at z direction

u: the displacement at r direction

and correspondingly, the stress vector is

$$\{\sigma\} = \begin{Bmatrix} \sigma_z \\ \sigma_r \\ \sigma_\theta \\ \tau_{rz} \end{Bmatrix} \tag{5.15}$$

The constitutive relationship between strain and stress, according to Hooke's law is:

$$\{\sigma\} = [D]\{\varepsilon\} \tag{5.16}$$

where:

$$[D] = \frac{E(1-v)}{(1+v)(1-v)}
\begin{bmatrix}
1 & \dfrac{v}{1-v} & \dfrac{v}{1-v} & 0 \\
 & 1 & \dfrac{v}{1-v} & 0 \\
 & & 1 & 0 \\
 & & & \dfrac{1-2v}{2(1-v)}
\end{bmatrix}$$

(5.17)

in which E is the elastic modulus, and v is the Poisson ratio.

Substitution of [D] given by Equation (5.17) into Equation (5.16) gives:

$$\sigma_z = \frac{E(1-v)}{(1+v)(1-2v)}\left[\varepsilon_z + \frac{v}{1-v}(\varepsilon_r + \varepsilon_\theta)\right]$$

(5.18.a)

$$\sigma_r = \frac{E(1-v)}{(1+v)(1-2v)}\left[\varepsilon_r + \frac{v}{1-v}(\varepsilon_z + \varepsilon_\theta)\right]$$

(5.18.b)

$$\sigma_\theta = \frac{E(1-v)}{(1+v)(1-2v)}\varepsilon_\theta$$

(5.18.c)

$$\tau_{rz} = \frac{E}{2(1+v)}\gamma_{rz} = G\gamma_{rz}$$

(5.18.d)

Compared with the theory of elasticity in which the streses are only the function of the strains, the purpose of sensitivity analysis is to study the variation of displacement caused by the variation of other parameters (design parameters). In this research, the design

48

parameters are defined as E and H. E is explicitly involved in the constitutive relationship, while another variable H is implicitly involved in the integration process. Differentiating the left hand side of Equations (5.18.a) to (5.18.d) with respect to E, ε_z, $\varepsilon_r, \varepsilon_\theta$ and γ_{rz}, results:

$$\delta\sigma_z = \frac{\partial\sigma_z}{\partial E}\delta E + \frac{\partial\sigma_z}{\partial\varepsilon_z}\delta\varepsilon_z + \frac{\partial\sigma_z}{\partial\varepsilon_r}\delta\varepsilon_r + \frac{\partial\sigma_z}{\partial\varepsilon_\theta}\delta\varepsilon_\theta$$

$$= \frac{1-v}{(1+v)(1-2v)}\left[\varepsilon_z + \frac{v}{1-v}(\varepsilon_r + \varepsilon_\theta)\right]\delta E + \frac{E(1-v)}{(1+v)(1-2v)}\delta\varepsilon_z + \frac{Ev}{(1+v)(1-2v)}\delta\varepsilon_r$$

$$+ \frac{Ev}{(1+v)(1-2v)}\delta\varepsilon_\theta$$

$$(5.19.a)$$

$$\delta\sigma_r = \frac{\partial\sigma_r}{\partial E}\delta E + \frac{\partial\sigma_r}{\partial\varepsilon_z}\delta\varepsilon_z + \frac{\partial\sigma_r}{\partial\varepsilon_r}\delta\varepsilon_r + \frac{\partial\sigma_r}{\partial\varepsilon_\theta}\delta\varepsilon_\theta$$

$$= \frac{1-v}{(1+v(1-2v))}\left[\varepsilon_r + \frac{v}{1-v}(\varepsilon_r + \varepsilon_\theta)\right]\delta E + \frac{E(1-v)}{(1+v)(1-2v)}\left[\delta\varepsilon_r + \frac{v}{1-v}(\delta\varepsilon_z + \delta\varepsilon_\theta)\right]$$

$$(5.19.b)$$

$$\delta\sigma_\theta = \frac{\partial\sigma_\theta}{\partial E}\delta E + \frac{\partial\sigma_\theta}{\partial\varepsilon_\theta}\delta\varepsilon_\theta$$

$$= \frac{1-v}{(1+v)(1+2v)}\varepsilon_\theta\delta E + \frac{E(1-v)}{(1+v)(1-2v)}\delta\varepsilon_\theta \qquad (5.19.c)$$

$$\delta\tau_{rz} = \frac{\partial\tau_{rz}}{\partial E}\delta E + \frac{\partial\tau_{rz}}{\partial\gamma_{rz}}\delta\gamma_{rz}$$

$$= \frac{\gamma_{rz}}{2(1+v)}\delta E + \frac{E}{(1+v)(1-2v)}\delta\varepsilon_\theta \qquad (5.19.d)$$

Since the primary structure is subjected to the constant load, therefore

49

$$\delta\sigma_z = 0 \tag{5.20.a}$$

$$\delta\sigma_r = 0 \tag{5.20.b}$$

$$\delta\sigma_\theta = 0 \tag{5.20.c}$$

$$\delta\tau_{rz} = 0 \tag{5.20.d}$$

Substituting Equations (5.19) into Equations (5.20) and solving them gives the strain variations with respect to δE

$$\delta\varepsilon_z = -\frac{\varepsilon_z}{E}\delta E \tag{5.21.a}$$

$$\delta\varepsilon_r = -\frac{\varepsilon_r}{E}\delta E \tag{5.21.b}$$

$$\delta\varepsilon_\theta = -\frac{\varepsilon_\theta}{E}\delta E \tag{5.21.c}$$

$$\delta\gamma_{rz} = -\frac{\gamma_{rz}}{E}\delta E \tag{5.21.d}$$

Now consider the change of permanent deflection of those three points, #1, #2, and #3, respectively, under the three conditions. For the sake of convenience, let's denote case 1 as the unreinforced case, case 2 as the case of geogrids reinforced in the middle of base layer, and case 3 as the case of geogrids reinforced at the base-subgrade interface. For a certain pass which is defined as the ith pass, the variation of deformation is calculated as the difference between the deformation (case 2) and the deformation (case 1) or as the difference between the deformation (case 3) and the deformation (case 1)

The description can be expressed by equations as follows:.

$$\delta v_{2i}^{1} = \delta v_{2i} - \delta v_{1i} \qquad \qquad (5.22.a)$$

$$\delta v_{3i}^{1} = \delta v_{3i} - \delta v_{1i} \qquad \qquad (5.22.b)$$

where

δv_{2i}^{1} : the change of deflection for case 2 with respect to case 1 associated with the ith pass.

δv_{3i}^{1} : the change of deflection for case 3 with respect to case 1 associated with the ith pass.

$\delta v_{1i}, \delta v_{2i}, \delta v_{3i}$: the deflection for the case 1, 2, 3, respectively, at the ith pass.

Incorporating the virtual work theorem, and substituting Equations (5.22) into Equation (5.13) results in:

$$\delta v_{ji}^{1} = \int_{v} -\frac{\delta E}{E}\left(\overline{\sigma}_{z}\,\varepsilon_{z} + \overline{\sigma}_{r}\,\varepsilon_{r} + \overline{\sigma}_{\theta}\,\varepsilon_{\theta} + \overline{\tau}_{rz}\,\gamma_{rz} \right) dV \qquad j=2,3$$

$$(5.23)$$

For the axisymmetric problem,

$$dV = 2\pi r\, dr\, dH \qquad \qquad (5.24)$$

In the scope of sensitivity analysis, it can be assume that δv_{ji}^{1} is caused by the change of modulus δE within the layer of thickness δH. For a given δv_{ji}^{1}, taking δH as constant,

51

substituting Equation (5.24) into Equation (5.23) and moving $\delta E/E$ out of the integration mark gives:

$$\delta v_{ij}^{l} = \frac{\delta E * \delta H * 2\pi}{E} \int_{r} (\overline{\sigma_{z}}\varepsilon_{z} + \overline{\sigma_{r}}\varepsilon_{r} + \overline{\sigma_{\theta}}\varepsilon_{\theta} + \overline{\tau_{rz}}\gamma_{rz})rdr \qquad (5.25)$$

where:

$\overline{\sigma_{z}}$:   the normal stress in z direction generated in adjoint structure

$\overline{\sigma_{r}}$:   the normal stress in r direction generated in adjoint structure

$\overline{\sigma_{\theta}}$:   the loop stress generated in adjoint structure

$\overline{\tau_{rz}}$:   the shear stress generated in adjoint structure

ε_{z} :   the normal strain in z direction generated in primary structure

ε_{r} :   the normal strain in r direction generated in primary structure

ε_{θ} :   the loop strain generated in primary structure

γ_{rz} :   the shear strain generated in primary structure

Equation (5.25) can be altered into:

$$\delta E * \delta H = \frac{\delta v_{ji}^{l} * E}{2\pi \int_{r} (\overline{\sigma_{z}}\,\varepsilon_{z} + \overline{\sigma_{r}}\,\varepsilon_{r} + \overline{\sigma_{\theta}}\,\varepsilon_{\theta} + \overline{\tau_{rz}}\,\gamma_{rz})rdr} \qquad (5.26)$$

Equation (5.26) shows that resulting formulation of displacement due to change of thickness of base layer and δE allows for the evaluation of coupling effect. Thus, the only possible way of further analysis is to assume one variable in order to analyze the other one.

5.3.4 Numerical Calculation

The derivation above is based on the application of the finite element method. Therefore, during the numerical calculation, all the stresses and strains involved in Equation (5.26) can be calculated or interpolated at the integration points of ABAQUS package.

Consequently, two input files in ABAQUS were performed, one named as "primary.inp", which was to analyze the primary structure subject to the tire pressure, and the other named as "adjoint.inp", which was to analyze the adjoint structure under unit concentrated load positioned at point #1, #2, and #3, respectively.

To accomplish the integration in the Equation (5.15), a program written in C Language was incorporated into the calculation. The program (sensitivity.c) is attached in the Appendix .

The analysis procedure was arranged as follows:

- Run *primary.inp*,
- Copy the data of *U2* in *primary.data* into Notepad, and print them out. This is to check the U2 of theoretical data to ensure the process of running is right,
- Copy the data of *E* (strain) in *primary.data* into *primary*, the file which will be opened by *sensitivity.c*,
- Run *adjoint.inp*, CLOAD=1,2,-1. the first "1" refers to Point #1,
- Copy the data of S (stress) into *adjoint*, the file which will be opened by *sensitivity.c*,
- Run *a.out* (the executable file of *sensitivity.c*), using the data of Point#1, namely, the change of permanent deformation as well as the resilient modulus of the base layer,
- Run *adjoint.inp*, CLOAD=401,2,-1. Node "401" refers to Point #2,
- Save the data of S (stress) into *adjoint*,
- Run *a.out*, using the data of Point #2,
- Run *adjoint.inp*, CLOAD=1201,2,-1. Node "1201" refers to Point #3,
- Save the data of S (stress) into *adjoint*,

- Run *a.out*, using the data of Point #3,

- Change the coordinates of *primary.inp*, based on the data of *U2* on Notepad, and change the moduli as well,

- Change the coordinates and moduli of *adjoint.inp* into those similar to *primary.inp*.

Calculations show that the modulus of newly-formed layer is much higher than that of the original layer. As pointed out previously, the change of thickness δH and change of modulus δE are coupled, thus the attempt has been made to separate these two parameters by assuming δH equal to *0.125H, 0.25H, 0.375H,* and *0.5H* (*H* is the thickness of base layer). It turns out that the increase of permanent resilient modulus varies linearly with respect to the number of passes. The results are illustrated as Table 5.7~ Table 5.10 and Figure 5.26 ~ Figure 5.29.

CHAPTER VI

OBSERVATIONS AND CONCLUSIONS

6.1 Observations

Through the experiments on soil with geotextiles, the following observations are obtained:

a) The inclusion of geotextiles definitely improves the performance of base material, in terms of both yielding stress and secant modulus.

b) Both yielding stress and secant modulus increase as the layers of geotextiles increase or the confining pressure increases. However, the extent of increase of yielding stress and secant modulus resulting from confining pressure is not as significant as that caused by geotextiles.

c) When the geotextiles are included as reinforcement/separator, the deformed shape of the part between two layers of geotextiles is the same as that of unreinforced soil sample. When the soil sample is reinforced with merely one layer of geotextile which divides the sample into two parts, one part will deform and the other part will keep its original shape. Which part will deform is unpredictable.

6.2 Conclusions

The following conclusions are made based on the numerical analysis associated with the experimental results published in Nejad et al (21) regarding to the effect of geogrids:

a) The analysis by means of FEM package is very sensitive to the model set-up. In the meanwhile, high-density meshing is always desirable to obtain better results, especially to avoid the stress concentration effect.

b) If properly applied, the analysis results from the multi-layer elastic theory can agree with those from finite element method (FEM) very well.

c) In the tests conducted by Nejad et al (21), permanent deformation of up to 20 mm after 3400 times of passes has been observed when the pavement was non-reinforced, and most portion of this deformation took place during the first several hundred passes. Therefore, this can be regarded as the study of gradual stiffening effect which became more pronounced with the inclusion of geogrids. When the gradual stiffing effect was evaluated by the introduction of concept of permanent resilient modulus (PRM), the increase of PRM with respect to the number of passes has been observed. Nonetheless, the permanent resilient modulus as the function of the number of passes for each layer can be expressed in quadratic expressions.

d) As having been pointed out by the paper (21), it is more effective if the geogrid is placed in the middle of base rather than at the base-subgrade interface. The effectiveness can be achieved by the rapid increase of permanent resilient modulus (PRM) when in the middle of base layer.

e) During the stage of stiffening, the variation of permanent deformation is very sensitive to the variation of thickness coupled with permanent resilient modulus (PRM) of base layer. By assuming that the change of thickness is constant, it is observed that permanent resilient modulus (PRM) varies linearly.

f) On the contrary, the variation of permanent deformation is very insensitive to the change of thickness of base layer. The same amount of variation of permanent deformation that can be obtained by a layer of geogrid will be achieved by big amount of base material in thickness. This, in turn, manifests the cost effectiveness of geogrids as the reinforcement in the flexible pavement.

FIGURES
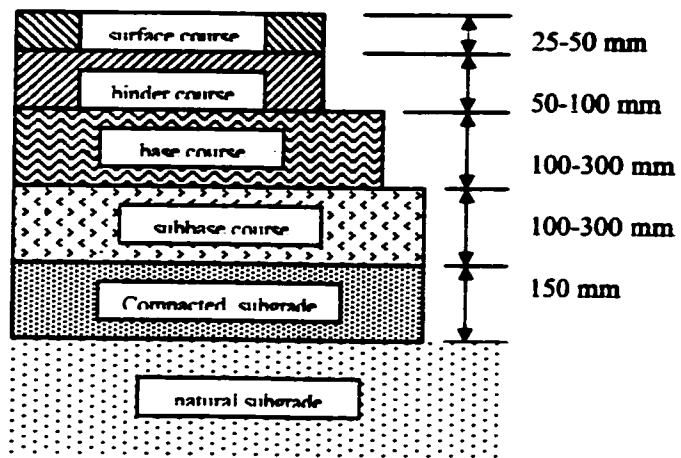
Figure 1.1   Typical cross section of a conventional pavement
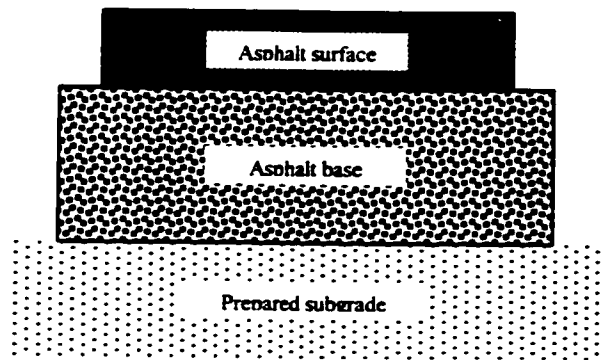
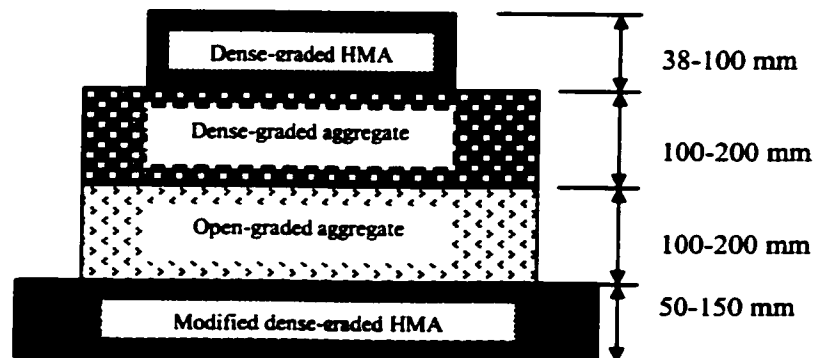**Figure 1.2   Typical cross section of a full-depth asphalt pavement**
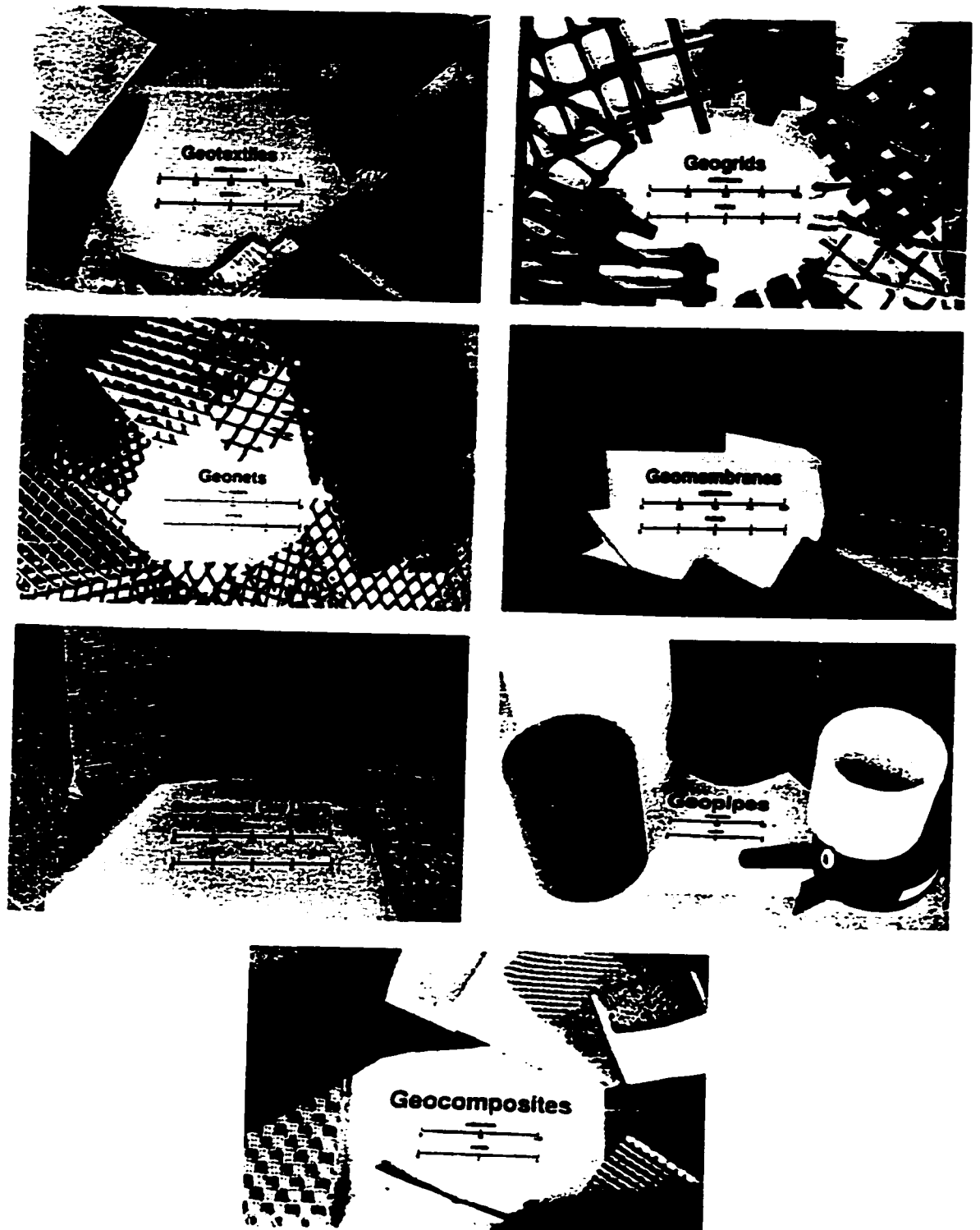

Figure 1.3   Typical CRAM cross section

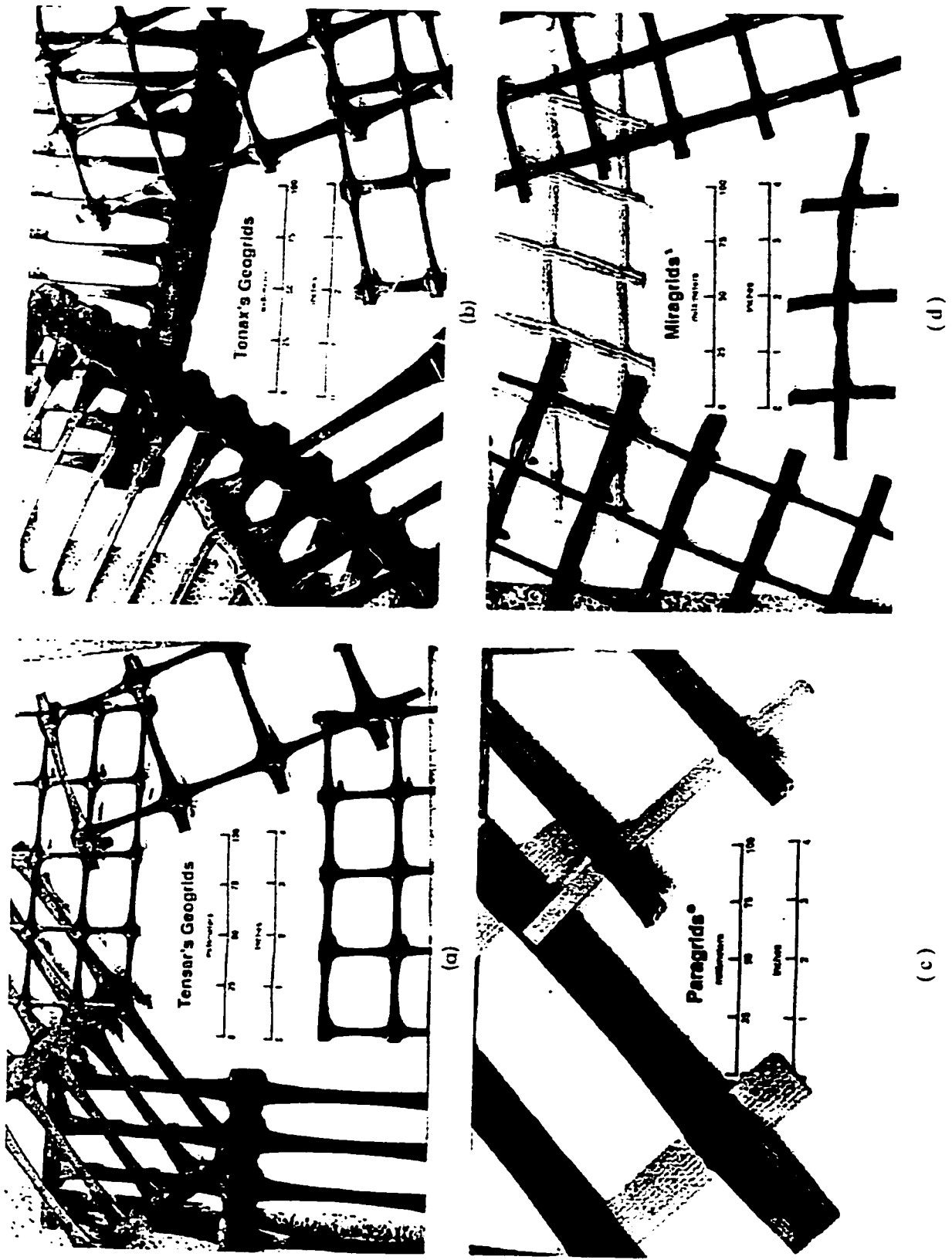**Figure 2.1   Typical geosynthetics materials**

Figure 2.2 (a) Geogrids of Tensor Corp. (b) Geogrids of Tenax Inc. (c) Geogirds of ICI Ltd. – Paragrids. (d) Geogirds of Mirafi/Ten Cate Corp. - Miragrids
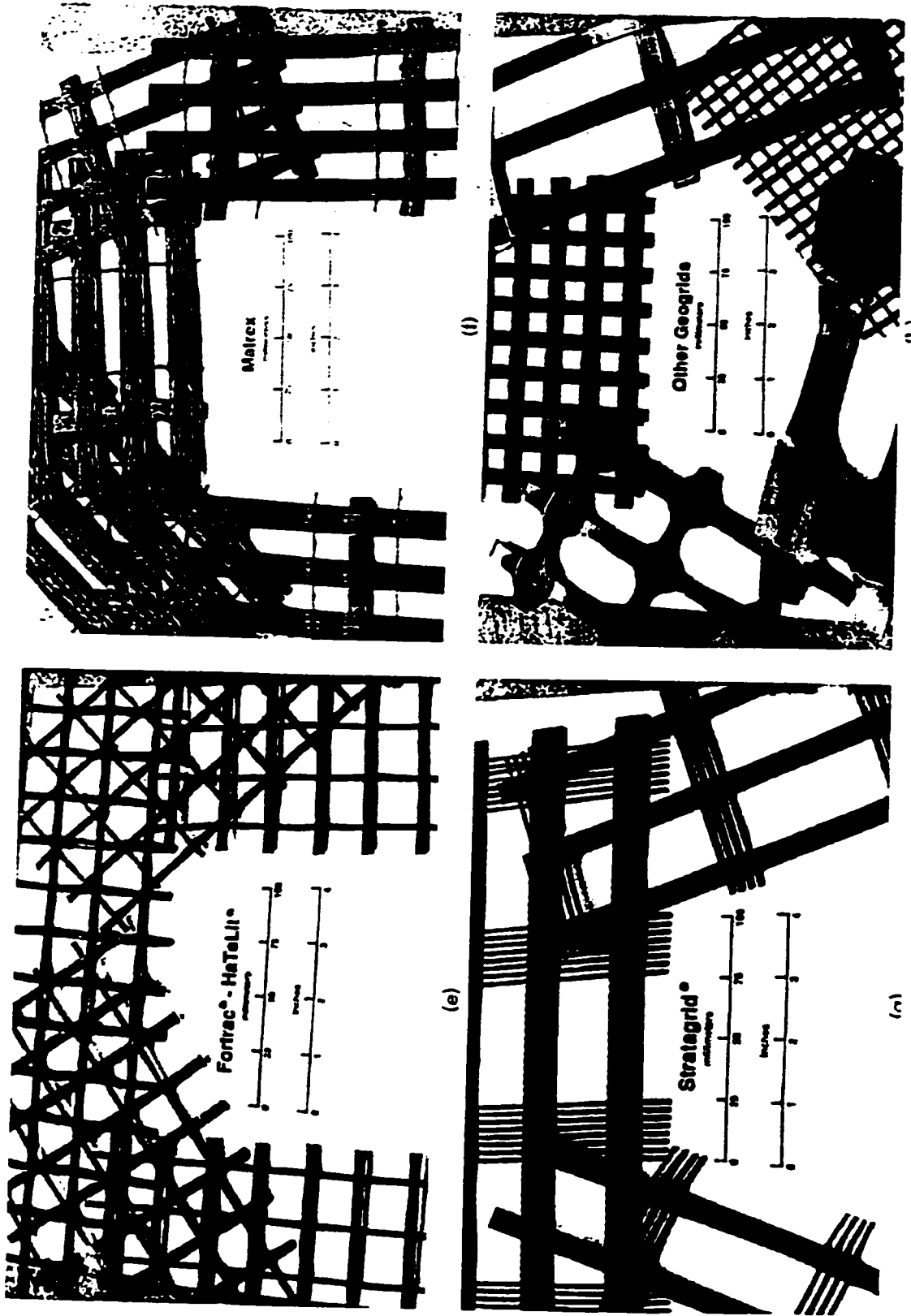
Figure 2.2 (contd) (e) Geogrids of Huesker, Inc., Fortrac and HaTeLit (f) Geogrids of Nicloon/Corps., Matrex. (g) Geogrids of Conwed, Inc. – Stratagrid. (h) other geogrids – mescellaneous.

61
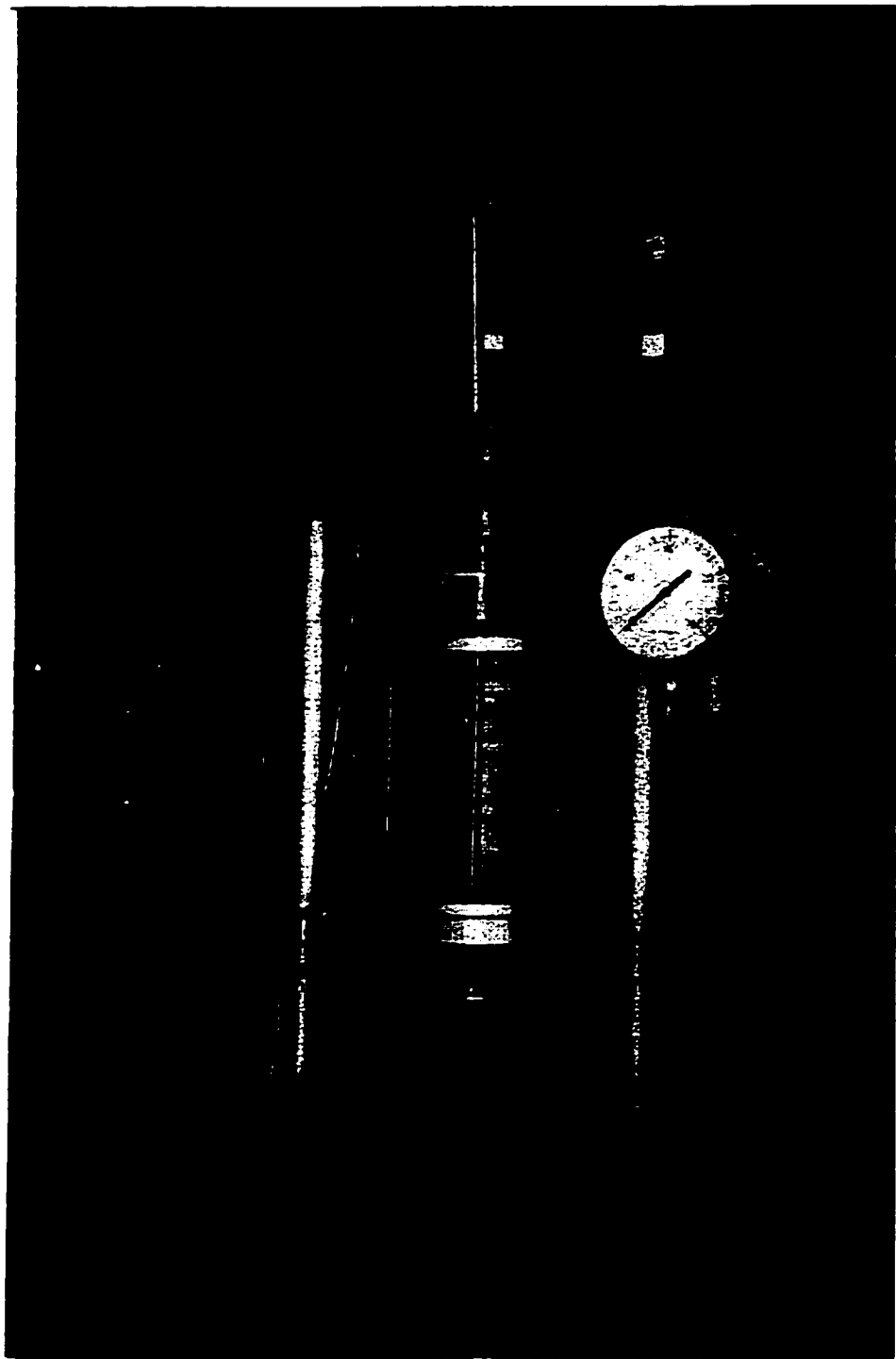
Figure 3.1 Lab set-up
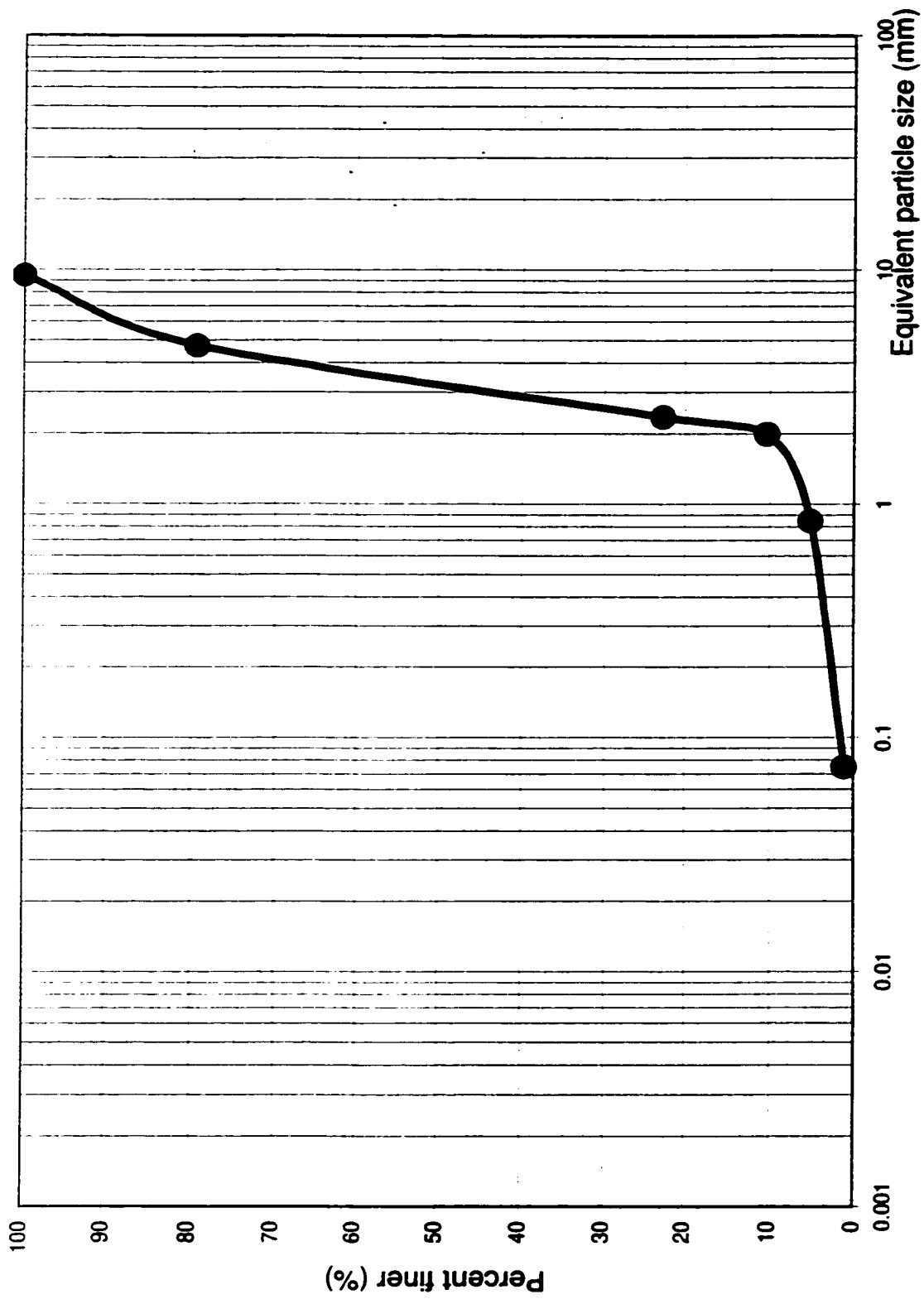
Figure 3.2   Soil gradation
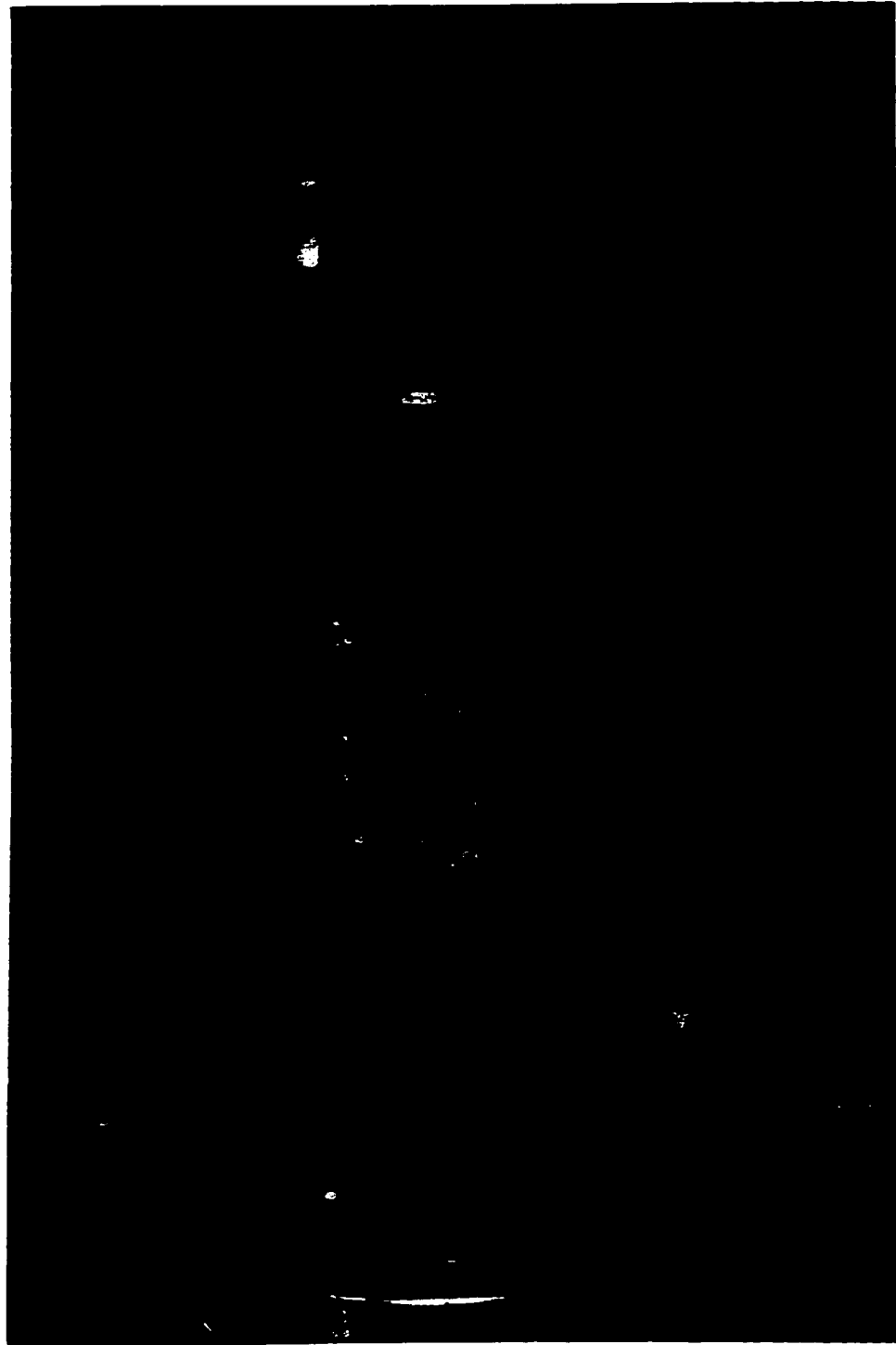
Figure 3.3   Prepared sample
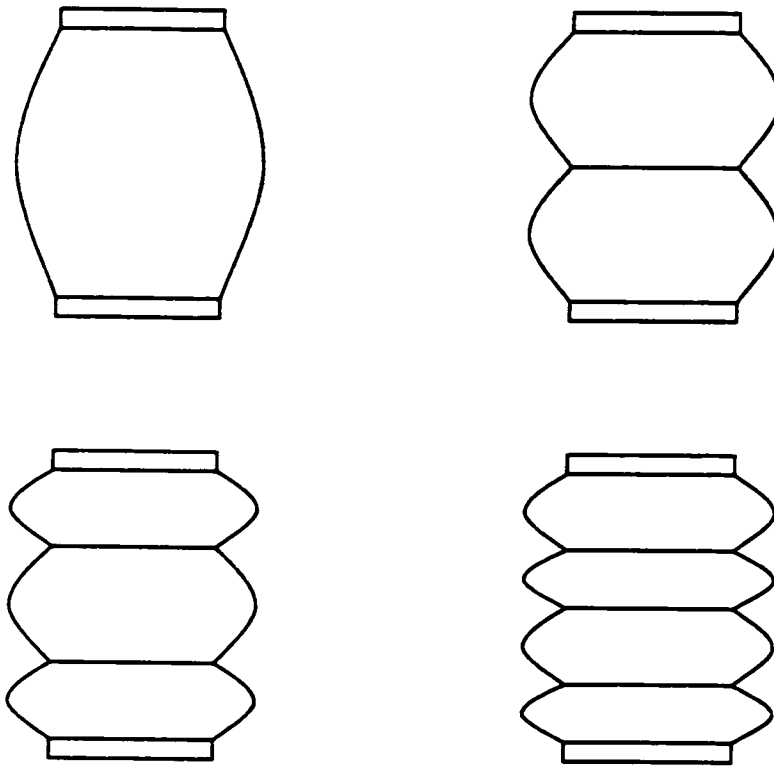
Figure 3.4 **Illustration of deformed-shape**
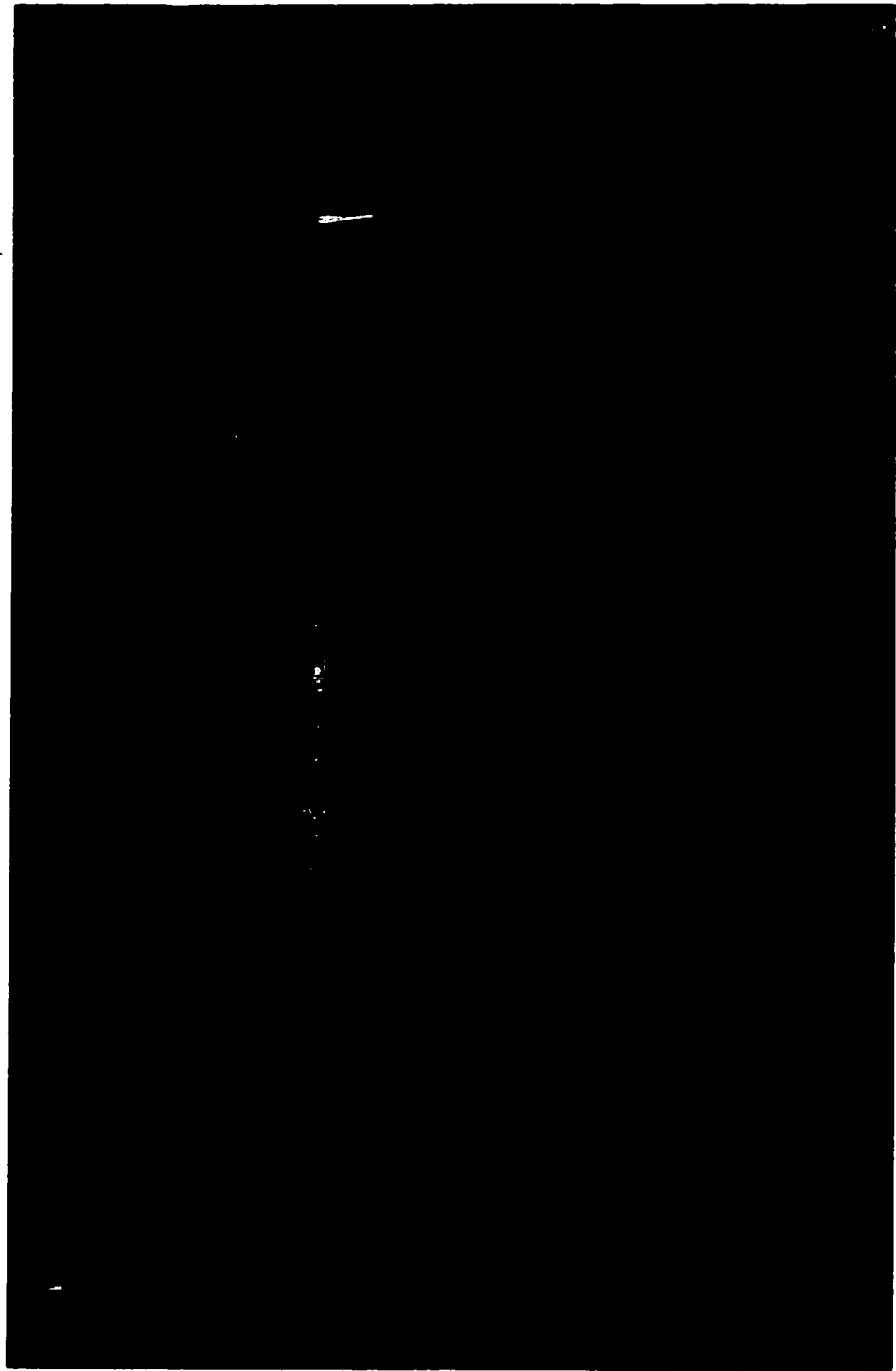
Figure 3.5   Deformed shape under unreinforced condition
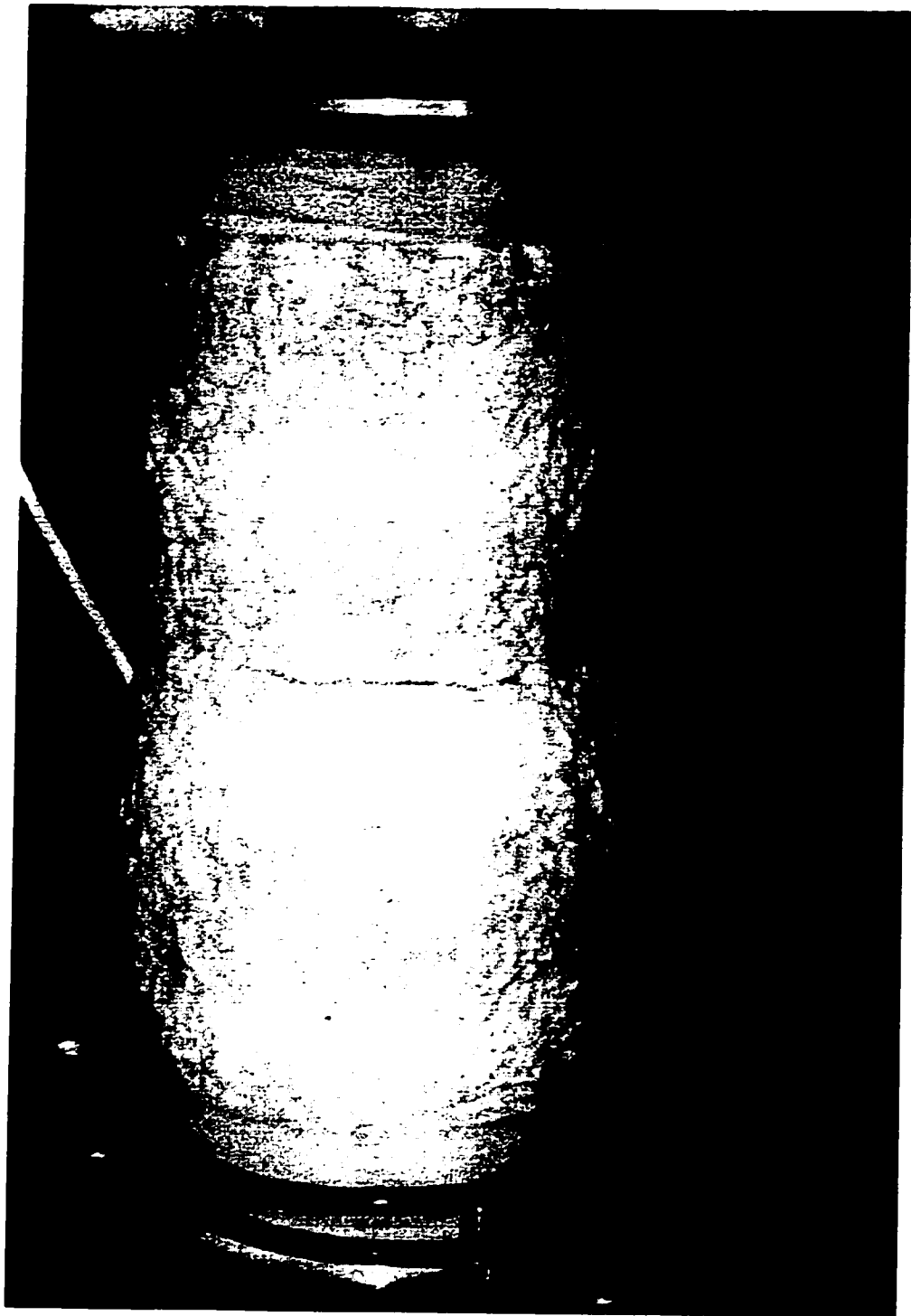
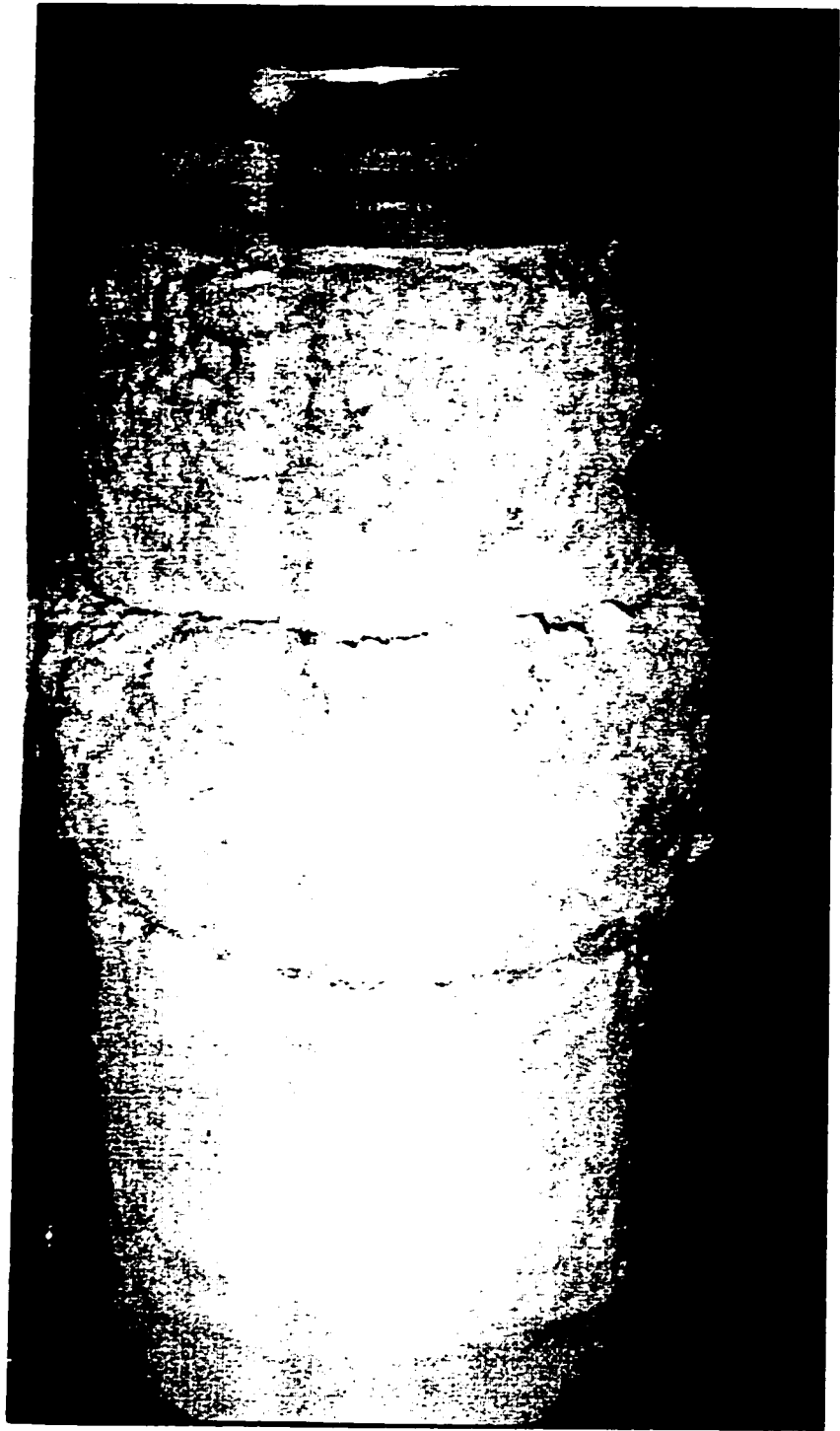**Figure 3.6   Deformed shape under one-layer reinforcement**

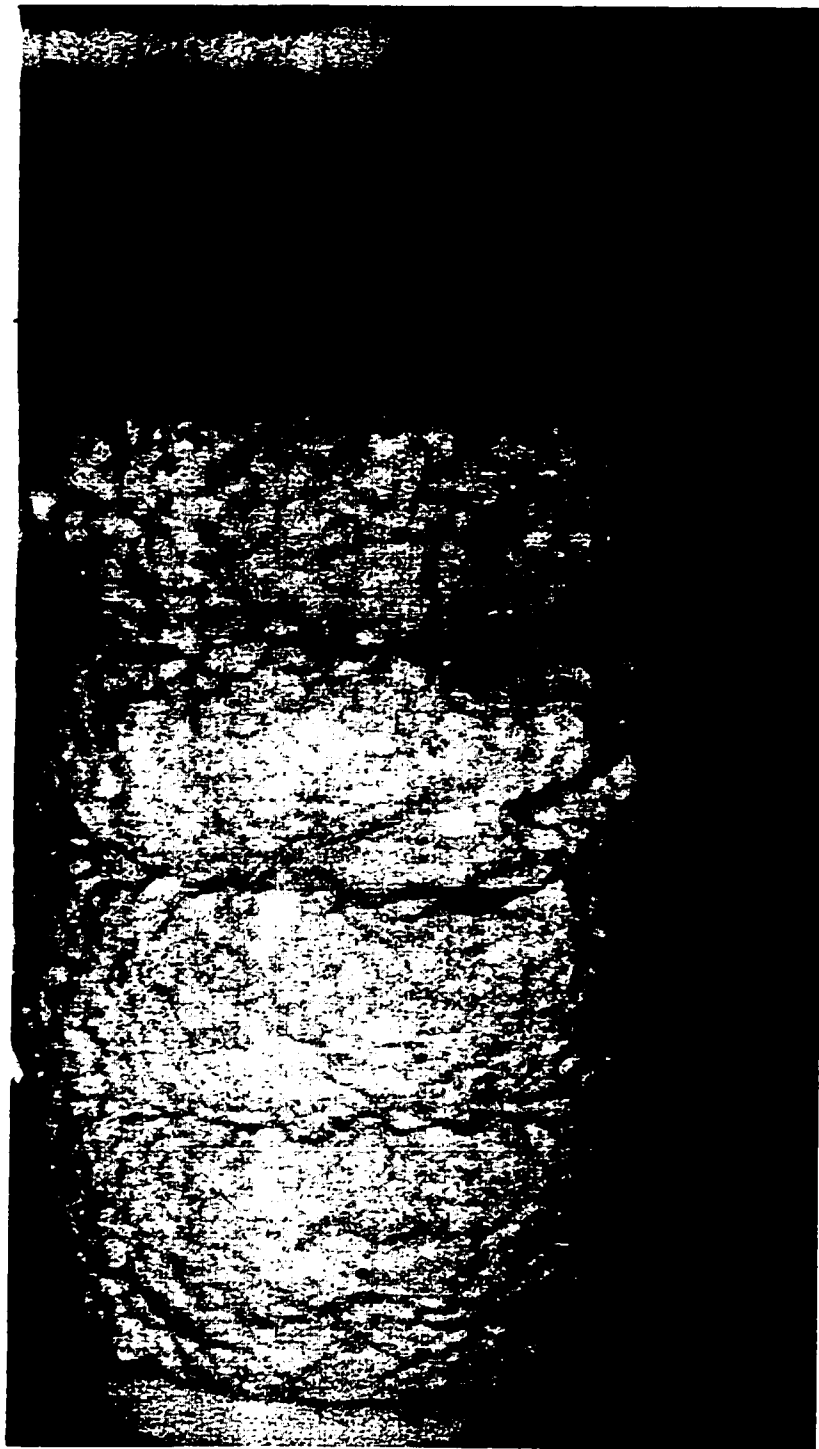**Figure 3.7   Deformed-shape under two-layer reinforcement**

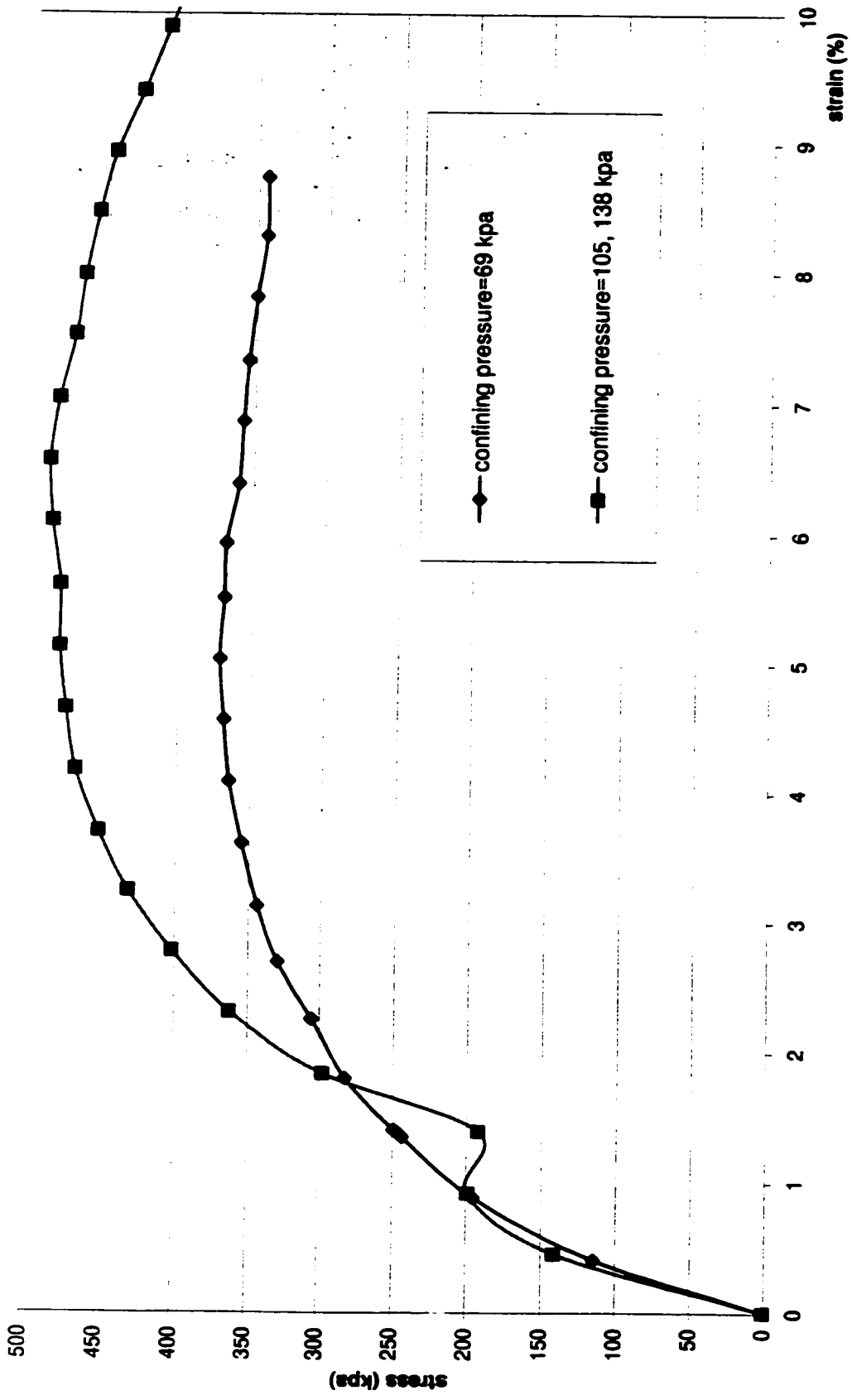**Figure 3.8   Deformed shape under three-layer reinforcement**
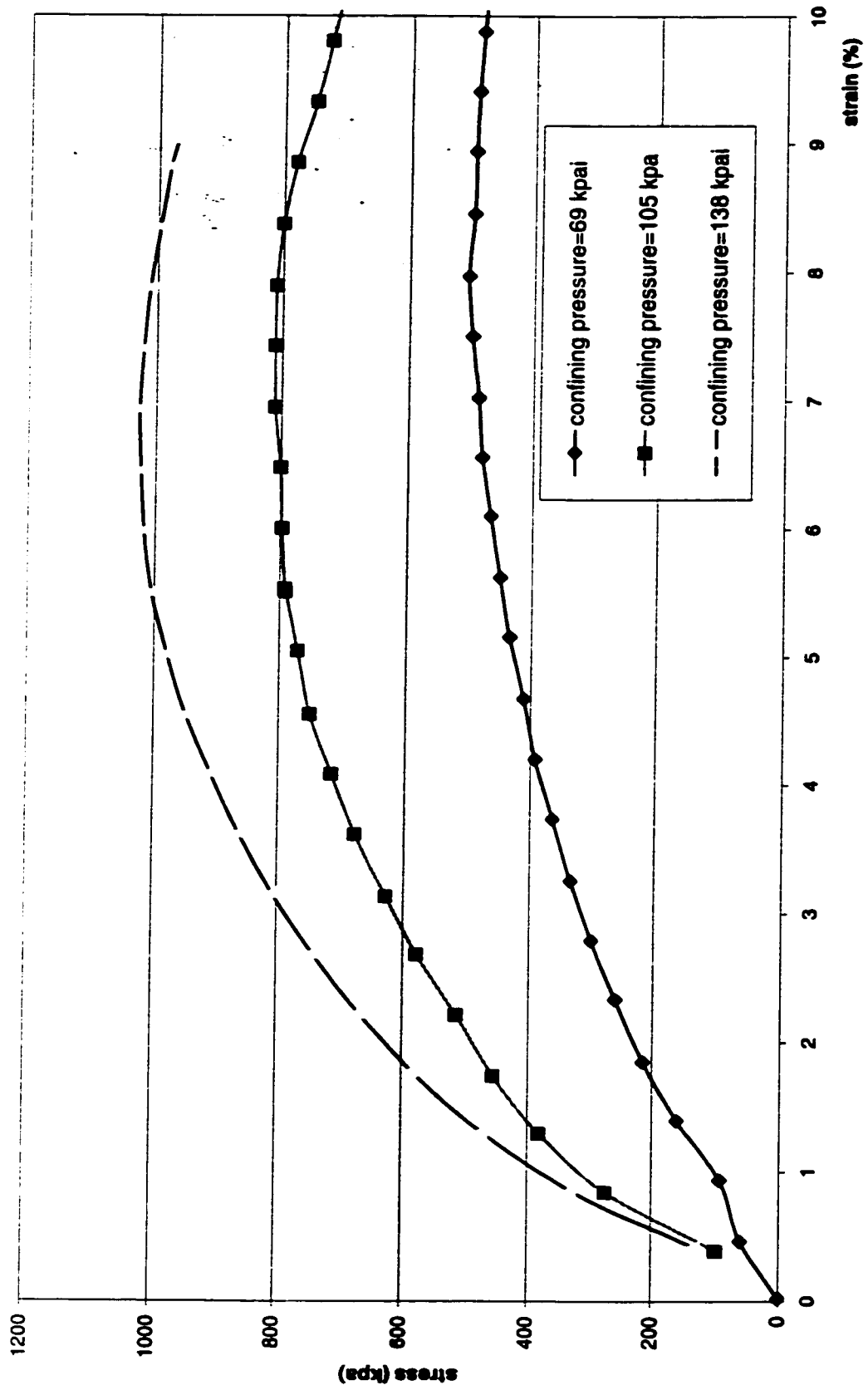
Figure 3.9   Stress-strain (reinforcement=0)
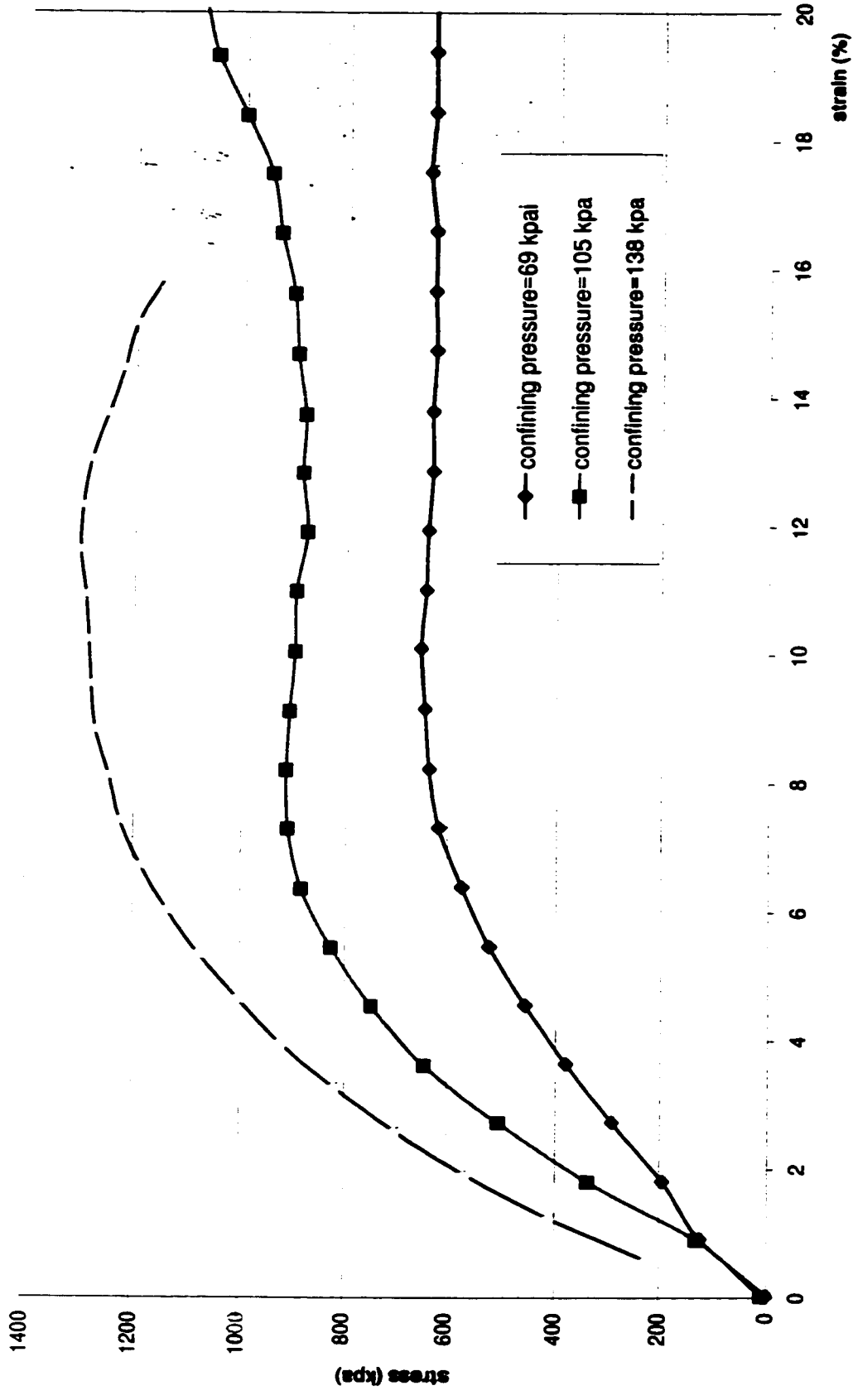
Figure 3.10 Stress-strain (reinforcement = 1 layer)

Legend:
— confining pressure=69 kpai
— confining pressure=105 kpa
-- confining pressure=138 kpai

Y-axis: stress (kpa) — 0, 200, 400, 600, 800, 1000, 1200
X-axis: strain (%) — 0, 1, 2, 3, 4, 5, 6, 7, 8, 9, 10

Figure 3.11 Stress-strain (reinforcment = 2 layers)

Legend:
— confining pressure=69 kpai
— confining pressure=105 kpa
— — confining pressure=138 kpa

Y-axis: stress (kpa) — 0, 200, 400, 600, 800, 1000, 1200, 1400

X-axis: strain (%) — 0, 2, 4, 6, 8, 10, 12, 14, 16, 18, 20
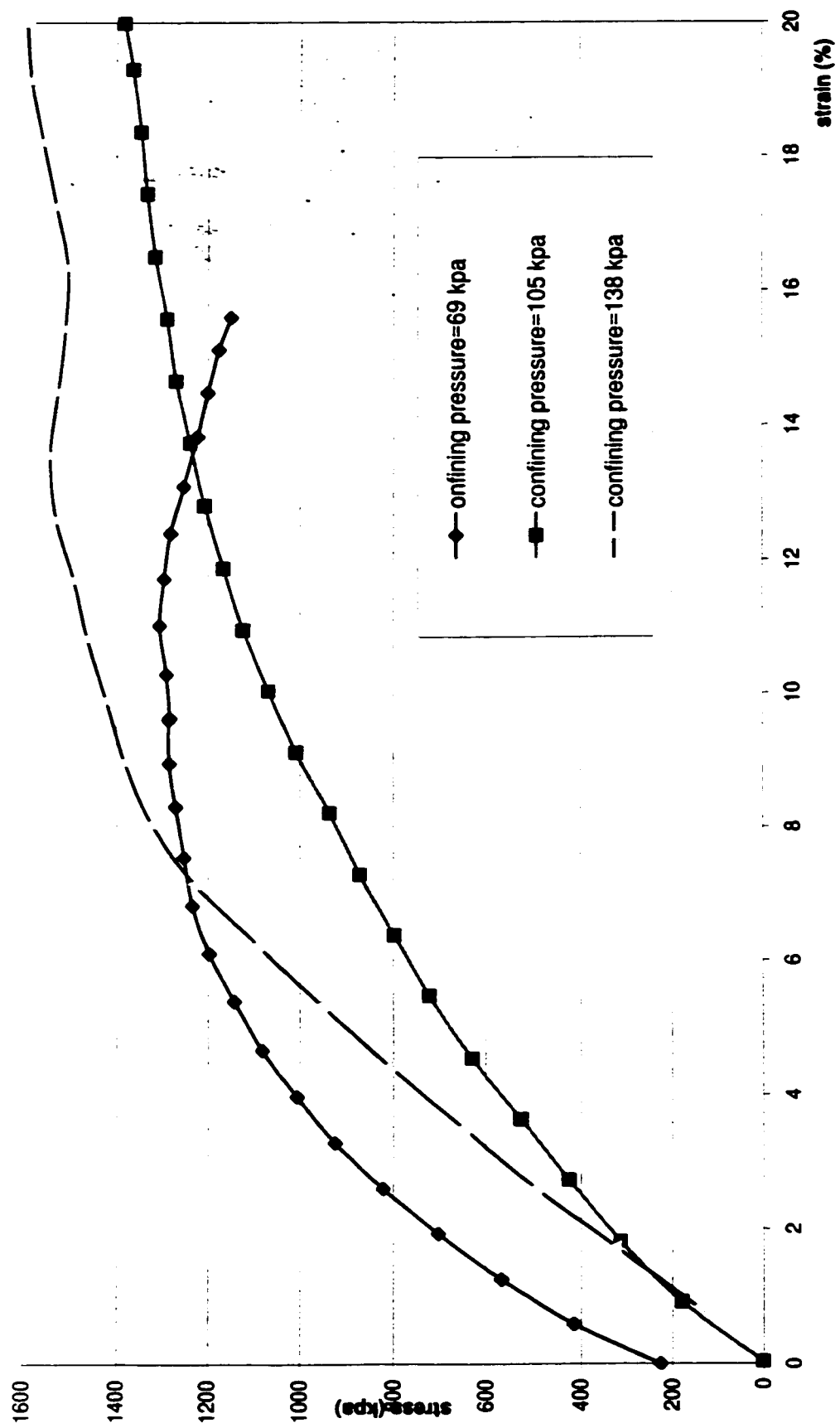
Figure 3.12 Stress-strain (reinforcement = 3 layers)

onfining pressure=69 kpa

confining pressure=105 kpa

confining pressure=138 kpa
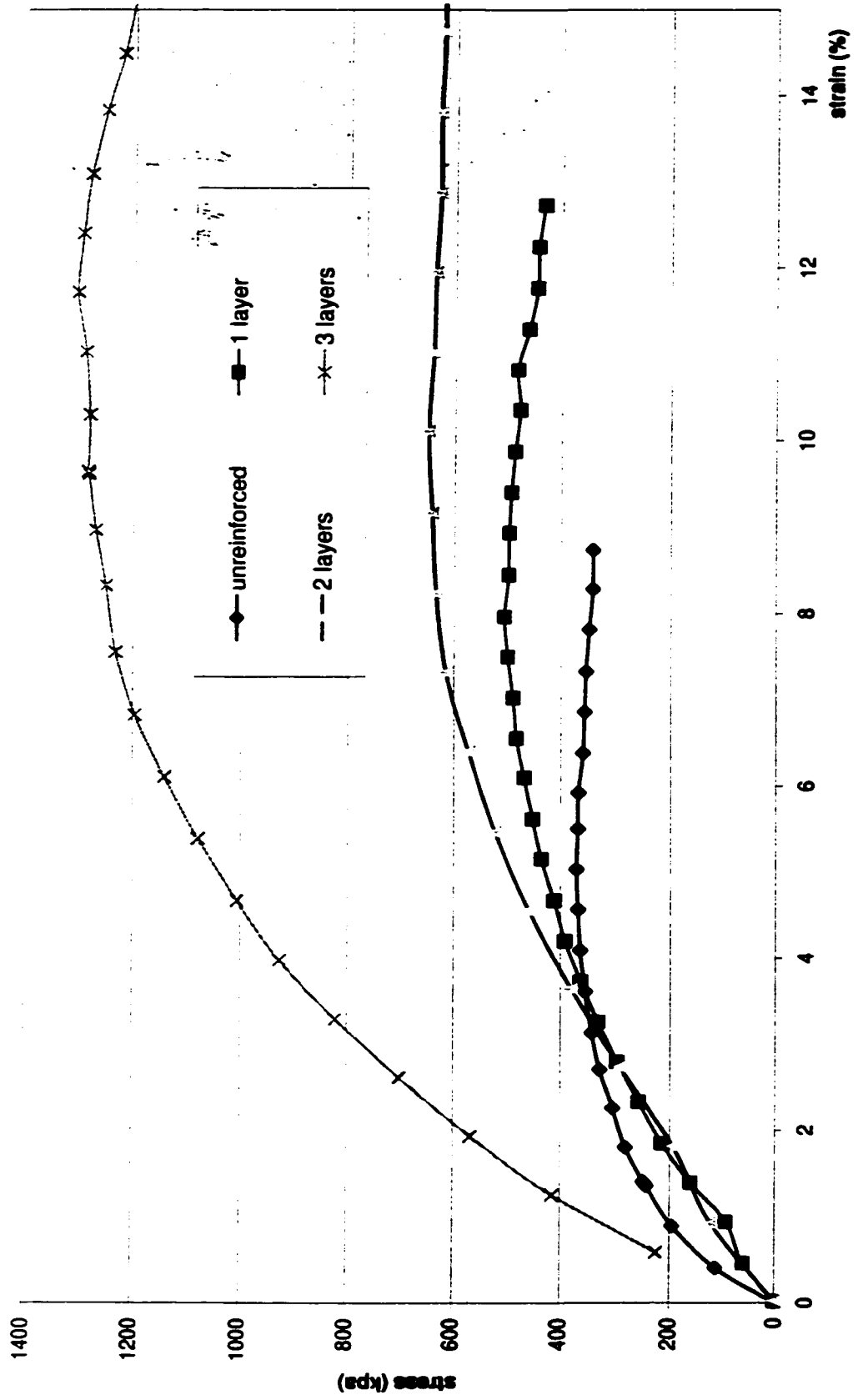
strain (%)

stress(kpa)

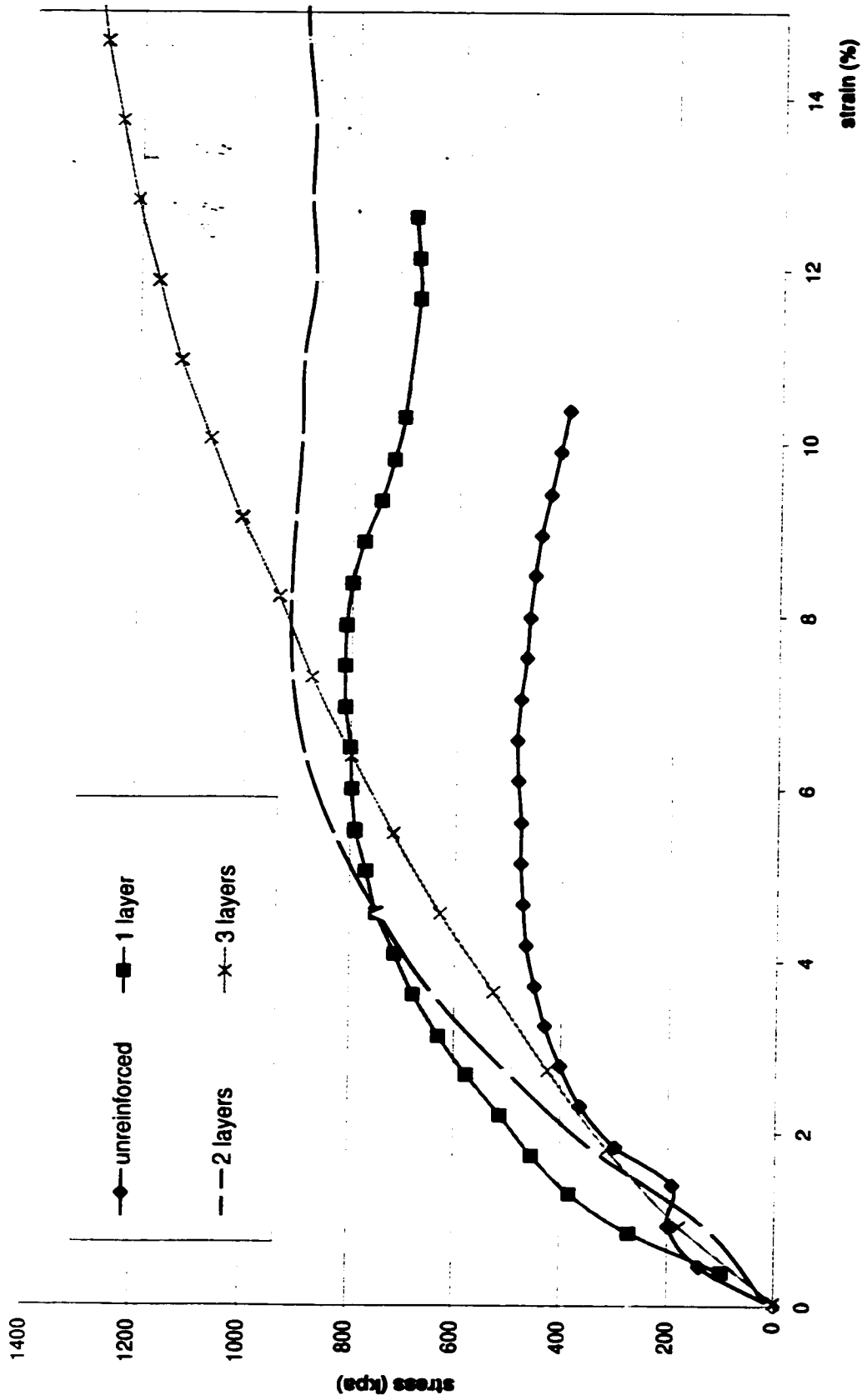Figure 3.13 Stress-strain (confining pressure = 69 kpa)

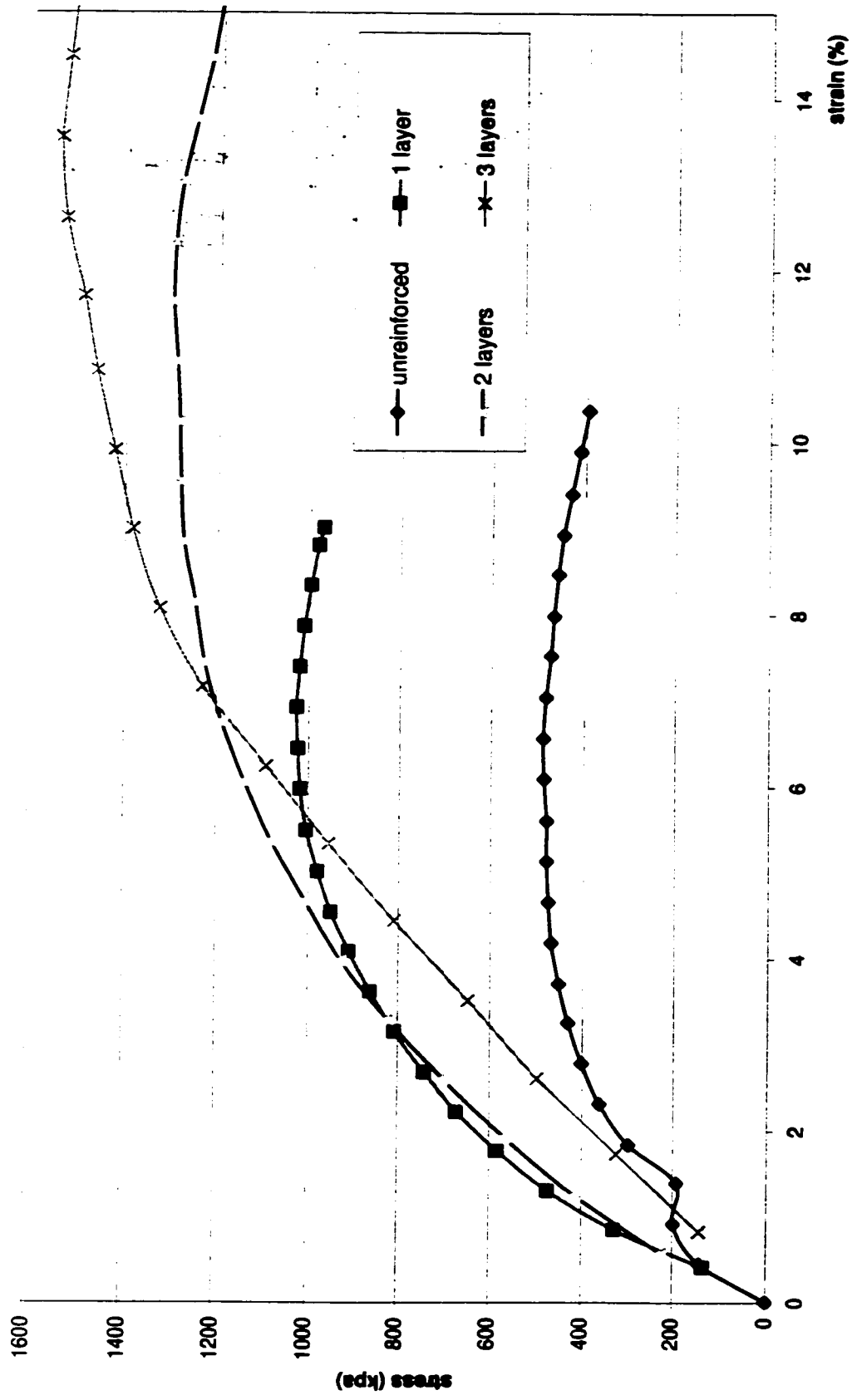Figure 3.14 Stress-strain (confining pressure = 105 kpa)

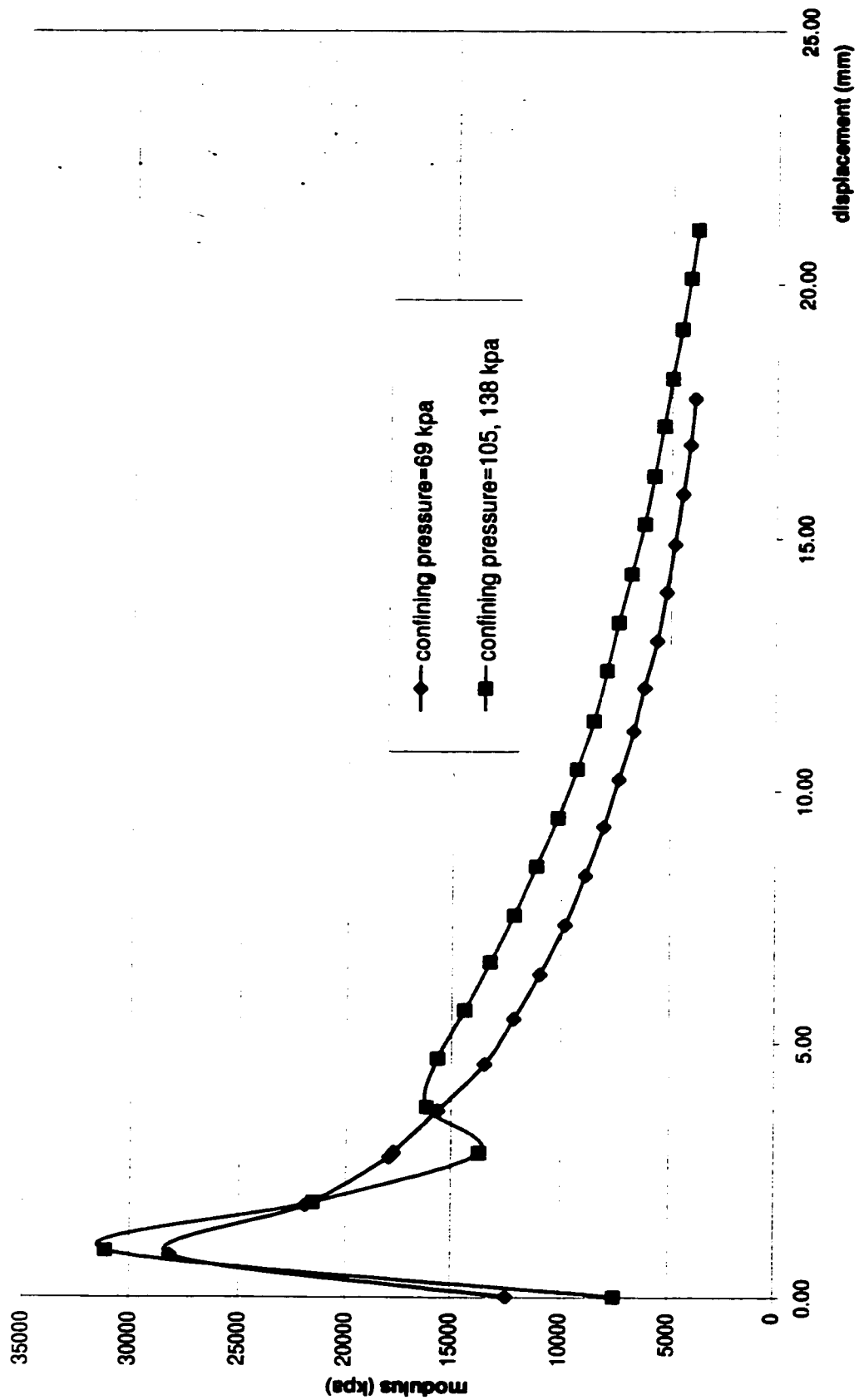Figure 3.15   Stress -strain (confining pressure = 138 kpa)

76

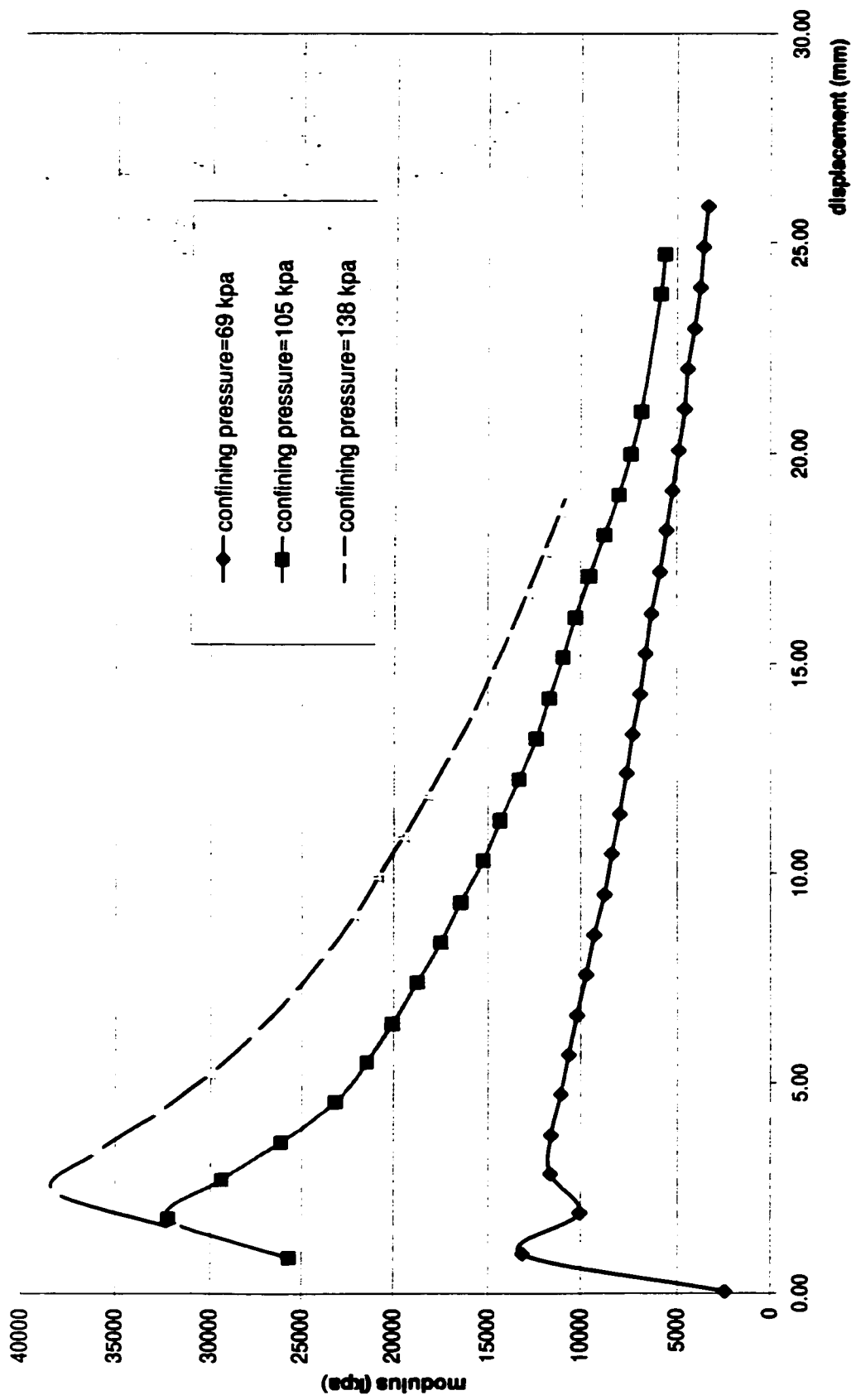**Figure 3.16 Modulus-dispalcement (reinforcement = 0)**

Figure 3.17 Modulus-displacement (reinforcement =1 layer)

confining pressure=69 kpa
confining pressure=105 kpa
confining pressure=138 kpa

displacement (mm)

modulus (kpa)

78
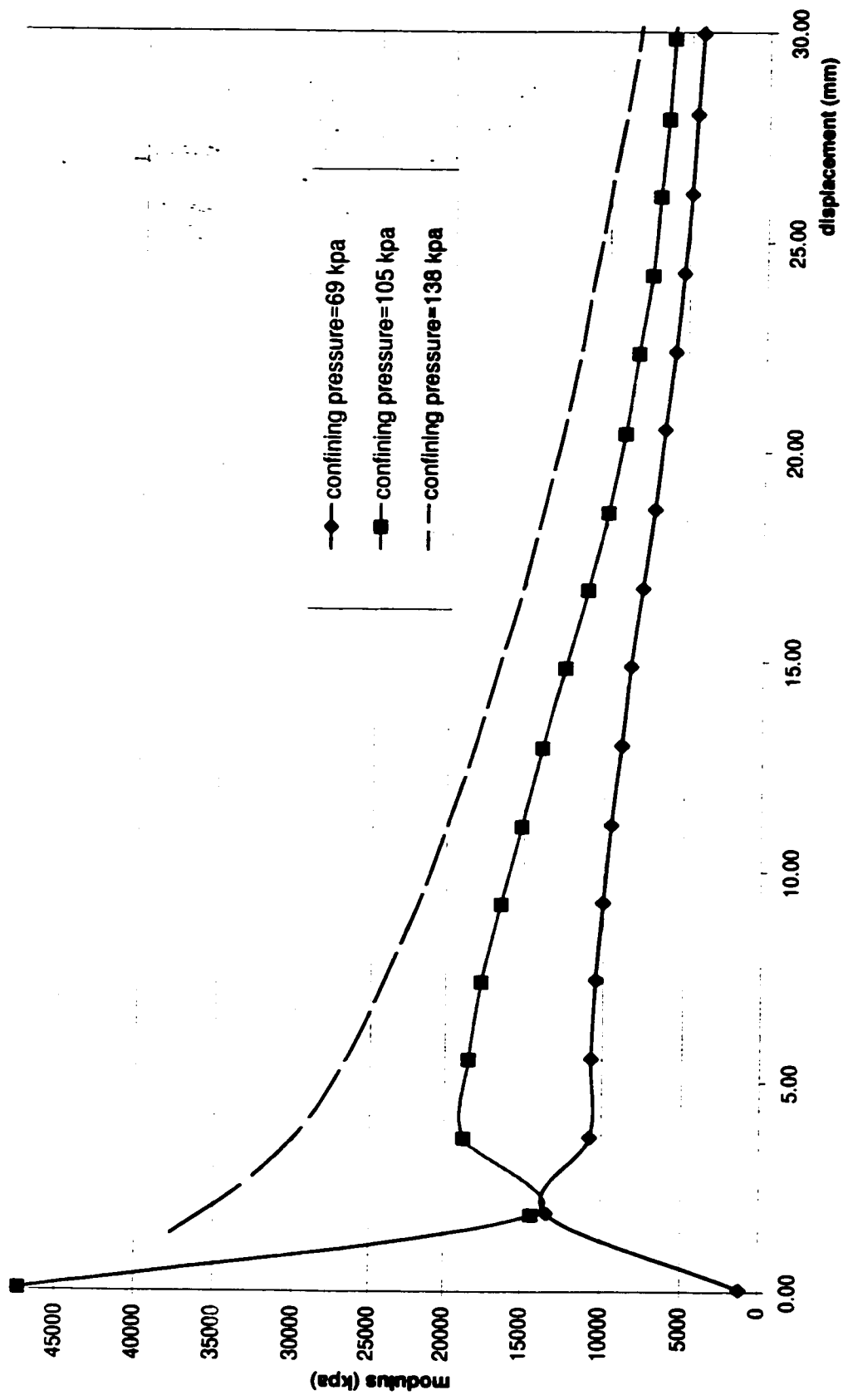
Figure 3.18 Modulus-displacement (reinforcement =2 layers)

legend:
- confining pressure=69 kpa
- confining pressure=105 kpa
- confining pressure=138 kpa

y-axis: modulus (kpa)
x-axis: displacement (mm)
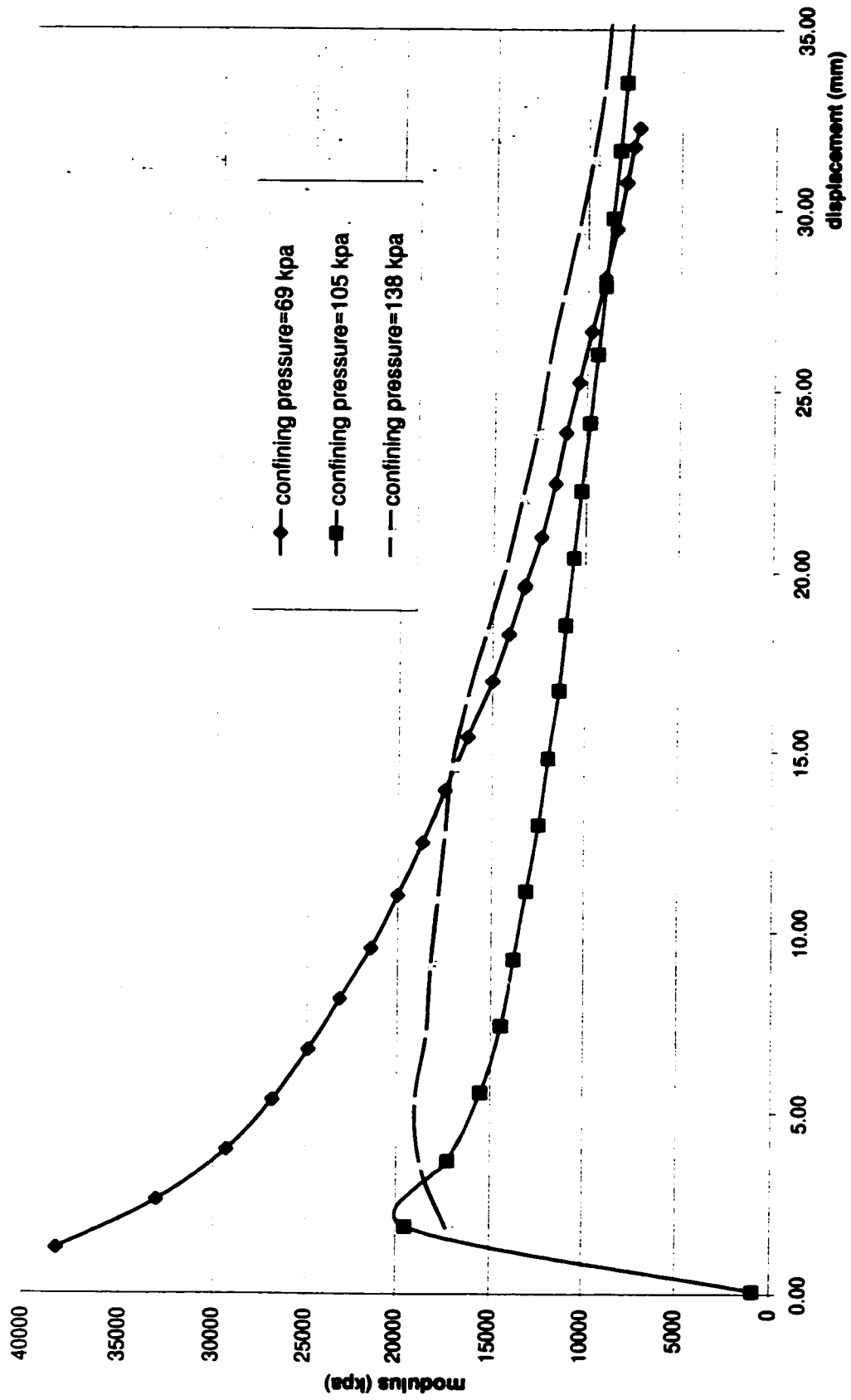
Figure 3.19 Modulus-displacement (reinforcement = 3 layers)

Legend:
- confining pressure=69 kpa
- confining pressure=105 kpa
- confining pressure=138 kpa

Figure 3.20 Modulus-displacement (confining pressure = 69 kpa)
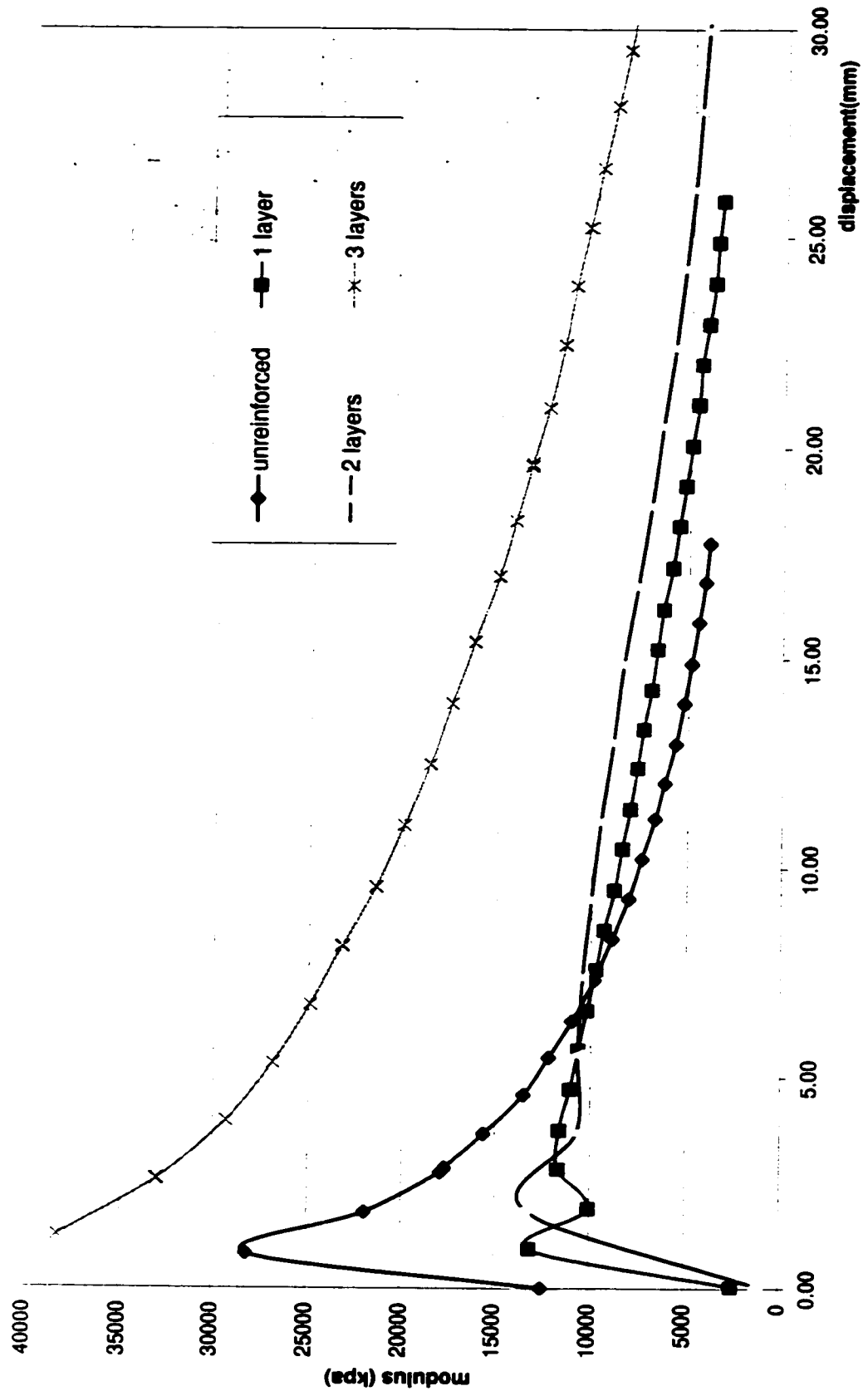
81
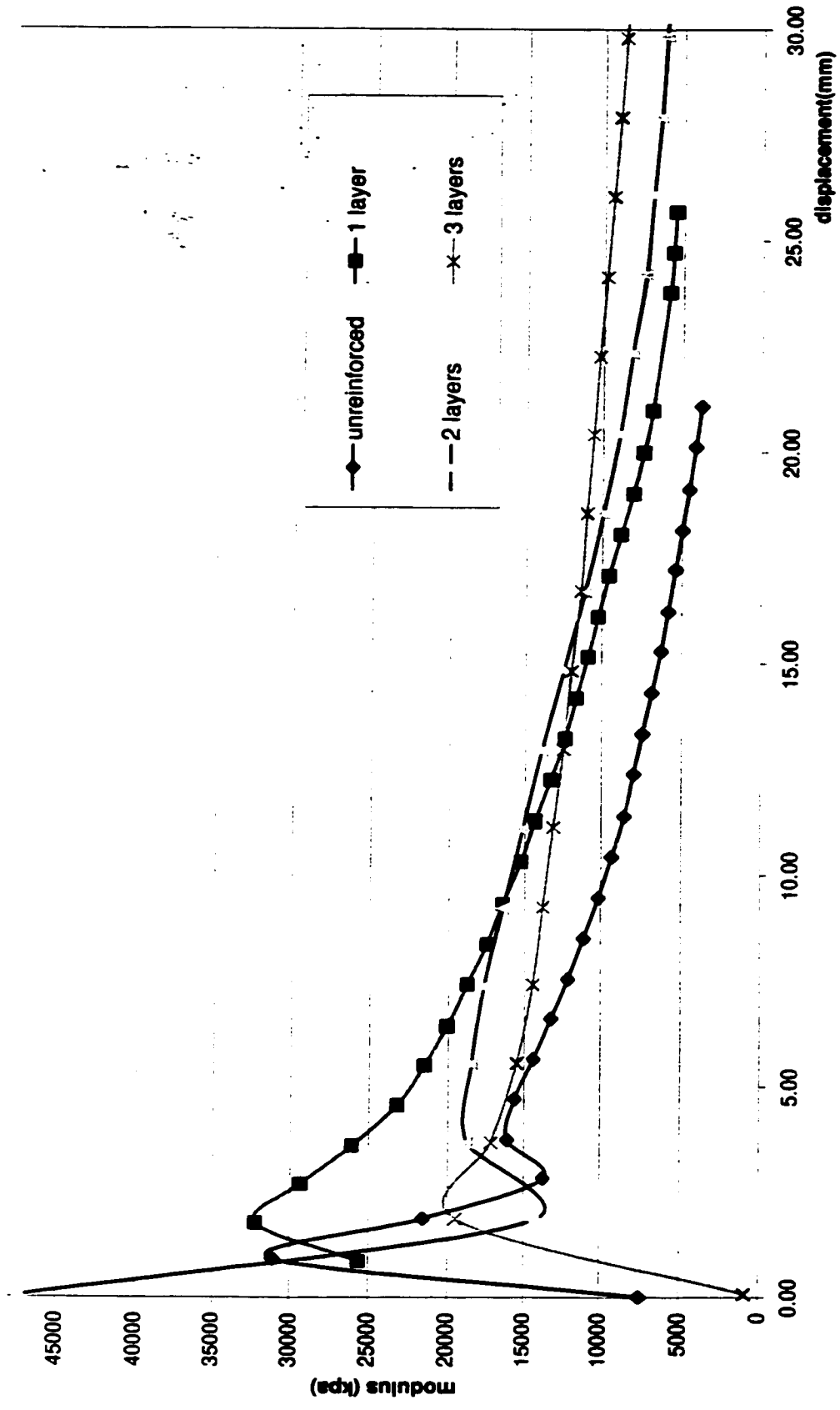
Figure 3.21 Modulus-displacement (confining pressure = 105 kpa)
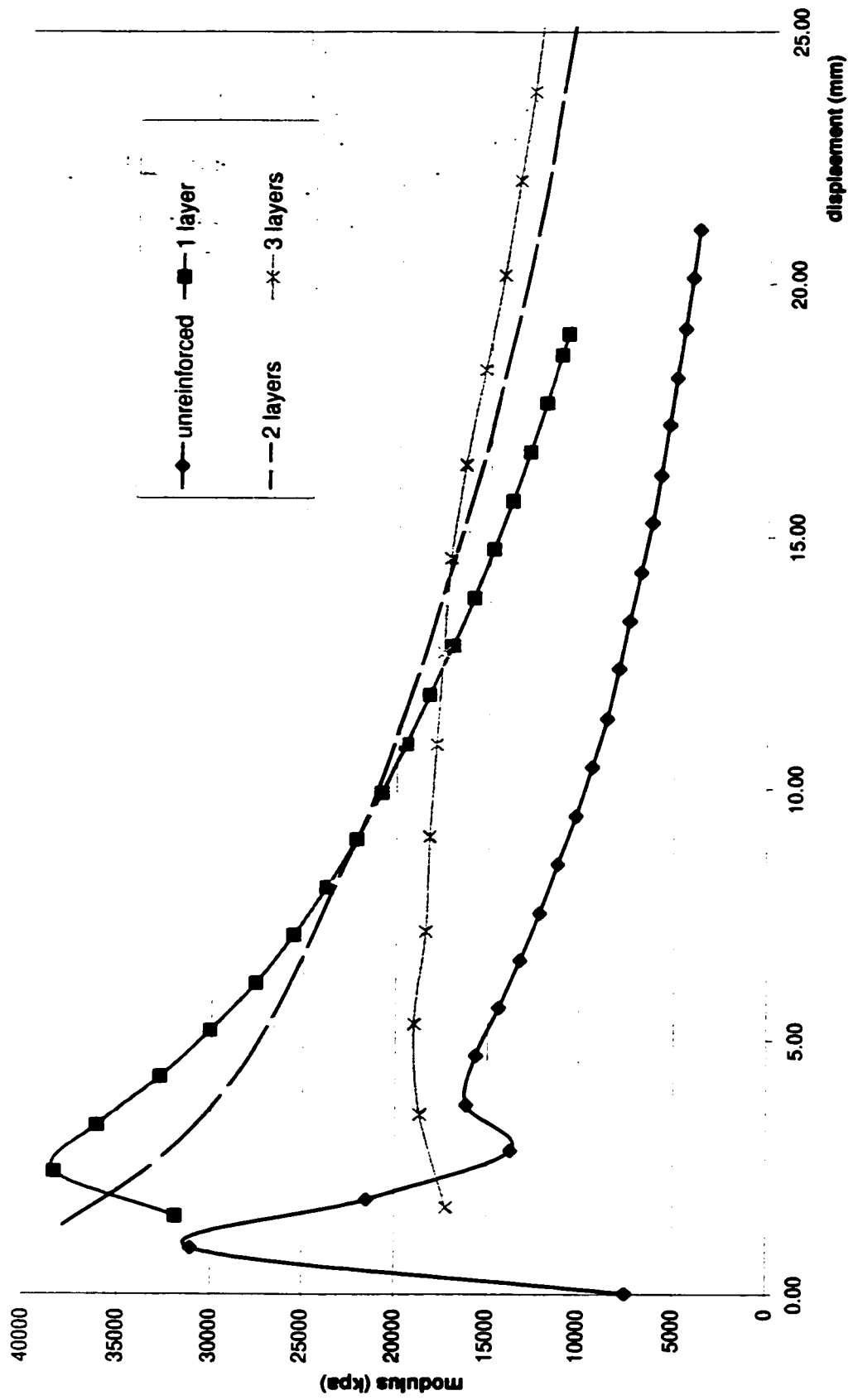
Figure 3.22 Modulus-displacement (confining pressure = 138 kpa)

83
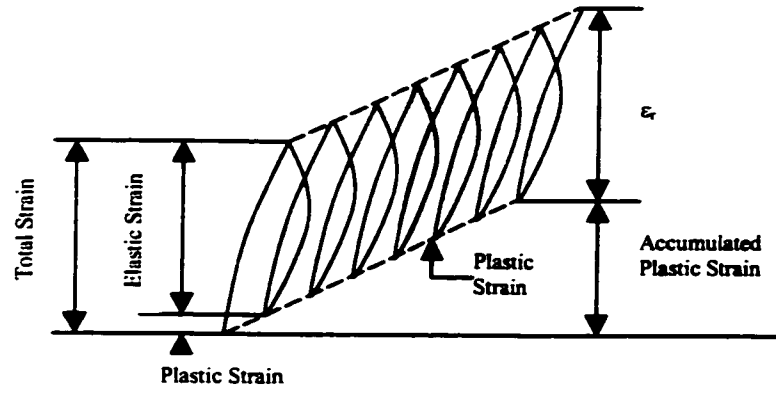
Figure 4.1   Strains under repeated loads
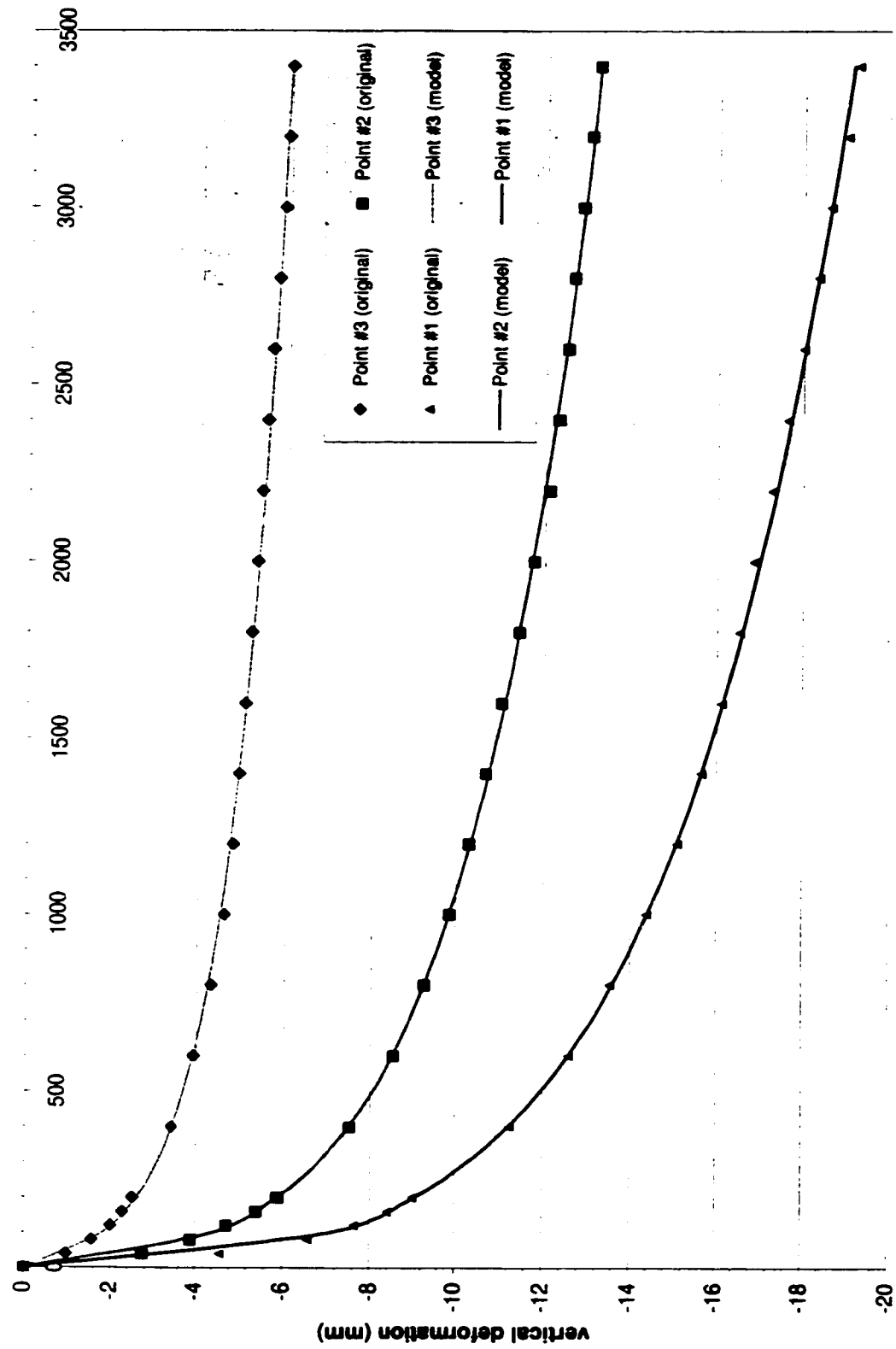
Figure 4.2 Permanent deformation under unreinforced condition

85
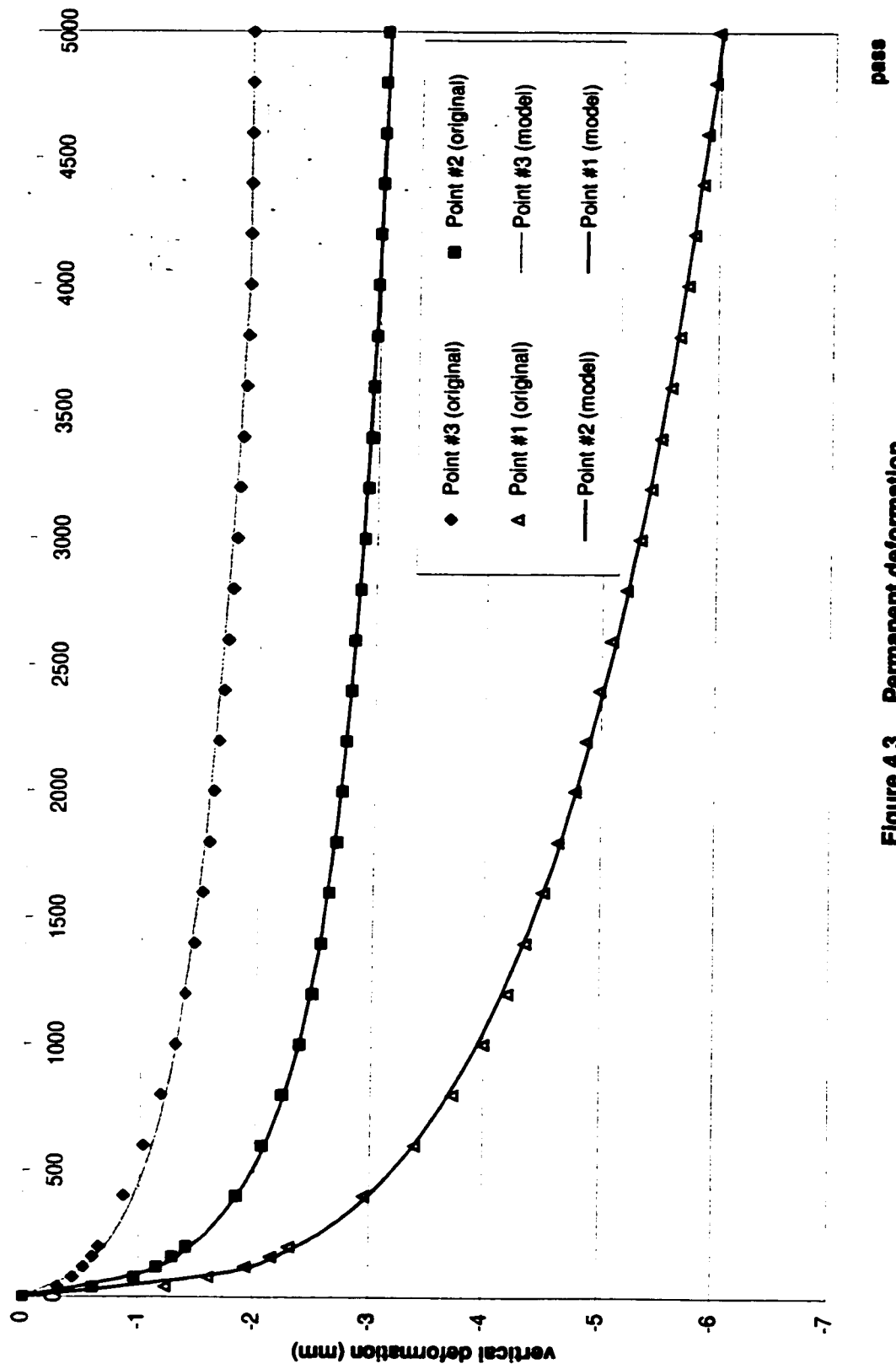
Figure 4.3 Permanent deformation
when geogrid is in the middle of base layer
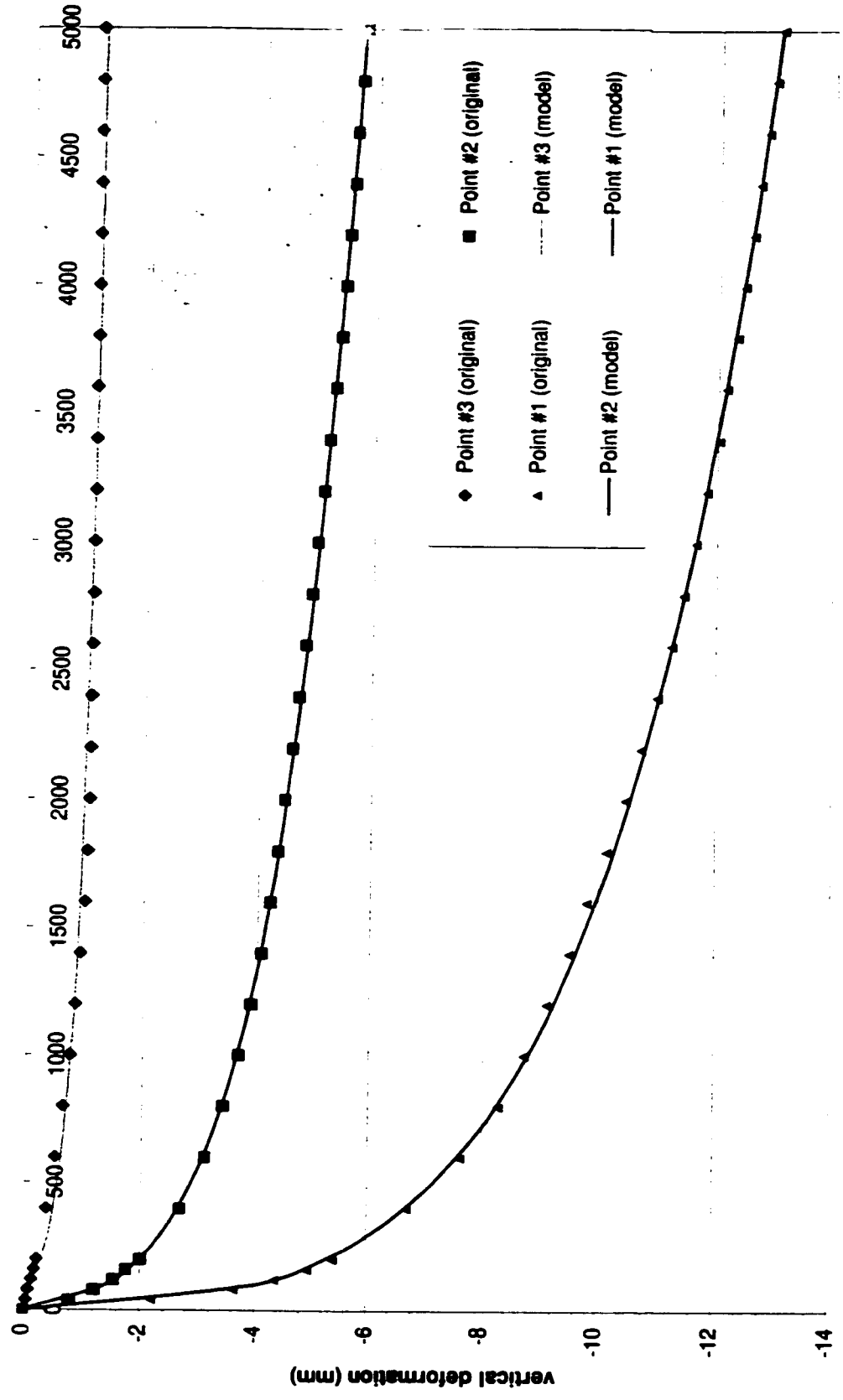
Figure 4.4   Permanent deformation
when geogrid is at base-subgrade interface
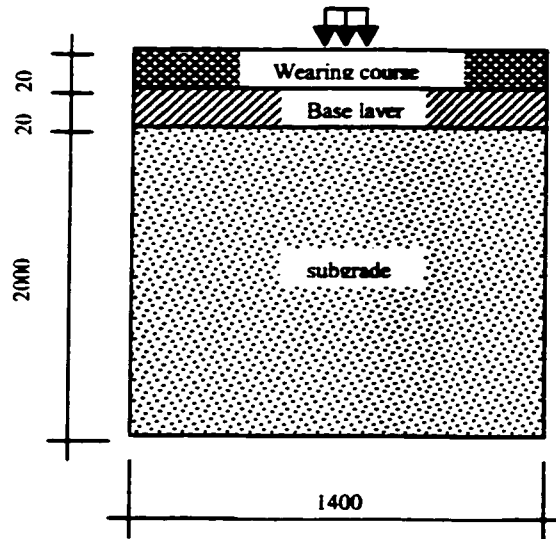
Figure 5.1   Geometry of the pavement tested in the lab (mm)
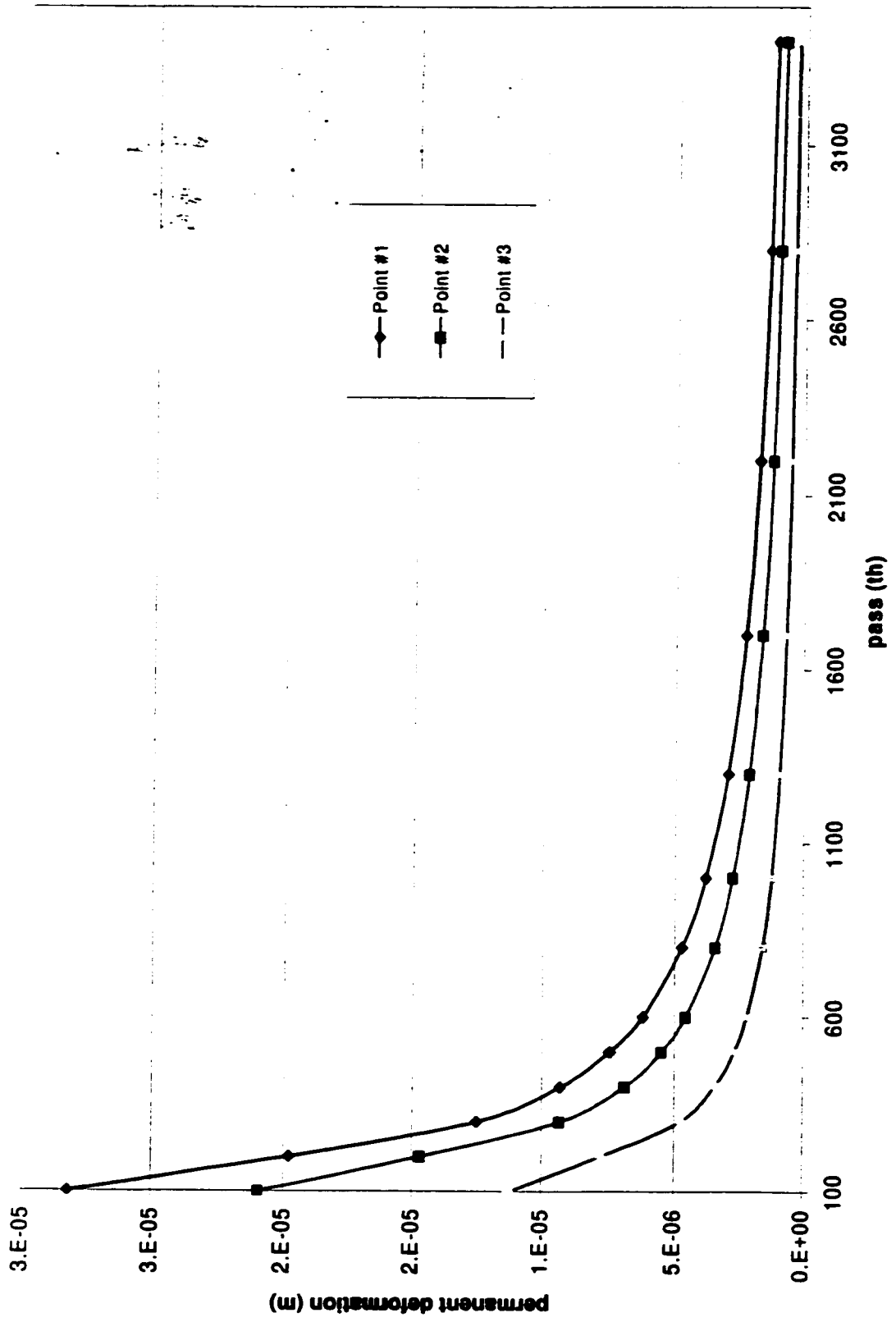
Figure 5.2 Permanent deformation generated by each pass
under unreinforced condition

89
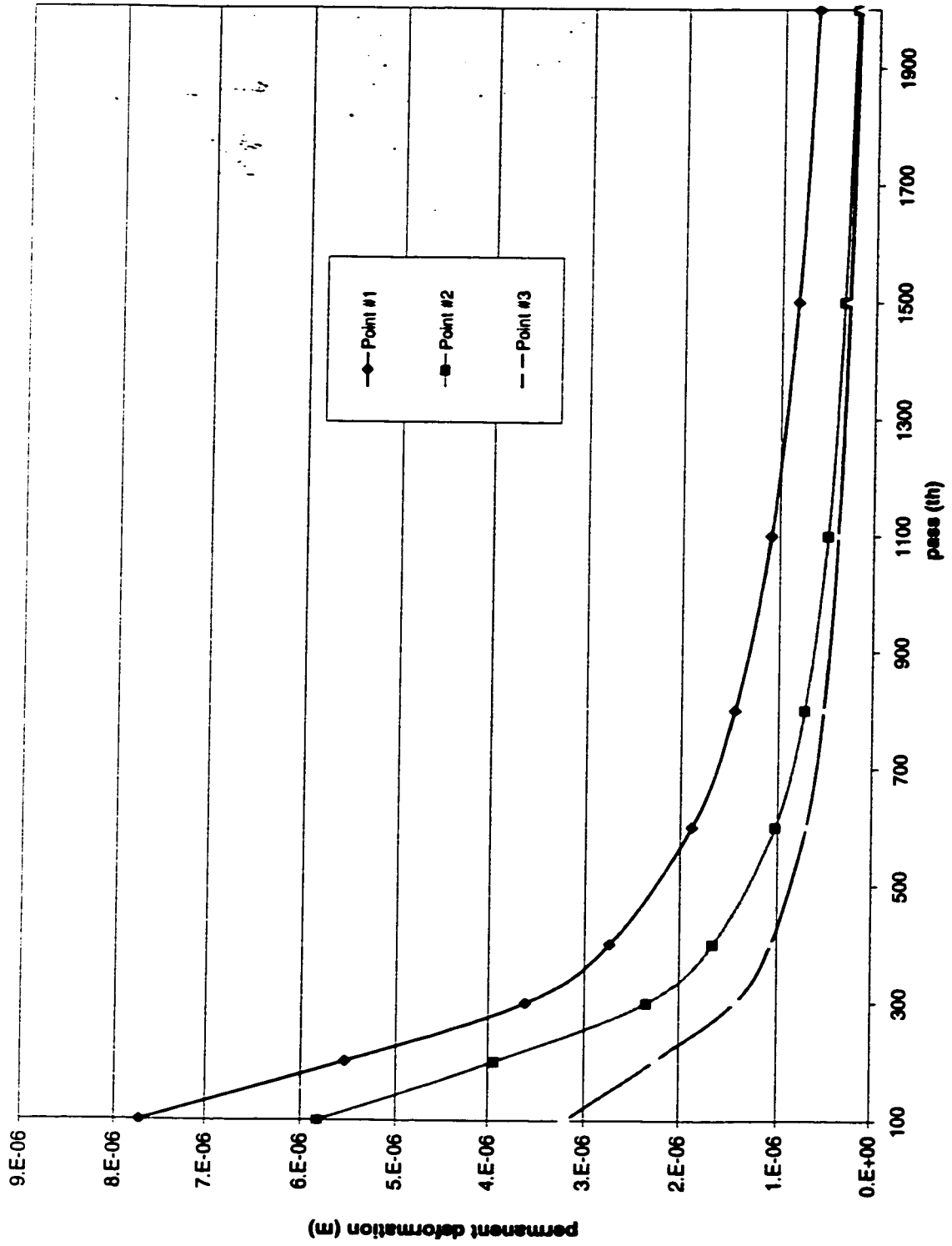
Figure 5.3 Permanent deformation generated by each pass when geogrid is in the middle of base layer

90
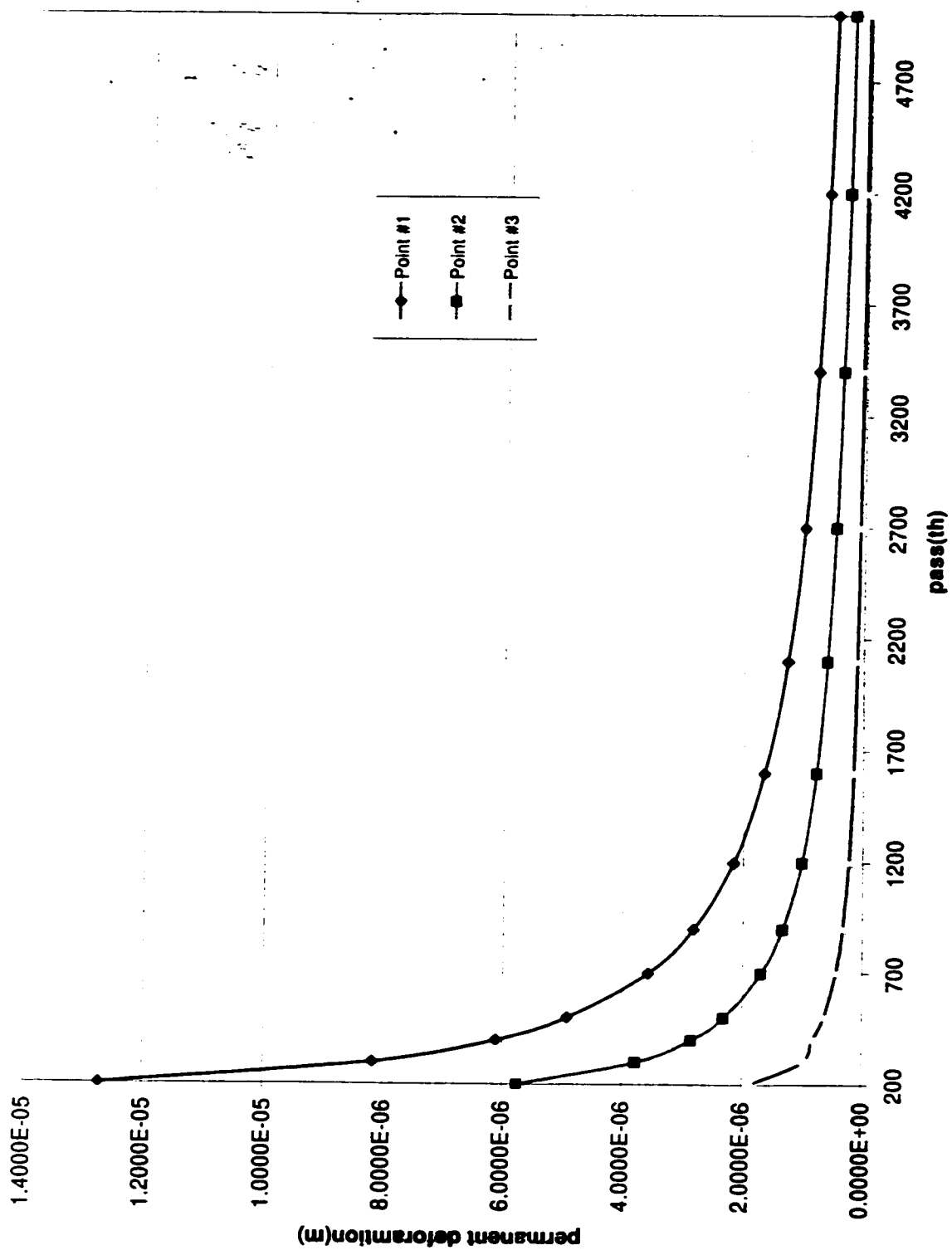
Figure 5.4 Permanent deformation generated by each pass when geogrid is at the base-subgrade interface

91
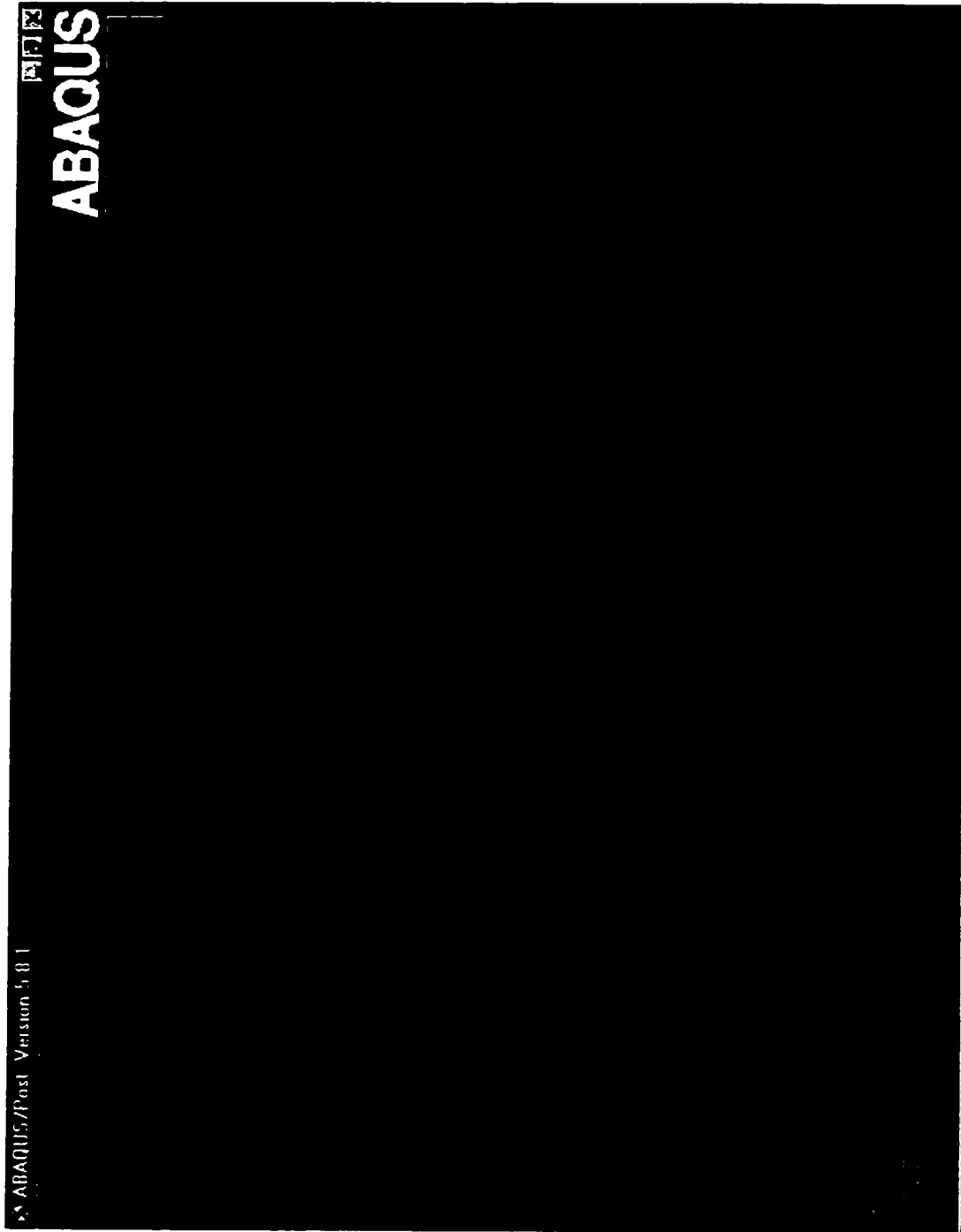
Figure 5.5   Geometry of pavement (model set-up)
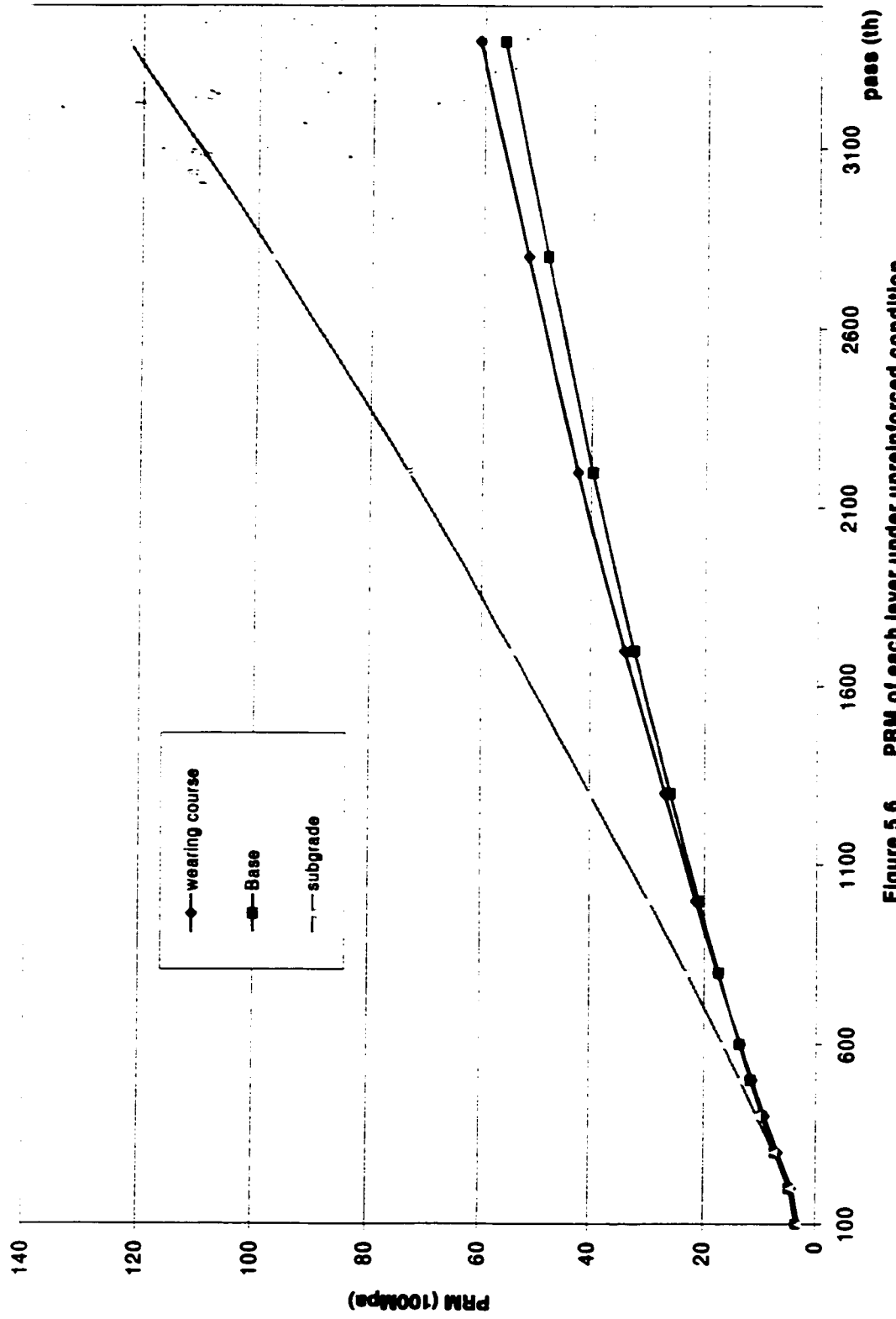
Figure 5.6   PRM of each layer under unreinforced condition

93
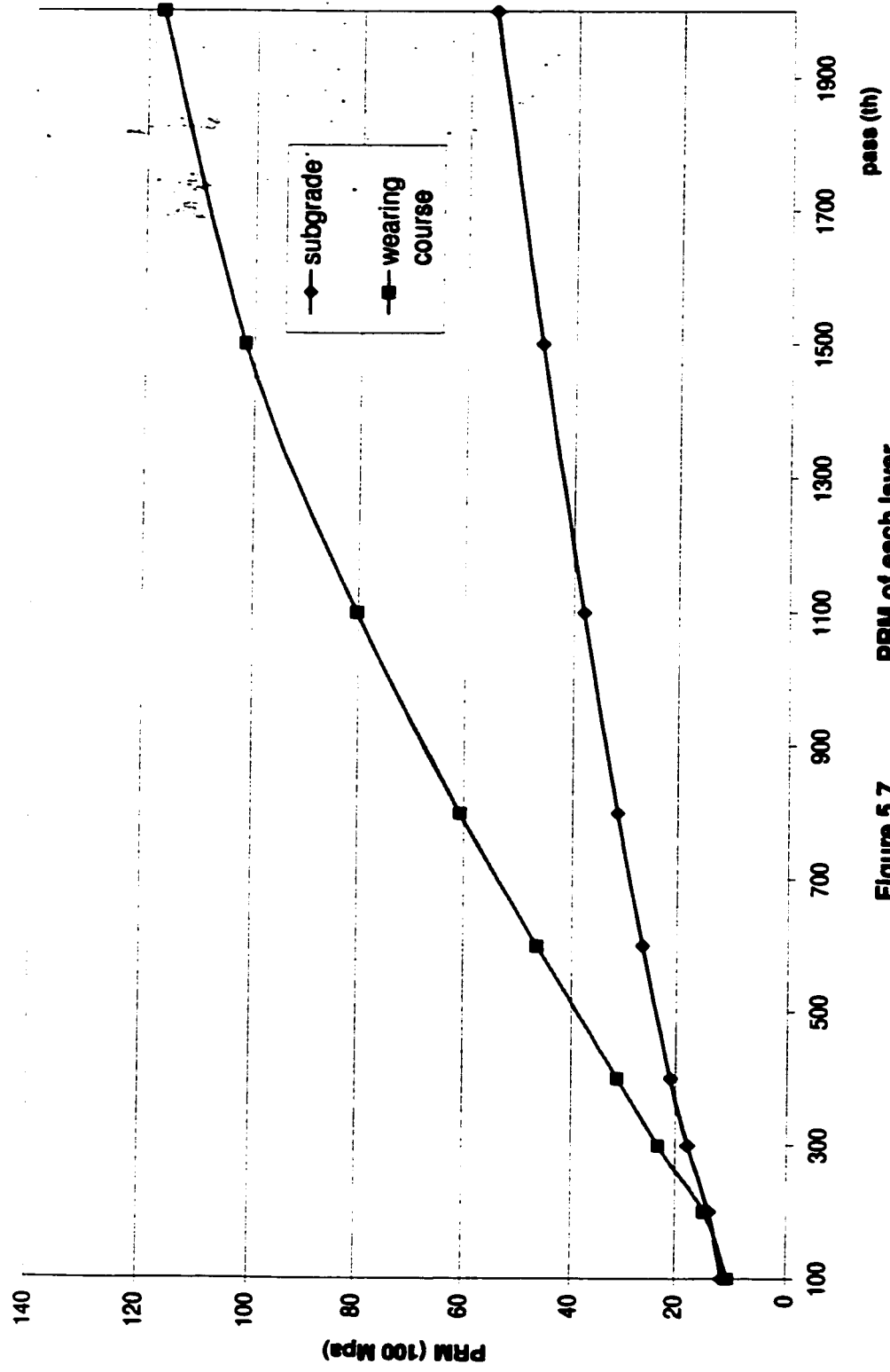
Figure 5.7   PRM of each layer
when geogrid is in the middle of base layer
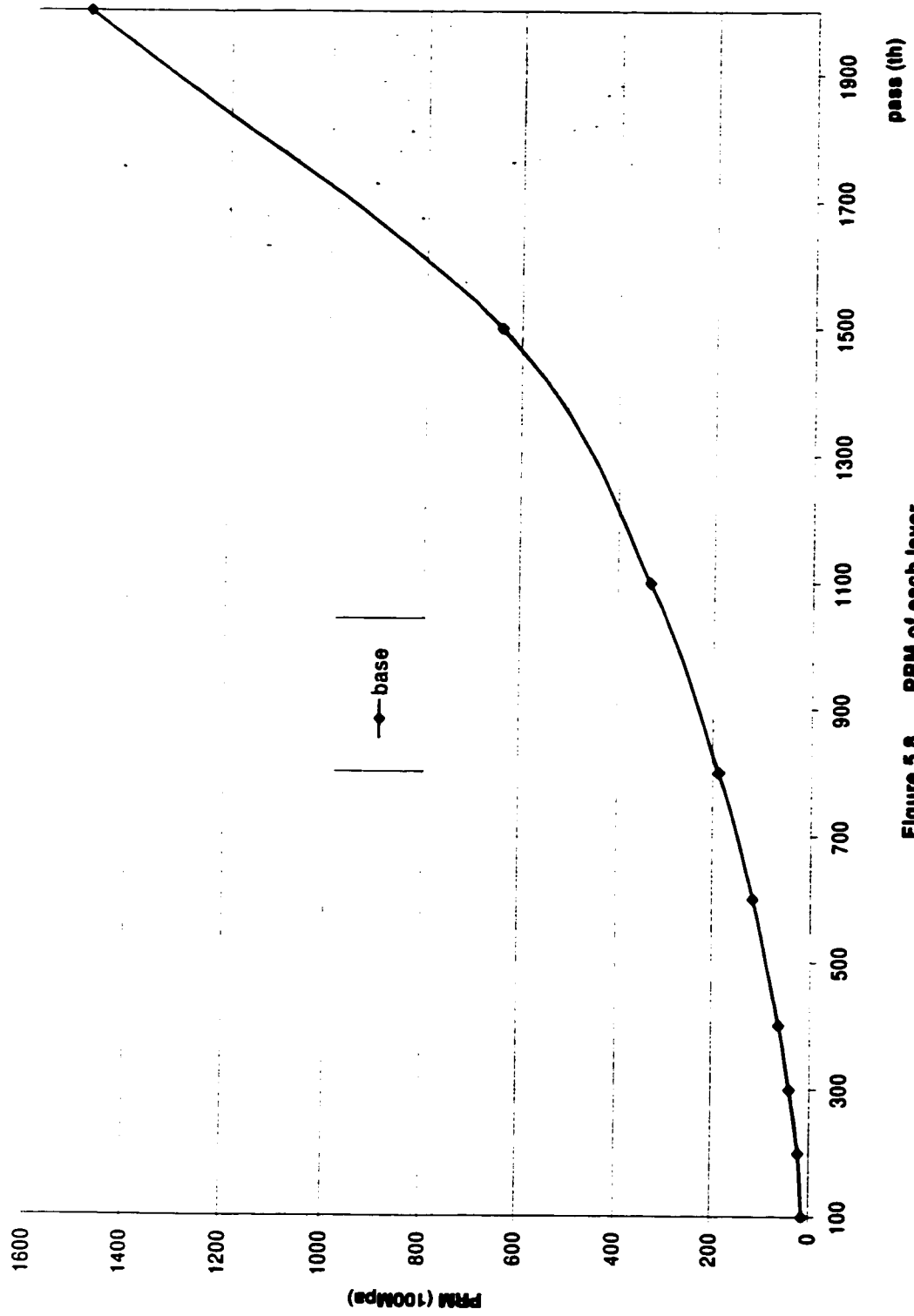
Figure 5.8   PRM of each layer
when geogrid is in the middle of base layer
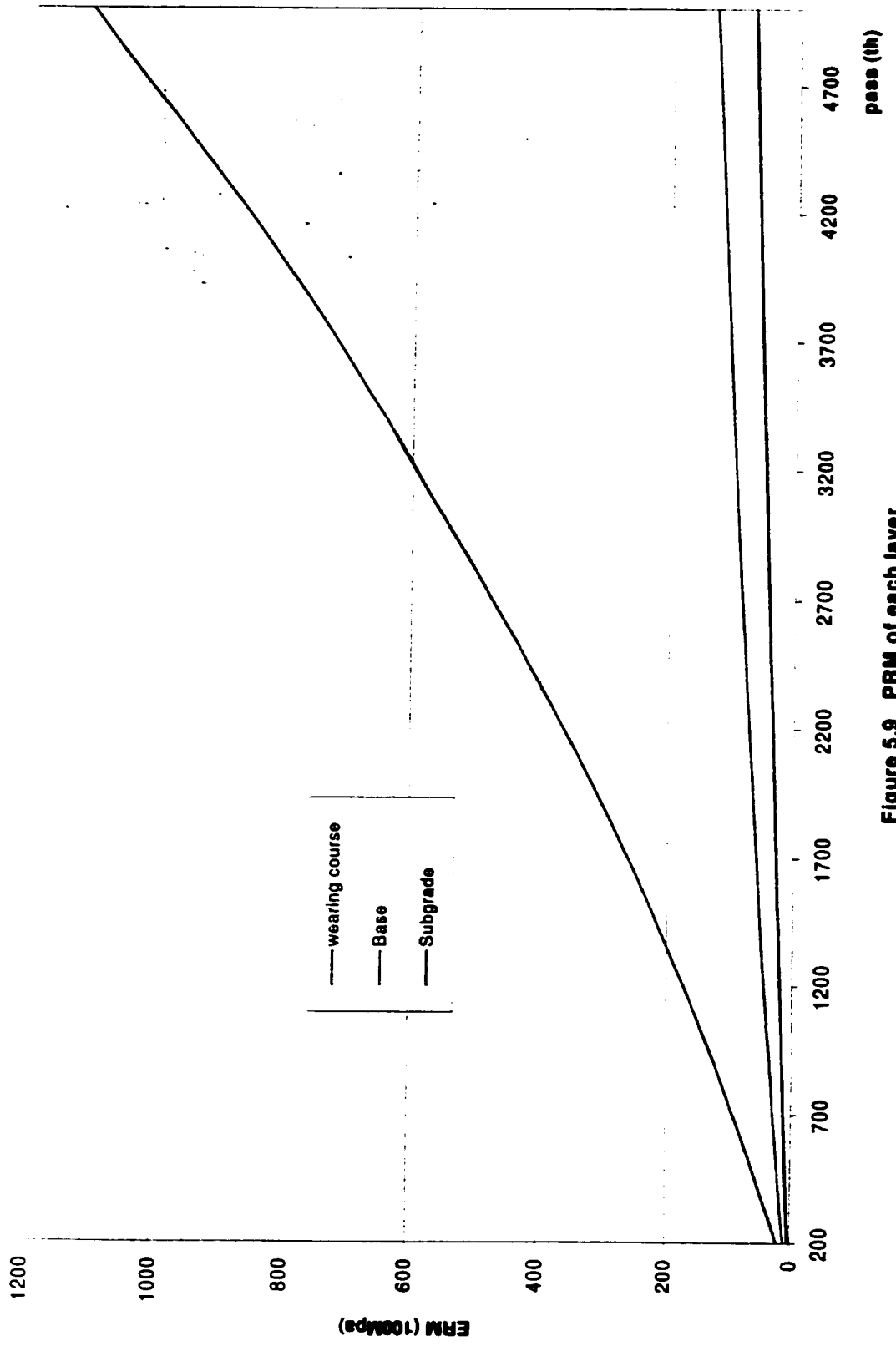
Figure 5.9 PRM of each layer
when geogrid is at the base-subgrade interface
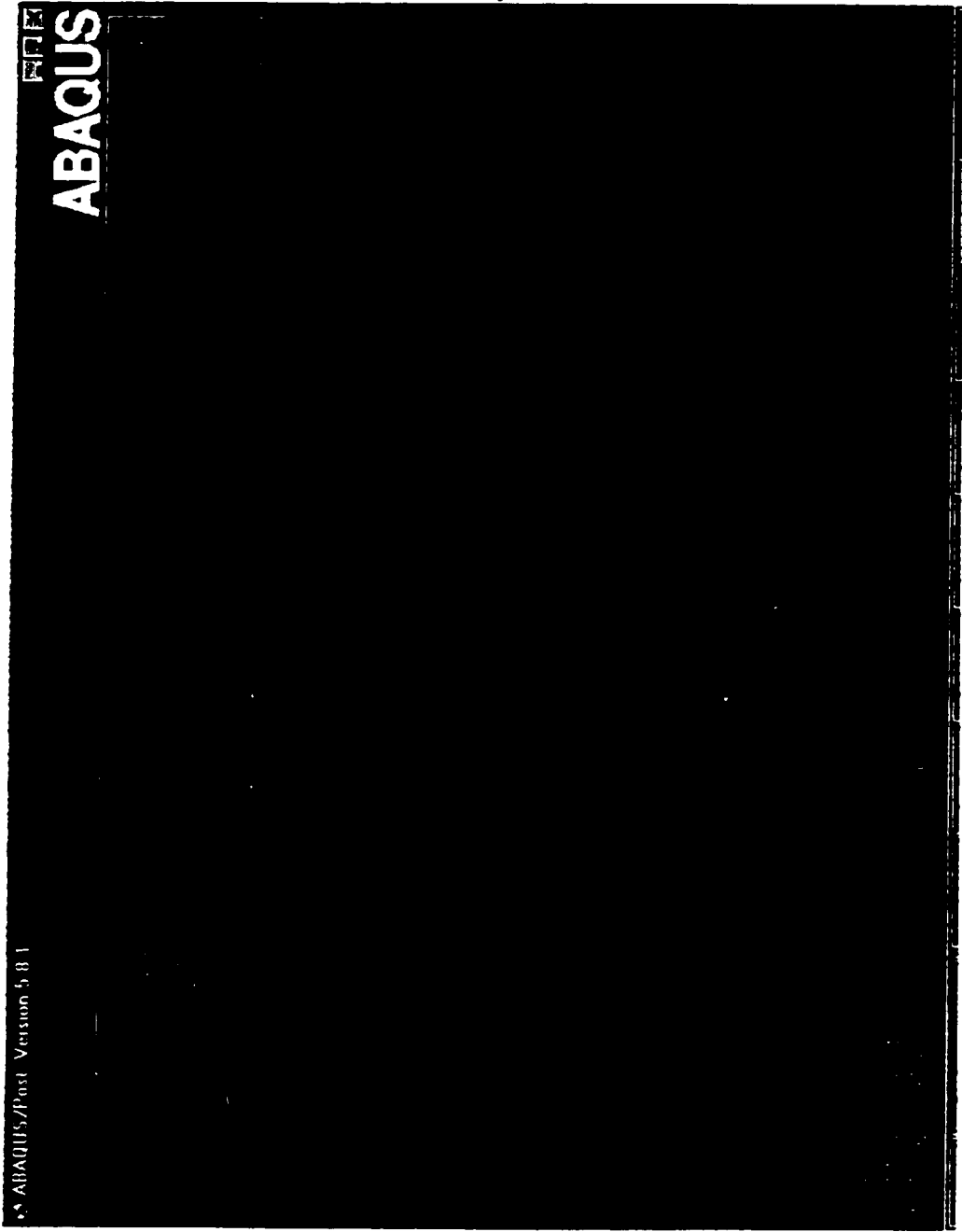
Figure 5.10 Contour of stress in the radial direction at 1st pass
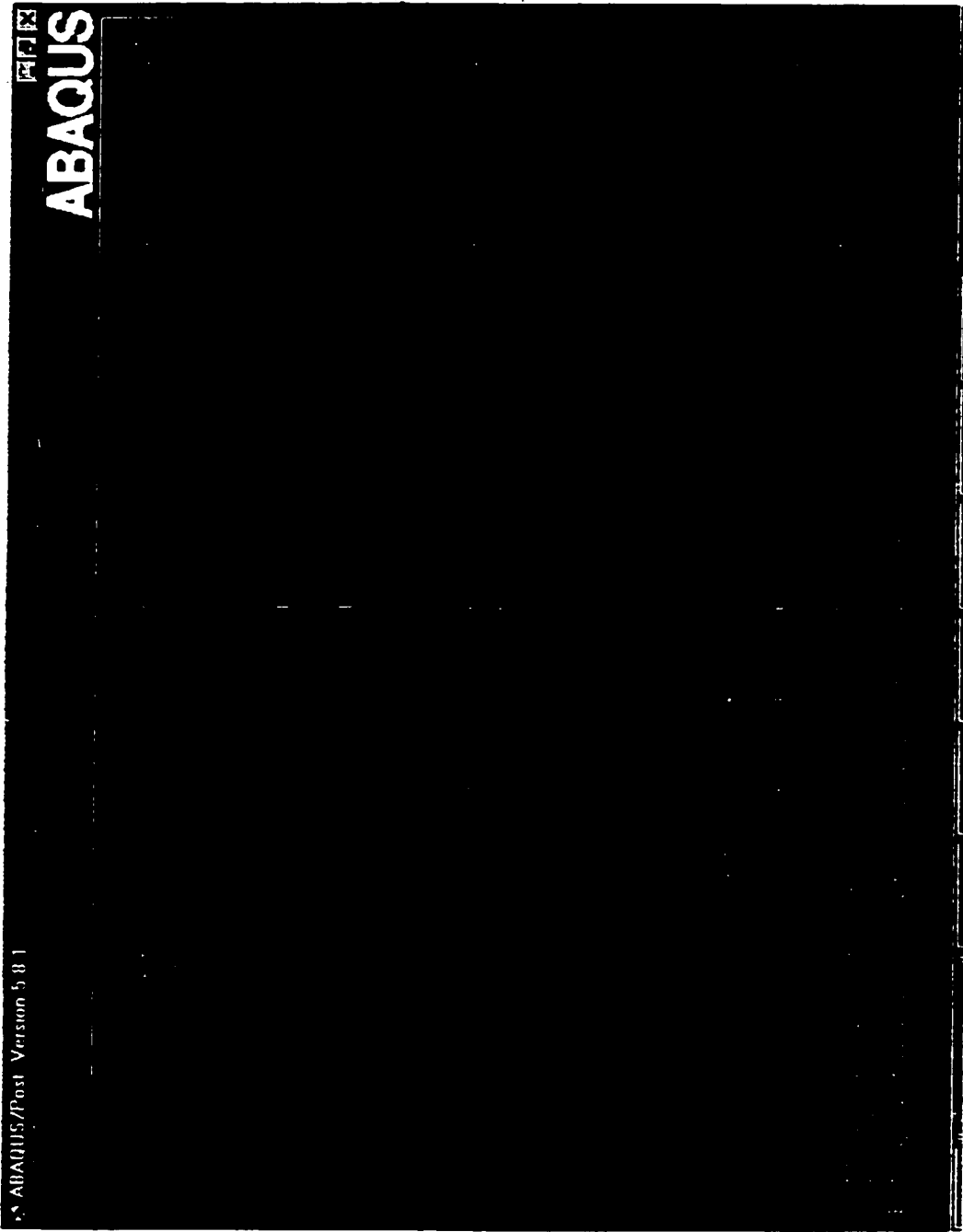
Figure 5.11   Contour of stress in the axial direction at 1st pass
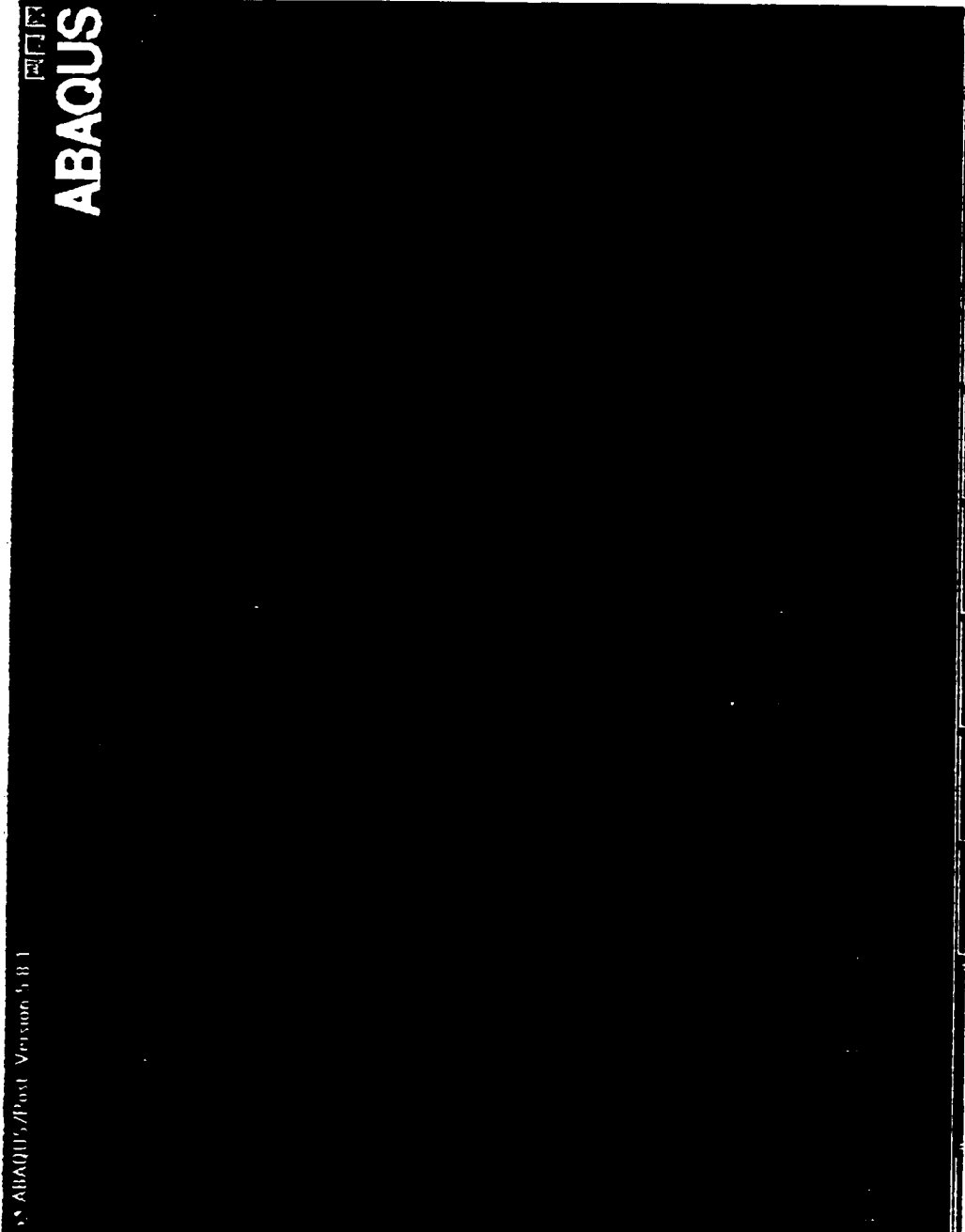
Figure 5.12   Contour of Von Mises stress at 1st pass
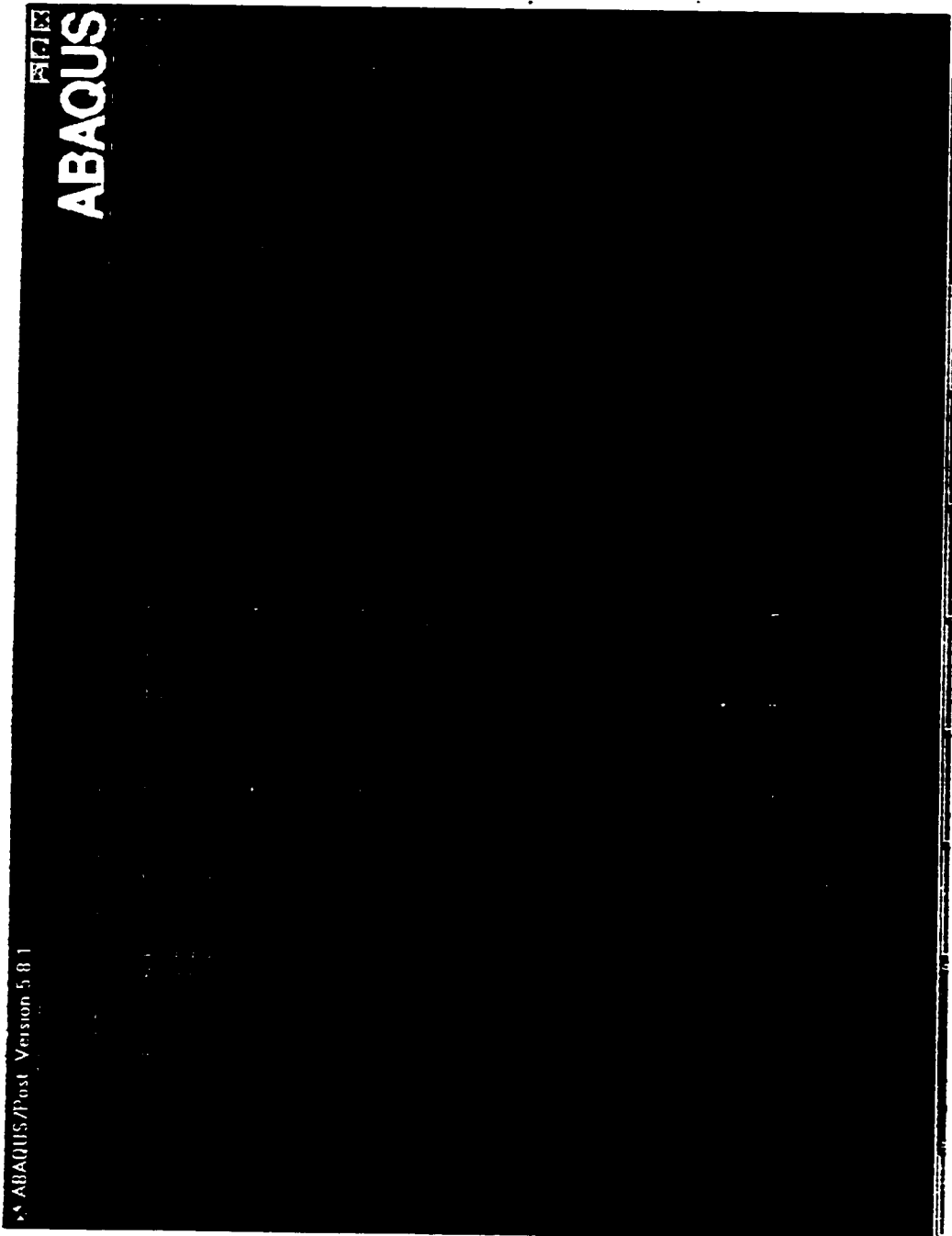
Figure 5.13 Contour of direct strain in the radial direction at 1st pass
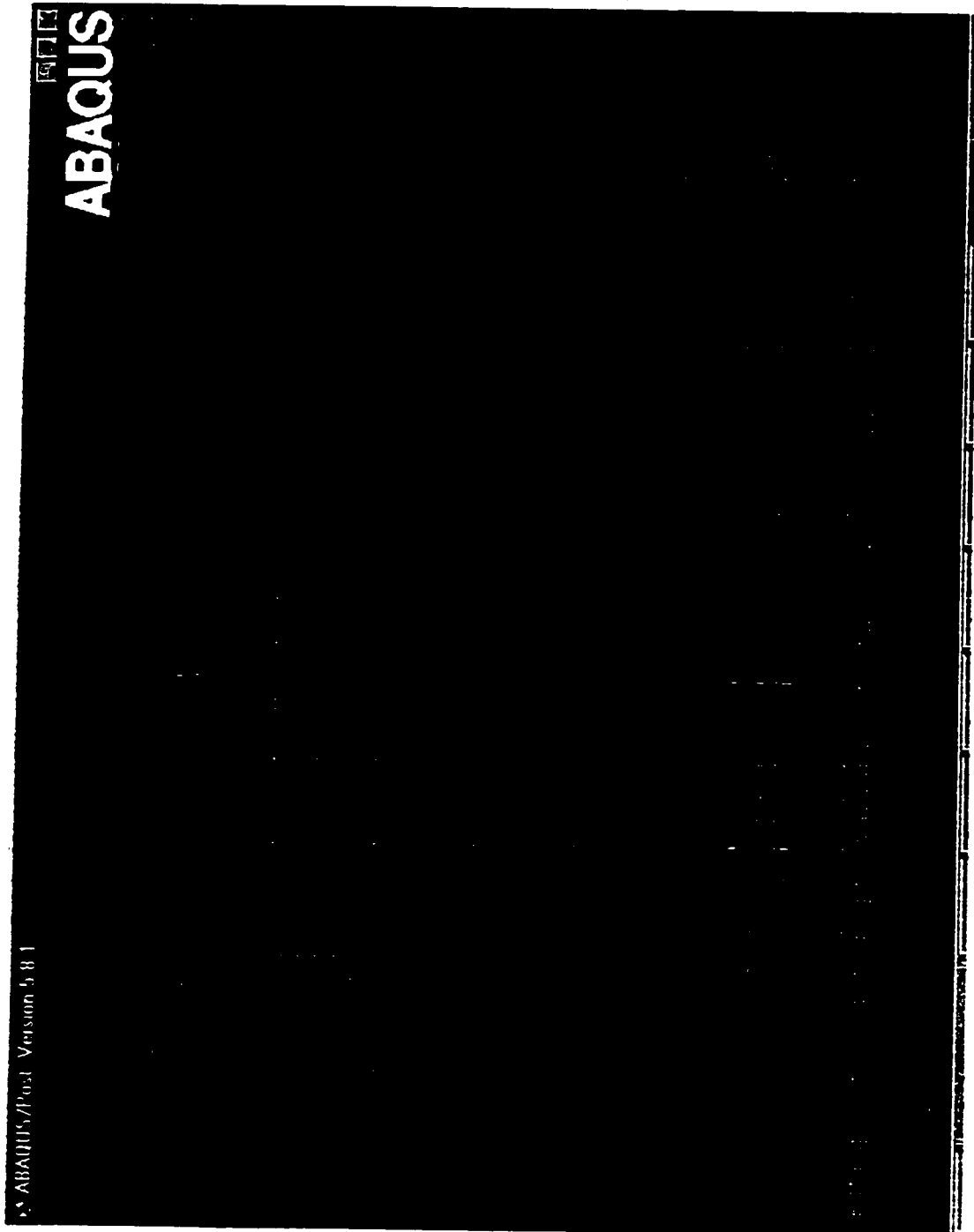
Figure 5.14   Contour of direct strain in the axial direction at 1st pass
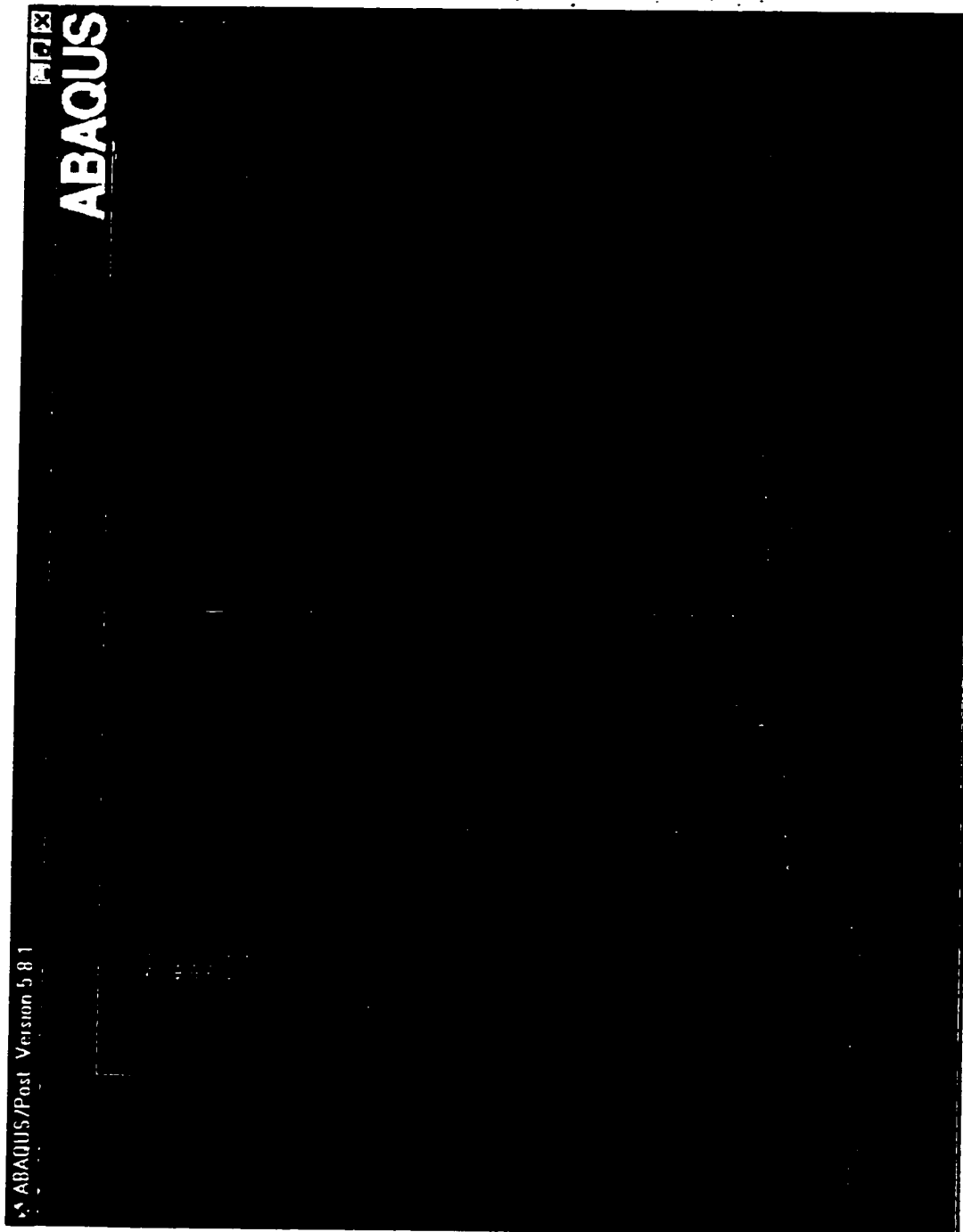
Figure 5.15   Contour of stress in the radial direction at 3400th pass
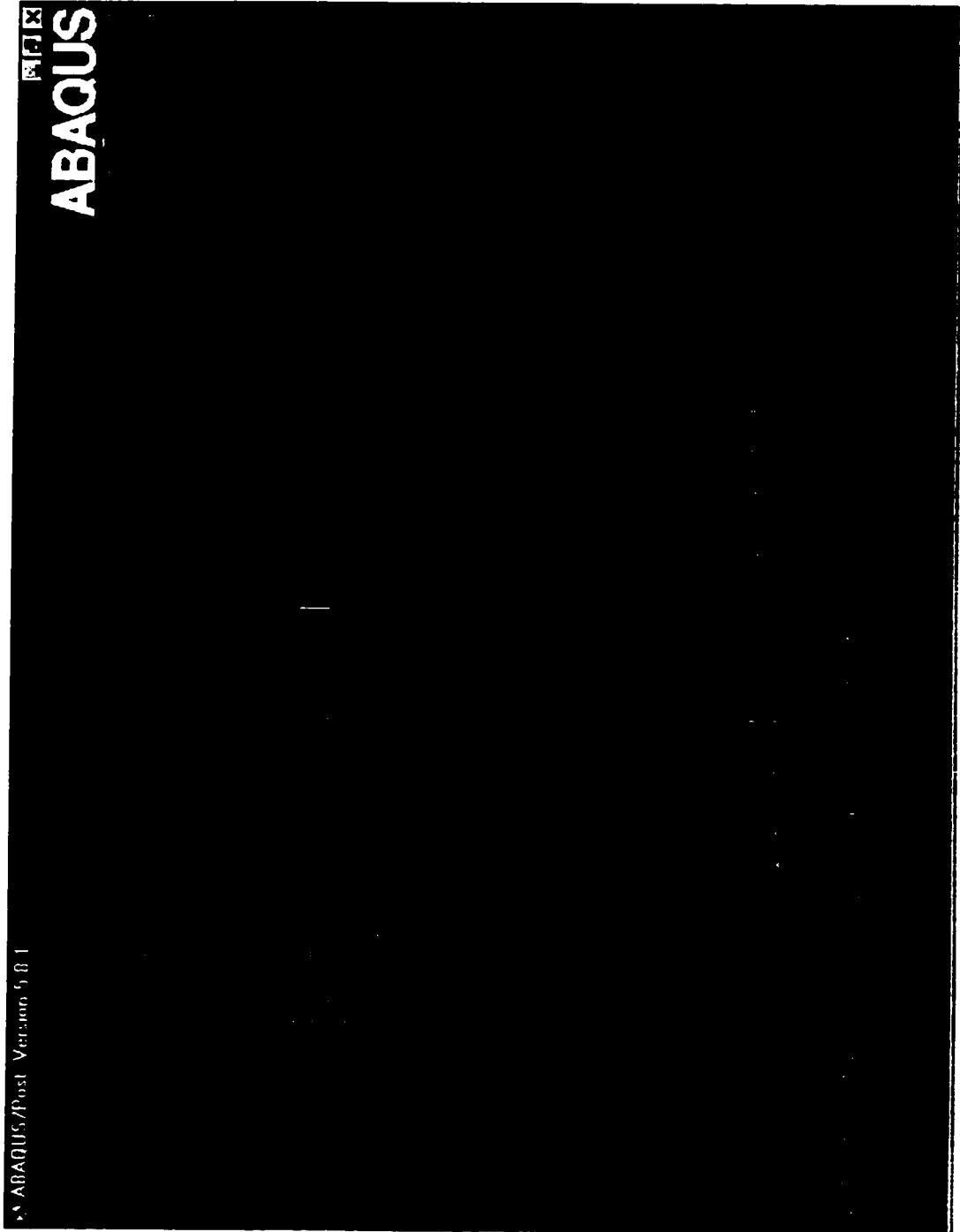
Figure 5.16   Contour of stress in the axial direction at 3400th pass
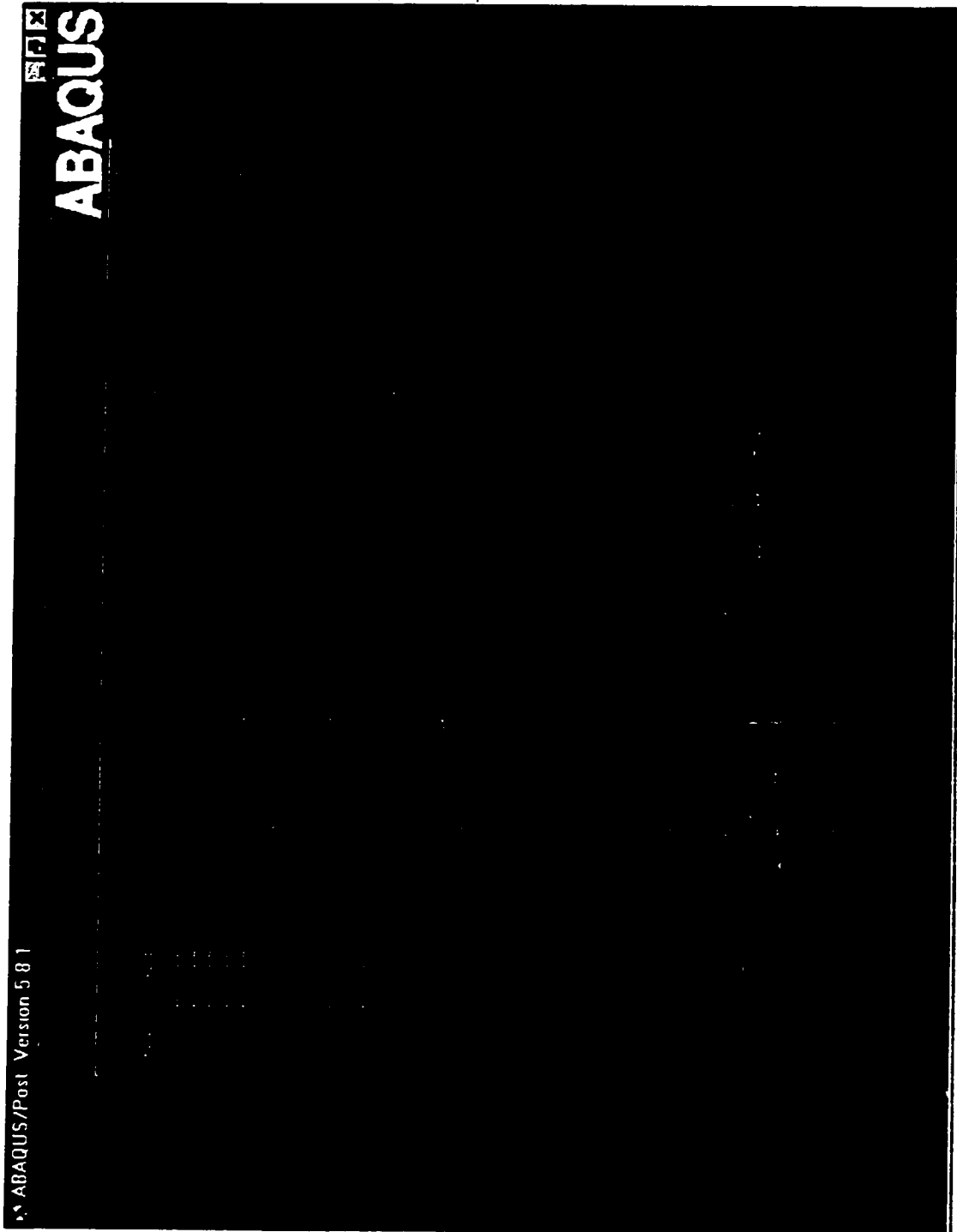
Figure 5.17 Contour of Von Mises stress at 3400th pass
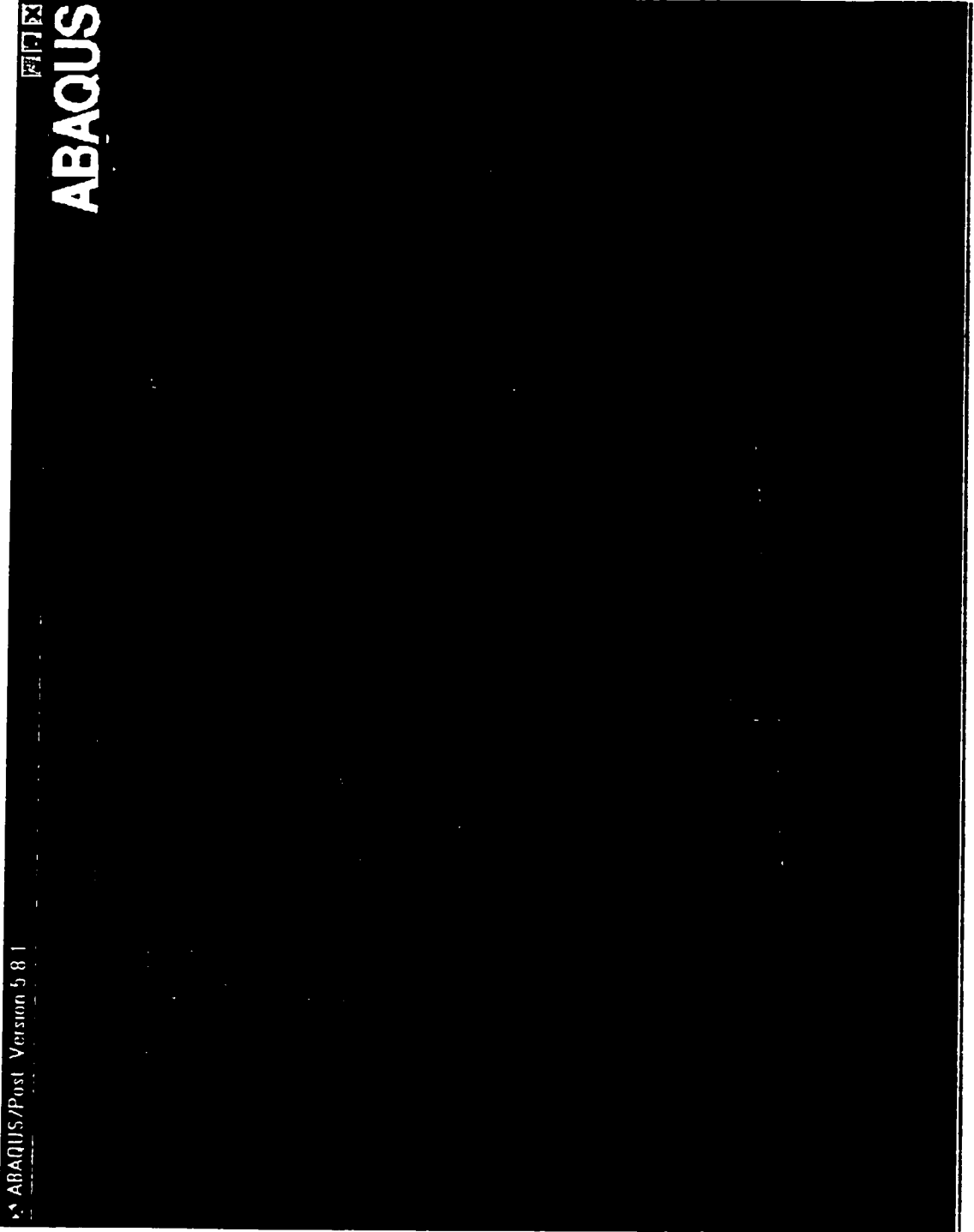
Figure 5.18 Contour of direct strain in the radial direction at 3400th pass.

ABAQUS

ABAQUS/Post Version 5 8 1

ABAQUS

ABAQUS/Post Version 5 8 1
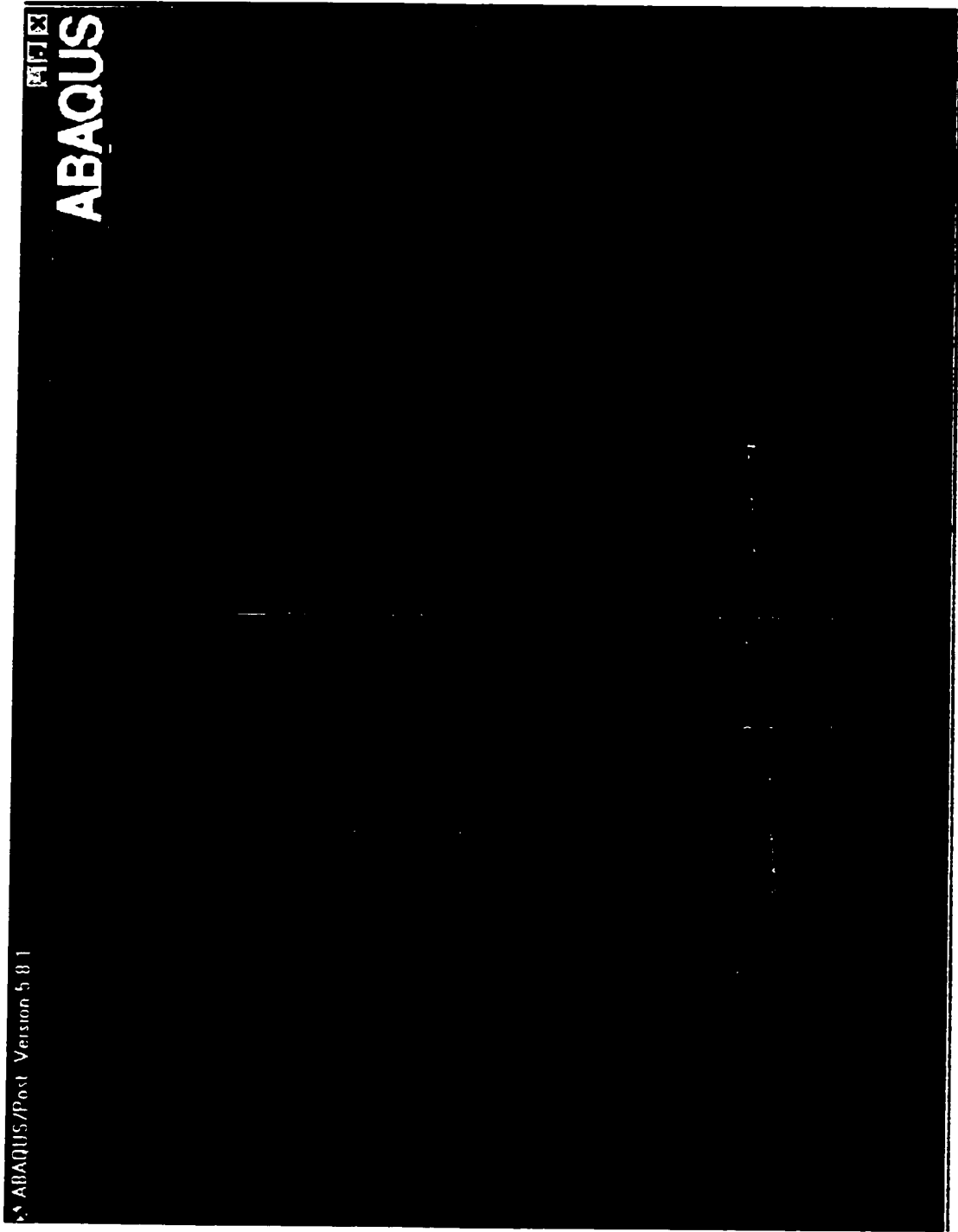
Figure 5.19   Contour of direct strain in the axial direction at 3400th pass
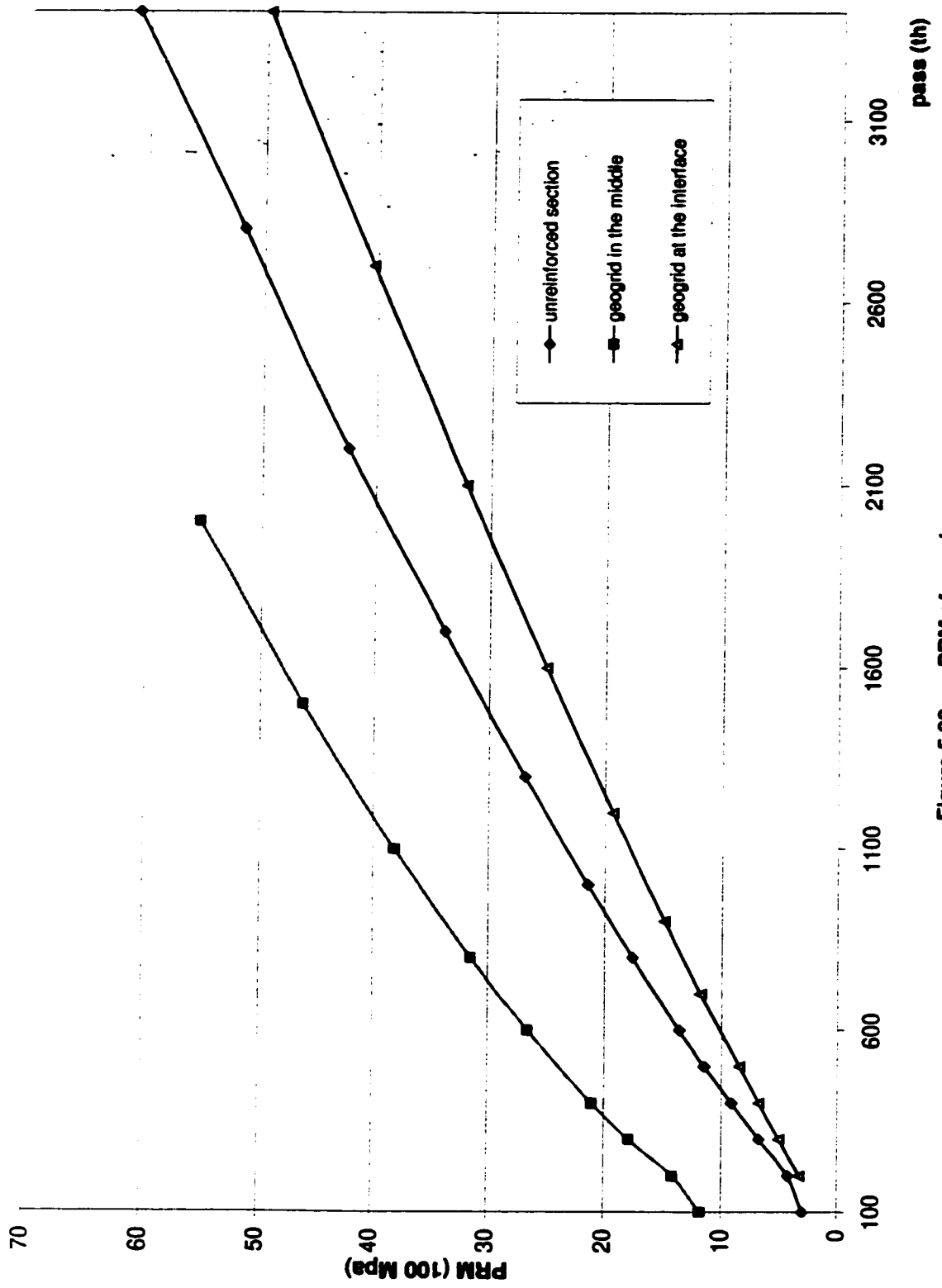
Figure 5.20   PRM of wearing course
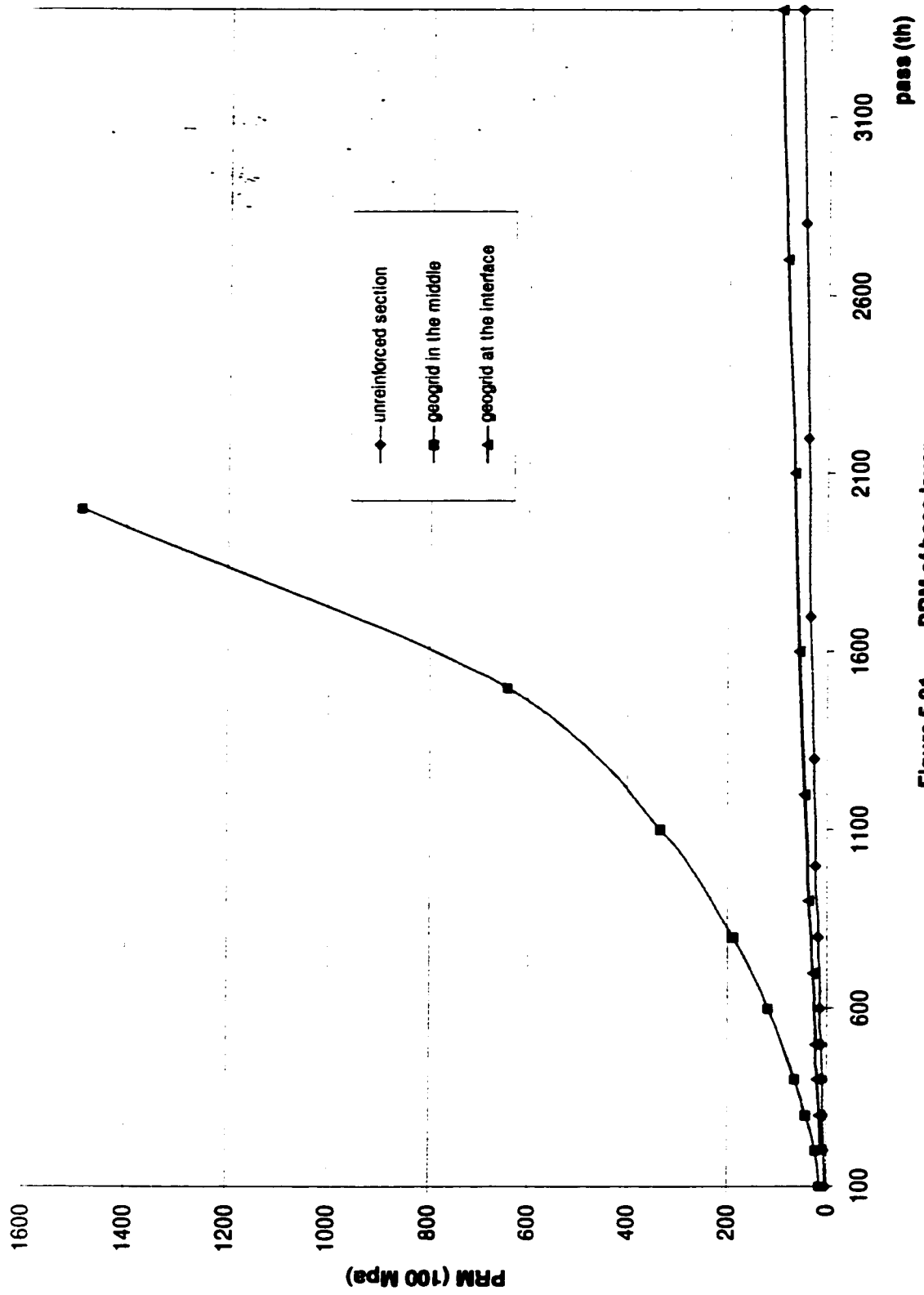
Figure 5.21   PRM of base layer
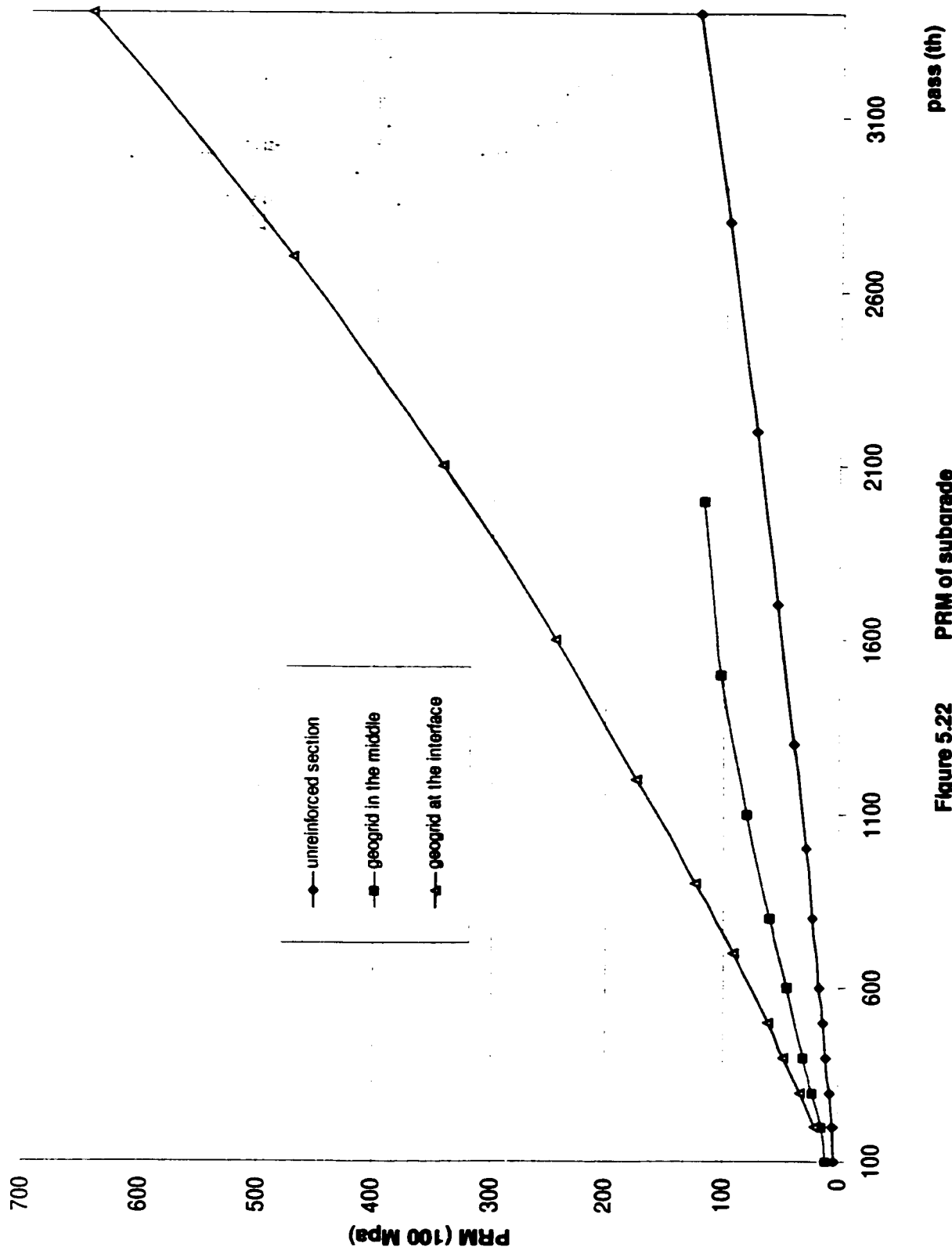
Figure 5.22 PRM of subgrade
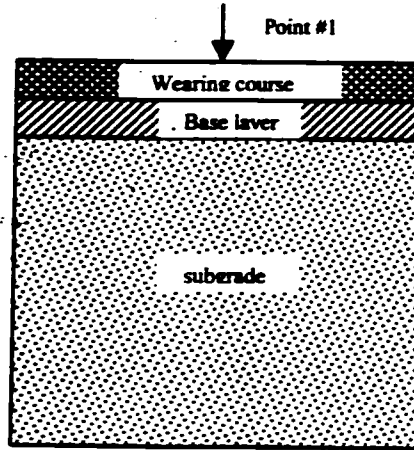
Figure 5.23   Adjoint structure for the case of

unit load at point #1
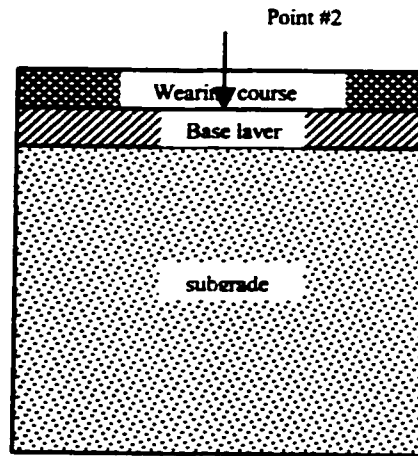
Figure 5.24   Adjoint structure for the case of

unit load at point #2
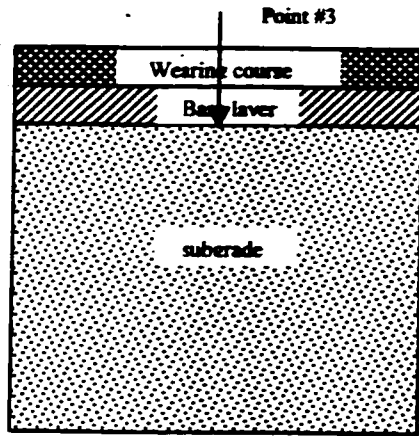
Figure 5.25 Adjoint structure for the case of
unit load at point #3
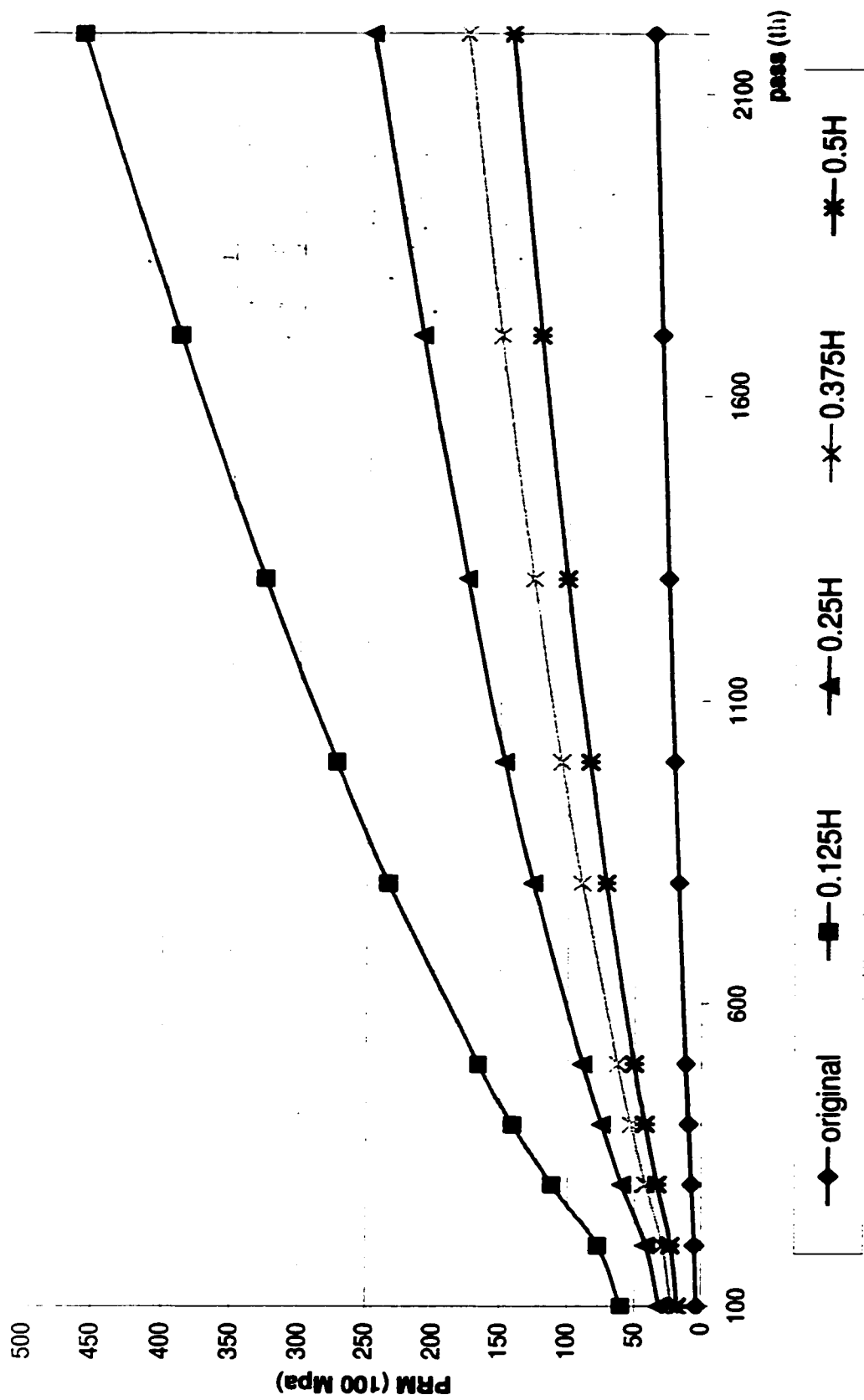
Figure 5.26 PRM of interlocking layer
(geogrid in the middle, controlling point = #1)
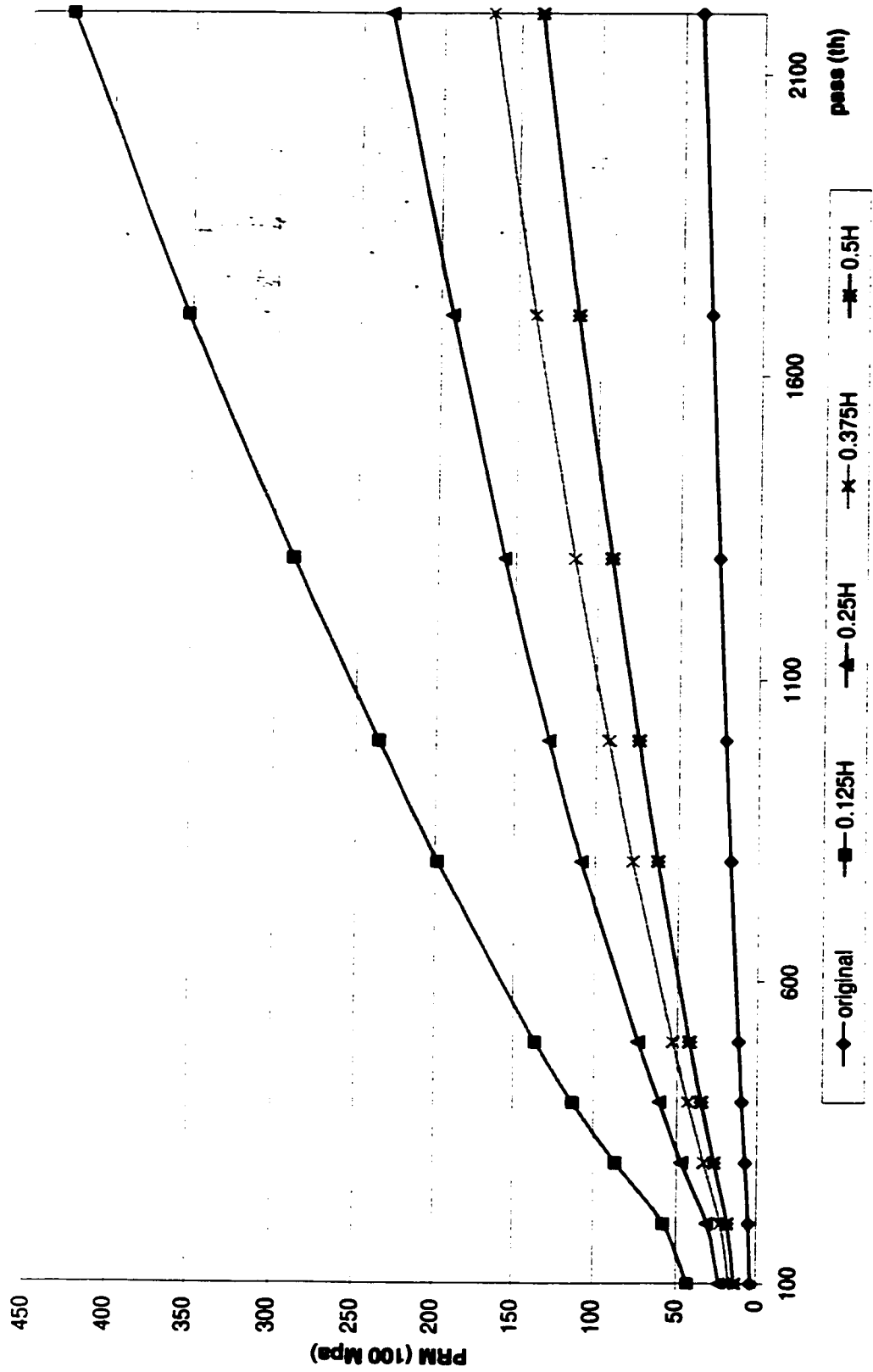
Figure 5.27 PRM of interlocking layer (geogrid in the middle, controlling point = #2)

113
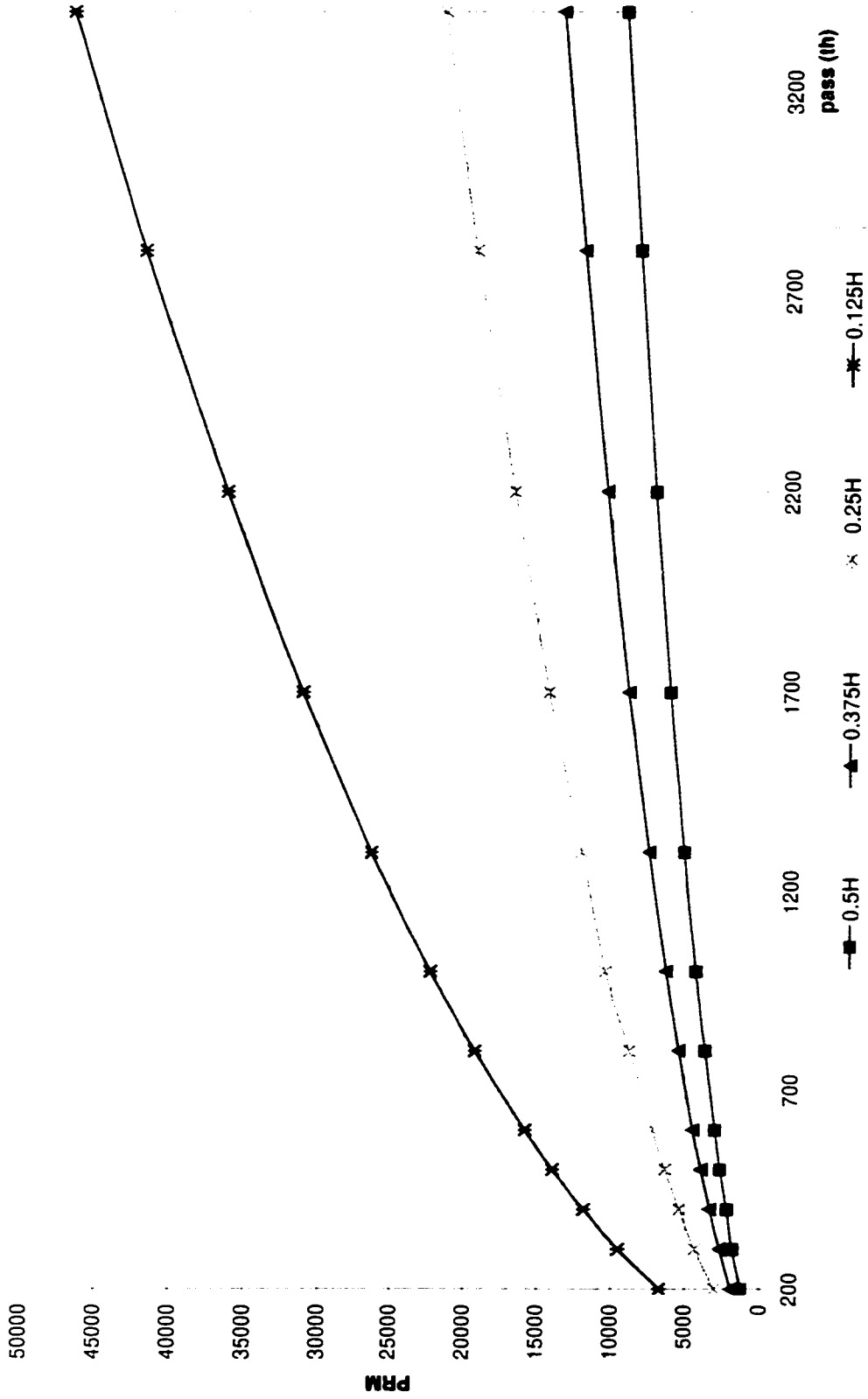
Figure 5.28 PRM of interlocking layer
(geogrid at the interface, controlling point =#1)
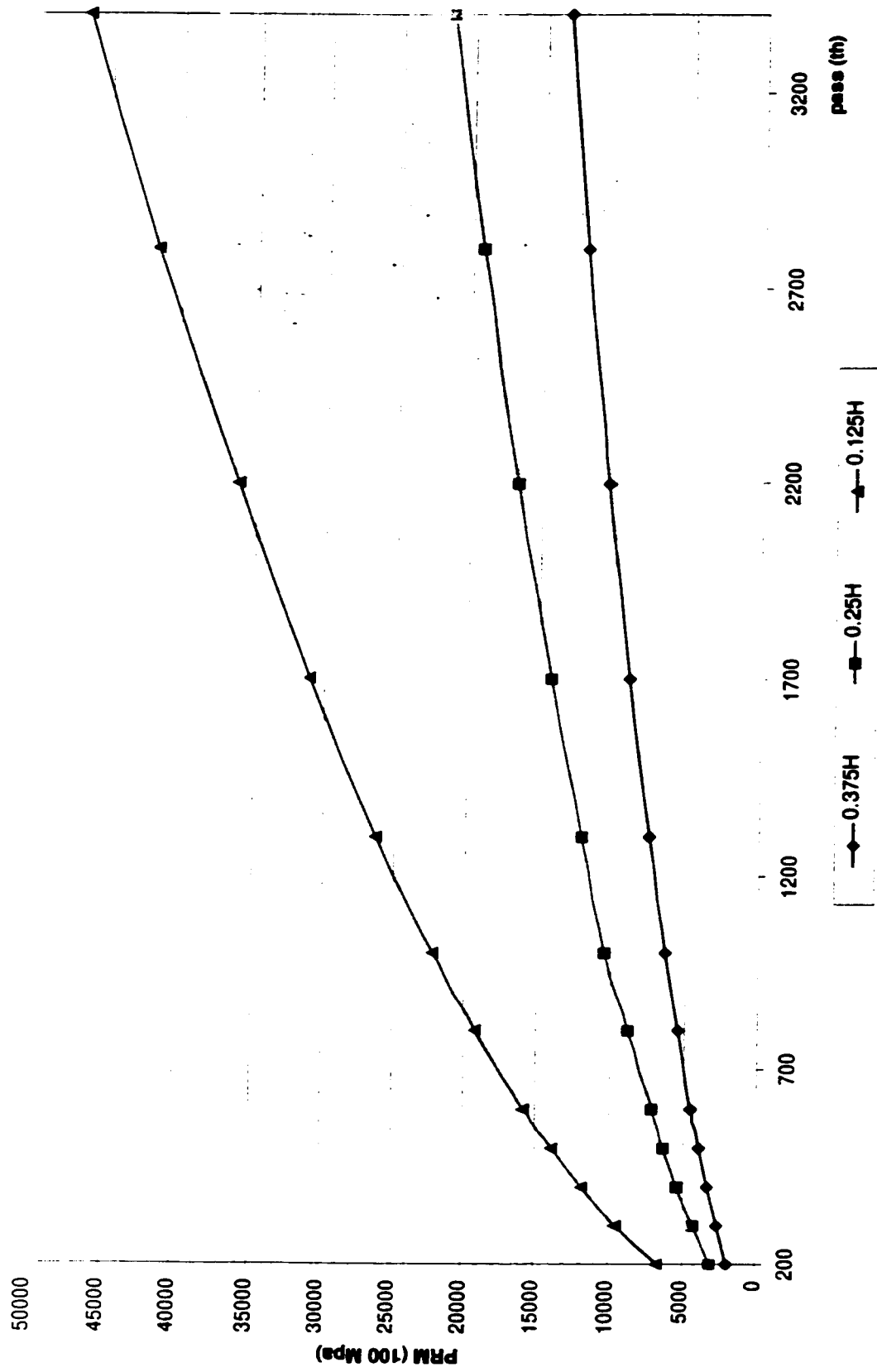
Figure 5.29 PRM of the interlocking layer
(geogrid at the interface, controlling point = #2)

TABLES

The sieve analysis of the soil

Sieve No.	Sieve Size (mm)	Retained weight 1 (g)	Retained weight 2 (g)	overall weight (g)	Retained percent	Passing percent
tan	Tan	22.5	9.77	32.27	1.0	0
200	0.075	89.9	39	128.9	4.1	1.0
20	0.85	112.35	48.45	160.8	5.2	5.2
10	2	336.75	50.2	386.95	12.4	10.3
8	2.36	1234.9	529.8	1764.7	56.6	22.8
4	4.75	448.7	192.91	641.61	20.6	79.4
3/8"	9.5					100
	Summation	2245.1	870.13	3115.23	100	

Table 3.1   Soil gradation

Properties	Test Method	Type 2006	
		American Standard	Metric
Physical			
Grab Tensile Strength	ASTM-D 4632	315	1.4
Grab Tensile Elongarion	ASTM-D 4632	15	
Wide Width Tensile	ASTM-D 4595	2400	35
Wide Width Elongation	ASTM-D 4595	M-10 X-8	
Mullen Burst	ASTM-D 3786	600	4130
Puncture	ASTM-D 4833	120	0.53
Trapezoid Tear	ASTM-D 4533	120	0.53
UV Resistance	ASTM-D 4355	70/500	
Hydraulic			
Apparent Opening Size (AOS)	ASTM-D 4751	40	0.425
Permittivity	ASTM-D 4491	0.05	
Flow Rate	ASTM-D 4491	4	160
Package			
Roll Width		12.5 18	3.81 5.48
Roll Length		360 252	109.7 76.8
Gross Weight		220	99
Area		500	418

Table 3.2   The properties of type 2006 (geotextile)

Yield stress (kpa)				
		confining pressure		
reinforcement		69 kpa	105 kpa	138 kpa
unreinforced		369.84	487.83	487.83
1-layer reinforced		505.77	814.89	1027.41
2-layer reinforced		656.19	1076.4	1297.89
3-layer reinforced		1305.48	1383.45	1589.76

Table 3.3 Comparison of yield stress of the soil under different conditions

Unreinforced Section

passes	PRM (100 Mpa)			Variation of displacement by ABAQUS(m)			Variation of displacement by modeling (m)		
0	course	base	subgrade	Point #1	Point #2	Point #3	Point #1	Point #2	Point #3
100	3.031	3.567	3.1345	2.8221E-05	2.0935E-05	1.1254E-05	2.8220E-05	2.0936E-05	1.1251E-05
200	4.34	4.868	4.579	1.9799E-05	1.4723E-05	7.8010E-06	1.9797E-05	1.4728E-05	7.8006E-06
300	6.858	7.34	7.534	1.2545E-05	9.3254E-06	4.8054E-06	1.2540E-05	9.3260E-06	4.8051E-06
400	9.198	9.57	10.525	9.3096E-06	6.9047E-06	3.4766E-06	9.3094E-06	6.9052E-06	3.4767E-06
500	11.41	11.655	13.573	7.4503E-06	5.5098E-06	2.7197E-06	7.4504E-06	5.5096E-06	2.7199E-06
600	13.53	13.64	16.68	6.2335E-06	4.5961E-06	2.2296E-06	6.2331E-06	4.5958E-06	2.2298E-06
800	17.58	17.4	23.065	4.7252E-06	3.4649E-06	1.6320E-06	4.7254E-06	3.4650E-06	1.6319E-06
1000	21.45	20.93	29.69	3.8220E-06	2.7891E-06	1.2804E-06	3.8221E-06	2.7890E-06	1.2808E-06
1300	26.94	25.975	39.975	2.9845E-06	2.1633E-06	9.6209E-07	2.9841E-06	2.1635E-06	9.6207E-07
1700	33.93	32.3	54.37	2.3203E-06	1.6695E-06	7.1609E-07	2.3200E-06	1.6699E-06	7.1613E-07
2200	42.4	39.7	73.33	1.8224E-06	1.3027E-06	5.3736E-07	1.8228E-06	1.3021E-06	5.3738E-07
2800	51.8	48.2	97.38	1.4551E-06	1.0315E-06	4.0928E-07	1.4551E-06	1.0315E-06	4.0925E-07
3400	60.95	56.26	122.78	1.2136E-06	8.5480E-07	3.2763E-07	1.2138E-06	8.5478E-07	3.2764E-07

Table 5.1   PRM of each layer in unreinforced section

120

Geogrid at the middle of the base

Passes	PRM (100 Mpa)			Variation of displacement by ABAQUS(m)			Variation of displacement by modeling(m)		
	Surface	Base	Subgrade	Surface	Base	Subgrade	Surface	Base	Subgrade
0									
100	11.716	14.055	10.57	7.73E-06	5.82E-06	3.20E-06	7.7269E-06	5.8242E-06	3.2015E-06
200	14.065	22.227	14.925	5.54E-06	3.95E-06	2.27E-06	5.5411E-06	3.9458E-06	2.2657E-06
300	17.85	41.57	23.37	3.62E-06	2.35E-06	1.44E-06	3.6158E-06	2.3480E-06	1.4372E-06
400	21.05	63.87	31.37	2.74E-06	1.66E-06	1.06E-06	2.7362E-06	1.6570E-06	1.0613E-06
600	26.6	118.47	46.532	1.88E-06	1.02E-06	7.01E-07	1.8795E-06	1.0229E-06	7.0114E-07
800	31.5	188.4	60.765	1.45E-06	7.26E-07	5.25E-07	1.4502E-06	7.2613E-07	5.2476E-07
1100	38.14	332.8	80.22	1.09E-06	4.94E-07	3.81E-07	1.0926E-06	4.9443E-07	3.8131E-07
1500	46.155	643.5	101.8	8.31E-07	3.37E-07	2.79E-07	8.3135E-07	3.3707E-07	2.7934E-07
2000	55.4	1490	117.27	6.46E-07	2.34E-07	2.09E-07	6.4595E-07	2.3365E-07	2.0907E-07

Table 5.2   PRM of each layer when geogrid is in the middle of base layer

Geogrid at the interface

Passes	PRM(100Mpa)			Variation of displacement by ABAQUS(m)			Variation of displacement by modeling(m)		
0	Surface	Base	Subgrade	Surface	Base	Subgrade	Surface	Base	Subgrade
200	3.265	9.803	21.25	1.2727E-05	5.7576E-06	1.8882E-06	1.2728E-05	5.7572E-06	1.8887E-06
300	5.113	14.365	34.54	8.1713E-06	3.7706E-06	1.0130E-06	8.1711E-06	3.7704E-06	1.1712E-06
400	6.846	18.395	48.193	6.1120E-06	2.8515E-06	8.4504E-07	6.1122E-06	2.8512E-06	8.4504E-07
500	8.51	22.125	62.264	4.9170E-06	2.3105E-06	6.5759E-07	4.9171E-06	2.3106E-06	6.5756E-07
700	11.713	28.983	91.725	3.5695E-06	1.6938E-06	4.5016E-07	3.5696E-06	1.6938E-06	4.5020E-07
900	14.81	35.3	122.8	2.8211E-06	1.3477E-06	3.3822E-07	2.8211E-06	1.3475E-06	3.3825E-07
1200	19.29	44.15	172.65	2.1601E-06	1.0391E-06	2.4255E-07	2.1603E-06	1.0390E-06	2.4254E-07
1600	25.08	55.095	244.57	1.6568E-06	8.0203E-07	1.7257E-07	1.6568E-06	8.0201E-07	1.7255E-07
2100	32.115	67.85	343.1	1.2901E-06	6.2810E-07	1.2394E-07	1.2902E-06	6.2812E-07	1.2390E-07
2700	40.34	82.18	474.27	1.0241E-06	5.0112E-07	9.0301E-08	1.0242E-06	5.0111E-07	9.0300E-08
3400	49.7	97.95	644.93	8.2865E-07	4.0725E-07	6.0846E-08	8.2867E-07	4.0724E-07	6.6844E-08
4200	60.18	115.03	864.35	6.8234E-07	3.3664E-07	5.0184E-08	6.8232E-07	3.3662E-07	5.0182E-08
5000	70.48	131.35	1111.4	5.8114E-07	2.8760E-07	3.9230E-08	5.8114E-07	2.8760E-07	3.9229E-08

Table 5.3   PRM of each layer when geogrid is at the base-subgrade interface

122

Unreinforced Section

passes	Variation of displacement by ABAQUS(m)			Variation of displacement by KENLAYER (m)			PRM by ABAQUS(100Mpa)		
	Point #1	Point #2	Point #3	Point #1	Point #2	Point #3	Course	Base	subgrade
0									
100	2.8221E-05	2.0935E-05	1.1254E-05	2.9200E-05	2.1700E-05	1.1100E-05	3.031	3.567	3.1345
200	1.9799E-05	1.4723E-05	7.8010E-06	2.0600E-05	1.5400E-05	7.6000E-06	4.34	4.868	4.579
300	1.2545E-05	9.3254E-06	4.8054E-06	1.3163E-05	9.8430E-06	4.6870E-06	6.858	7.34	7.534
400	9.3096E-06	6.9047E-06	3.4766E-06	9.8190E-06	7.3370E-06	3.3820E-06	9.198	9.57	10.525
500	7.4503E-06	5.5098E-06	2.7197E-06	7.8950E-06	5.8890E-06	2.6410E-06	11.41	11.655	13.573
600	6.2335E-06	4.5961E-06	2.2296E-06	6.6360E-06	4.9400E-06	2.1610E-06	13.53	13.64	16.68
800	4.7252E-06	3.4649E-06	1.6320E-06	5.0690E-06	3.7590E-06	1.5770E-06	17.58	17.4	23.065
1000	3.8220E-06	2.7891E-06	1.2804E-06	4.1290E-06	3.0510E-06	1.2340E-06	21.45	20.93	29.69
1300	2.9845E-06	2.1633E-06	9.6209E-07	3.2530E-06	2.3920E-06	9.2500E-07	26.94	25.975	39.975
1700	2.3203E-06	1.6695E-06	7.1609E-07	2.5560E-06	1.8690E-06	6.8600E-07	33.93	32.3	54.37
2200	1.8224E-06	1.3027E-06	5.3736E-07	2.0300E-06	1.4780E-06	5.1400E-07	42.4	39.7	73.33
2800	1.4551E-06	1.0315E-06	4.0928E-07	1.6400E-06	1.1860E-06	3.9000E-07	51.8	48.2	97.38
3400	1.2136E-06	8.5480E-07	3.2763E-07	1.3820E-06	9.9500E-07	3.1100E-07	60.95	56.26	122.78

Table 5.4 Comparison of displacements by KENLAYER and ABAQUS in unreinforced section

Passes	Variation of dispalcement by ABAQUS			Variation of dispalcement by KENLAYER			PRM by ABAQUS(100 Mpa)		
0	Point #1	Point #2	Point #3	Point #1	Point #2	Point #3	Surface	Base	Subgrade
100	7.7269E-06	5.8244E-06	3.2012E-06	7.8060E-06	5.8920E-06	3.2090E-06	1.1716E+01	1.4055E+01	1.0570E+01
200	5.5412E-06	3.9460E-06	2.2656E-06	5.6210E-06	4.0010E-06	2.2680E-06	1.4065E+01	2.2227E+01	1.4925E+01
300	3.6156E-06	2.3484E-06	1.4369E-06	3.6900E-06	2.3860E-06	1.4390E-06	1.7850E+01	4.1570E+01	2.3370E+01
400	2.7361E-06	1.6573E-06	1.0612E-06	2.8060E-06	1.6850E-06	1.0630E-06	2.1050E+01	6.3870E+01	3.1370E+01
600	1.8793E-06	1.0227E-06	7.0115E-07	1.9420E-06	1.0400E-06	7.0200E-07	2.6600E+01	1.1847E+02	4.6532E+01
800	1.4504E-06	7.2615E-07	5.2473E-07	1.5080E-06	7.3800E-07	5.2500E-07	3.1500E+01	1.8840E+02	6.0765E+01
1100	1.0926E-06	4.9439E-07	3.8131E-07	1.1450E-06	5.0200E-07	3.8100E-07	3.8140E+01	3.3280E+02	8.0220E+01
1500	8.3134E-07	3.3705E-07	2.7933E-07	8.7900E-07	3.4100E-07	2.7900E-07	4.6155E+01	6.4350E+02	1.0180E+02
2000	6.4595E-07	2.3361E-07	2.0910E-07	6.8900E-07	2.3500E-07	2.0900E-07	5.5400E+01	1.4900E+03	1.1727E+02

Geogrid in the middle of the base

Table 5.5   Comparison of displacements by KENLAYER and ABAQUS
when geogrid is in the middle of base layer

Geogrid at the interface

Passes	Variation of displacement by ABAQUS(m)			Variation of displacement by KENLAYER (m)			PRM by ABAQUS(100Mpa)		
0	Point #1	Point #2	Point #3	Point #1	Point #2	Point #3	Surface	Base	Subgrade
200	1.2727E-05	5.7576E-06	1.8882E-06	1.3839E-05	6.1950E-06	1.8700E-06	3.265	9.803	21.25
300	8.1713E-06	3.7706E-06	1.0130E-06	8.9900E-06	4.1100E-06	1.1600E-06	5.113	14.365	34.54
400	6.1120E-06	2.8515E-06	8.4504E-07	6.7820E-06	3.1370E-06	8.3300E-07	6.846	18.395	48.193
500	4.9170E-06	2.3105E-06	6.5759E-07	5.4970E-06	2.5630E-06	6.4700E-07	8.51	22.125	62.264
700	3.5695E-06	1.6938E-06	4.5016E-07	4.0380E-06	1.9050E-06	4.4200E-07	11.713	28.983	91.725
900	2.8211E-06	1.3477E-06	3.3822E-07	3.2200E-06	1.5330E-06	3.3200E-07	14.81	35.3	122.8
1200	2.1601E-06	1.0391E-06	2.4255E-07	2.4940E-06	1.1950E-06	2.3700E-07	19.29	44.15	172.65
1600	1.6568E-06	8.0203E-07	1.7257E-07	1.9360E-06	8.3800E-07	1.6800E-07	25.08	55.095	244.57
2100	1.2901E-06	6.2810E-07	1.2394E-07	1.5250E-06	6.4600E-07	1.2000E-07	32.115	67.85	343.1
2700	1.0241E-06	5.0112E-07	9.0301E-08	1.2250E-06	5.0400E-07	8.7000E-08	40.34	82.18	474.27
3400	8.2865E-07	4.0725E-07	6.0846E-08	9.0200E-07	4.0800E-07	6.5000E-08	49.7	97.95	644.93
4200	6.8234E-07	3.3664E-07	5.0184E-08	7.3400E-07	3.3800E-07	4.8000E-08	60.18	115.03	864.35
5000	5.8114E-07	2.8760E-07	3.9230E-08	6.1700E-07	2.8900E-07	3.8000E-08	70.48	131.35	1111.4

Table 5.6   Comparison of displacements by KENLAYER and ABAQUS
when geogrid is at the base-subgrade interface

125

PRM of interlocking layer (geogrid in the middle, #1 as controlling point)

pass(th)	PRM (100 Mpa) original	δE*δH (10Mpa)	δH=	PRM (100 Mpa)			
				0.125H	0.25H	0.375H	0.5H
100	3.5670E+00	2.8290E+00		6.0147E+01	3.1857E+01	2.2427E+01	1.7712E+01
200	4.8680E+00	3.6513E+00		7.7894E+01	4.1381E+01	2.9210E+01	2.3125E+01
300	7.3400E+00	5.2190E+00		1.1172E+02	5.9530E+01	4.2133E+01	3.3435E+01
400	9.5700E+00	6.5508E+00		1.4059E+02	7.5078E+01	5.3242E+01	4.2324E+01
500	1.1655E+01	7.7398E+00		1.6645E+02	8.9053E+01	6.3254E+01	5.0354E+01
800	1.7400E+01	1.0818E+01		2.3376E+02	1.2558E+02	8.9520E+01	7.1490E+01
1000	2.0930E+01	1.2588E+01		2.7269E+02	1.4681E+02	1.0485E+02	8.3870E+01
1300	2.5975E+01	1.5017E+01		3.2632E+02	1.7615E+02	1.2609E+02	1.0106E+02
1700	3.2300E+01	1.7902E+01		3.9034E+02	2.1132E+02	1.5165E+02	1.2181E+02
2200	3.9700E+01	2.1083E+01		4.6136E+02	2.5053E+02	1.8025E+02	1.4512E+02

Table 5.7   PRM of interlocking layer
(geogrid in the middle of base, controlling point = #1)

PRM of interlocking layer (geogrid in the middle, #2 as the controlling point)

pass(th)	PRM (100 Mpa) original	δE*δH (10Mpa.m)	PRM (100 Mpa)			
		δH=	0.125H	0.25H	0.375H	0.5H
100	3.5670E+00	1.9948E+00	4.3463E+01	2.3515E+01	1.6866E+01	1.3541E+01
200	4.8680E+00	2.6804E+00	5.8476E+01	3.1672E+01	2.2737E+01	1.8270E+01
300	7.3400E+00	3.9984E+00	8.7308E+01	4.7324E+01	3.3996E+01	2.7332E+01
400	9.5700E+00	5.1587E+00	1.1274E+02	6.1157E+01	4.3961E+01	3.5364E+01
500	1.1655E+01	6.2208E+00	1.3607E+02	7.3863E+01	5.3127E+01	4.2759E+01
800	1.7400E+01	9.0656E+00	1.9871E+02	1.0806E+02	7.7837E+01	6.2728E+01
1000	2.0930E+01	1.0758E+01	2.3609E+02	1.2851E+02	9.2650E+01	7.4720E+01
1300	2.5975E+01	1.3130E+01	2.8858E+02	1.5728E+02	1.1351E+02	9.1625E+01
1700	3.2300E+01	1.6024E+01	3.5278E+02	1.9254E+02	1.3913E+02	1.1242E+02
2200	3.9700E+01	1.9306E+01	4.2582E+02	2.3276E+02	1.6841E+02	1.3623E+02

Table 5.8   PRM of interlocking layer
(geogrid in the middle of base, controlling point = #2)

PRM of interlocking layer (geogrid at the interface, #1 as controlling point)					
pass	PRM of base (100 Mpa)	δE*δH (100 Mpa.m)			
		δH=0.5H	δH=0.375H	δH=0.25H	δH=0.125H
200	4.8680E+00	2.6073E+01	2.8586E+01	3.0696E+01	3.3585E+01
300	7.3400E+00	3.6760E+01	4.0318E+01	4.3324E+01	4.7480E+01
400	9.5700E+00	4.4188E+01	5.0224E+01	5.3985E+01	5.9205E+01
500	1.1655E+01	5.3824E+01	5.9021E+01	6.3446E+01	6.9591E+01
600	1.3640E+01	6.1176E+01	6.7065E+01	7.2087E+01	7.9060E+01
800	1.7400E+01	7.4481E+01	8.1606E+01	8.7681E+01	9.6112E+01
1000	2.0930E+01	8.6274E+01	9.4455E+01	1.0415E+02	1.1109E+02
1300	2.5975E+01	1.0238E+02	1.1197E+02	1.2017E+02	1.3140E+02
1700	3.2300E+01	1.2137E+02	1.3257E+02	1.4211E+02	1.5508E+02
2200	3.9700E+01	1.4214E+02	1.5501E+02	1.6596E+02	1.8064E+02
2800	4.8200E+01	1.6486E+02	1.7950E+02	1.9272E+02	2.0835E+02
3400	5.6260E+01	1.8519E+02	2.0134E+02	2.1500E+02	2.3283E+02
		PRM (100 Mpa)			
		1.3037E+03	1910.601333	3.0745E+03	6.7219E+03
		1.8380E+03	2695.206667	4.3397E+03	9.5033E+03
		2.2094E+03	3357.836667	5.4081E+03	1.1851E+04
		2.6912E+03	3946.388333	6.3563E+03	1.3930E+04
		3.0588E+03	4484.64	7.2223E+03	1.5826E+04
		3.7241E+03	5457.8	8.7855E+03	1.9240E+04
		4.3137E+03	6317.93	1.0436E+04	2.2239E+04
		5.1190E+03	7490.641667	1.2043E+04	2.6306E+04
		6.0685E+03	8870.3	1.4243E+04	3.1048E+04
		7.1070E+03	10373.7	1.6636E+04	3.6168E+04
		8.2430E+03	12014.86667	1.9320E+04	4.1718E+04
		9.2595E+03	13478.92667	2.1556E+04	4.6622E+04

Table 5.9   PRM of interlocking layer
(geogrid at the base-subgrade interface, controlling point = #1)

PRM of interlocking layer (geogrid at the interface, #2 as controlling point)				
pass	PRM of base (100 Mpa)	δE*δH (100 Mpa.m)		
		δH=0.375H	δH=0.25H	δH=0.125H
200	4.8680E+00	2.8586E+01	3.0696E+01	3.3585E+01
300	7.3400E+00	4.0318E+01	4.3324E+01	4.7480E+01
400	9.5700E+00	5.0224E+01	5.3985E+01	5.9205E+01
500	1.1655E+01	5.9021E+01	6.3446E+01	6.9591E+01
600	1.3640E+01	6.7065E+01	7.2087E+01	7.9060E+01
800	1.7400E+01	8.1606E+01	8.7681E+01	9.6112E+01
1000	2.0930E+01	9.4455E+01	1.0415E+02	1.1109E+02
1300	2.5975E+01	1.1197E+02	1.2017E+02	1.3140E+02
1700	3.2300E+01	1.3257E+02	1.4211E+02	1.5508E+02
2200	3.9700E+01	1.5501E+02	1.6596E+02	1.8064E+02
2800	4.8200E+01	1.7950E+02	1.9272E+02	2.0835E+02
3400	5.6260E+01	2.0134E+02	2.1500E+02	2.3283E+02
		PRM (100 Mpa)		
		1.9106E+03	3.0745E+03	6.7219E+03
		2.6952E+03	4.3397E+03	9.5033E+03
		3.3578E+03	5.4081E+03	1.1851E+04
		3.9464E+03	6.3563E+03	1.3930E+04
		4.4846E+03	7.2223E+03	1.5826E+04
		5.4578E+03	8.7855E+03	1.9240E+04
		6.3179E+03	1.0436E+04	2.2239E+04
		7.4906E+03	1.2043E+04	2.6306E+04
		8.8703E+03	1.4243E+04	3.1048E+04
		1.0374E+04	1.6636E+04	3.6168E+04
		1.2015E+04	1.9320E+04	4.1718E+04
		1.3479E+04	2.1556E+04	4.6622E+04

Table 5.10   PRM of interlocking layer
(geogrid at the base-subgrade interface, controlling point = #2)

APPENDIX

Program: *sensitivity.c*

```c
#include <stdio.h>
#include <math.h>

#define NUMBER 104
#define PI 3.14159

struct load_effect
{
        int element;
        int force;
        double s11;                     /*stress or strain in z direction*/
        double s22;                     /*stress or strain in r direction*/
        double s33;                     /*loop stress or loop strain*/
        double s12;                     /*shear stress or shear strain*/
};

load_effect  primary[NUMBER];    /*analysis results for the primary structure*/
load_effect  adjoint[NUMBER];    /*analysis results for the adjoint structure*/

int main(void)
{
        FILE *in1, *in2, *out1, *out2;
        int i,j;
        double r[26],s[26];
        double G11,G22,G33,G12,S11,S22,S33,S12,E11,E22,E33,E12;
        double sum,S, factor, Delta_d, E, Delta_E_H;

        in1=fopen("primary", "r");    /* "primary" is the file containing strain data
```

```c
                                            * for the primary structure*/
in2=fopen("adjoint", "r");      /* "secondary" is the file containing stress data
                                            * for the secondary structure*/


/*read the data into the file*/
for(i=1;i<=NUMBER; i++)
{
        fscanf(in1, "%d%d%lf%lf%lf%lf\n", &primary[i].element,
                &primary[i].foot, &primary[i].s11, &primary[i].s22,
                &primary[i].s33,&primary[i].s12);


        fscanf(in2, "%d%d%lf%lf%lf%lf\n", &adjoint[i].element,
                &adjoint[i].foot, &adjoint[i].s11, &adjoint[i].s22,
                &adjoint[i].s33, &adjoint[i].s12);}
printf("the variation of displacement is :");
scanf("%lf", &Delta_d);


printf("the Modulus is :");
scanf("%lf", %E);


factor=1.0/sqrt(3.0);


/*generate the distance from Gaussian Points to the axis center*/
for(i=1;i<=26;i++)
{
        if(i<=6)
        {
                if(i%2==1) r[i]=(i-1)*0.0045+0.0045*(1-factor);
                else        r[i]=(i-2)*0.0045+0.0045*(1+factor);
```

132

```c
                s[i]=r[i]*2*PI*0.027/6;}
        else if(i<=12)
        {
                if(i%2==1) r[i]=0.027+(i-7)*0.009+0.009*(1-factor);
                else        r[i]=0.027+(i-7)*0.009+0.009*(1+factor);
                s[i]=r[i]*2*PI*0.009;}
        else if(i<=20)
        {
                if(i%2==1) r[i]=0.081+(i-13)*0.219/8+0.219/8*(1-factor);
                else        r[i]=0.081+(i-14)*0.219/8+0.219/8*(1+factor);
                s[i]=r[i]*2*PI*0.219/8;}
        else
        {
                if(i%2==1) r[i]=0.3+(i-21)*0.03+0.03*(1-factor);
                else        r[i]=0.3+(i-22)*0.03+0.03*(1+factor);
                s[i]=r[i]*2*PI*0.03;}
}

out1=fopen("data_strain", "w");
out2=fopen("data_stress", "w");

sum=0.0;

for(i=1;i<=NUMBER/2;i++)
{
        j=(primary[i].element)%100;

        if(primary[i].foot==1||primary[i].foot==2)
        {
```

```c
E11=(primary[i].s11+primary[i+54].s11)/2;
E22=(primary[i].s22+primary[i+54].s22)/2;
E33=(primary[i].s33+primary[i+54].s33)/2;
E12=(primary[i].s12+primary[i+54].s12)/2;


S11=(adjoint[i].s11+adjoint[i+54].s11)/2;
S22=(adjoint[i].s22+adjoint[i+54].s22)/2;
S33=(adjoint[i].s33+adjoint[i+54].s33)/2;
S12=(adjoint[i].s12+adjoint[i+54].s12)/2;


fprintf(out1, "%f\t%f\t%f\n", E11, E22, E33, E12);


fprintf(out2, "%f\t%f\t%f\n", S11, S22, S33, S12);


if(primary[i].foot==1)   S=s[2*j-1];
else                     S=s[2*j];


G11=S11*E11;
G22=S22*E22;
G33=S33*E33;
G12=S12*E12;


sum=sum+(G11+G22+G33+G12)*S;
}


}


Delta_E_H=Delta_d*E/sum;


printf("dE*dH=%.4e\n",Delta_E_H);
```

```
        fclose(in1);

        fclose(in2);

        fclose(out1);

        fclose(out2);
}
```

REFERENCES

1. AASHTO Guide for Design of Pavement Structures, 1986, American Association of State Highway and Transportation Officials, Washington, D.C.

2. ABAQUS Standard Users Manual, 1998, Version 5.8, Habbbit, Karlsson & Sorensen, Inc., USA.

3. Bathe, K.J., and Wilson, E.L., 1976, Numerical Methods in Finite Element Analysis, Prentice Hall, Inc., Englewood Cliffs, New Jersey.

4. Budkowska, B.B., 1997, "Sensitivity Analysis of Short Piles Subject to Bending Embedded in Homogeneous Soil, Part I – Theoretical Formulation", Computers and Geotechnics, An Internal Journal, Vol. 21, 87-102.

5. Budkowska, B.B., 1997, "Sensitivity Analysis of Short Piles Subject to Bending Embedded in Homogeneous Soil, Part II – Numerical Analysis", Computers and Geotechnics, An Internal Journal, Vol. 21, 103-120.

6. Canadian Geotechnical Engineering Manual, 1992, 3rd Edition, Canadian Geotechnical Society, BiTech Publishers Ltd., Richmond, B.C.

7. Chan, F., Barksdale, R.D., and Brown, S.F., 1989, "Aggregate Base Reinforcement of Surface Pavements", Geotextiles and Geomembranes, 8, 165-189.

8. Cividini, A., Gioda, G., and Sterpi, D., 1997, "An Experimental and Numerical Study of the Behavior of Reinforced Sands", Computer Methods and Advances in Geomechanics, 15-30.

9. Giroud, J.P.,and Noiray, L., 1981, "Geotextile-Reinforced Unpaved Road Design", Journal of the Geotechnical Division, ASCE, Vol. 107, No. GT9, 1233-1254.

10. Giroud, J.P., Ah-Line, C., and Bonaparte, R., 1984, "Design of Unpaved Roads and Trafficked Areas With Geogrids", Proceeding of the Symposium on Polymer Grid Reinforcement in Civil Engineering, 116-127.

11. Giroud, J.P., 1985,Geotextile and Geomembranes Definitions, Properties and Design, 2nd Edition, Industrial Fabrics Association International, St. Paul

12. Hass, R., Walls, J., and Carroll, R.G., 1988, "Geogrid Reinforcement of Granular Base in Flexible Pavements", Transportation Research Board, Washington, D.C., 19-27.

13. Houben, L.J.M., Molenaar, A.A.A., Fuchs, G.H.A.M., Moll, H.O., 1984, "Analysis and Design of Concrete Block Pavements", Second International Conference on Concrete Block Paving, 86-99.

14. Huang, Y.H., Pavement Analysis and Design, 1993, Prentice Hall Inc, A Division of Simon & Schuster Englewood Cliffs, New Jersey 07632.

15. ICPI, 1995, Interlocking Concrete Pavement Institute, Technical Specification.

16. Koerner, R. M., Designing with Geosynthetics, 1986, 2nd Edition, Prentice Hall Inc; A Division of Simon & Schuster Englewood Cliffs, New Jersey 07632.

17. Washizu, K., 1968, Variational Methods in Elasticity and Plasticity, Pergamon Press.

18. Marvin, K.C., 1984, "Site and Laboratory Testing of Interlocking Concrete Block Pavements", Second International Conference on Concrete Block Paving, 55-60.

19. Miura, N., Sakai, A., and Taesiri, Y., 1990, "Polymer Grid Reinforced Pavement on Soft Clay Grounds", Geotextiles and Geomembranes, Vol 9, 99-123.

20. Manual, 1984 , "Thickness Design – Asphalt Pavements For Highways and Streets", Asphalt Institute, Series No. 1.

21. Nejad, F.M., and Small, J.C., 1996, "Effect of Geogrid Reinforced in Model Track Tests on Pavements", Journal of Transportation Engineering, Vol 122, No. 6, 468-474.

22. Rada, G.R., Smith, D.R., Miller, J.S., and Witczak, M.W., 1990, "Structural Design of Concrete Block Pavements", Journal of Transportation Engineering, Vol. 116, No. 5, 615-635.

23. Shackel, B., 1984, "The Analysis and Design of Concrete Block Paving Subject to Road Traffic and Heavy Industrial Loading", Second International Conference on Concrete Block Paving, 139-146.

24. Siriwardane, H., and Kutuk, B., 1990, "Evaluation of Flexible Pavement Reinforced with Glass Fiber Grids", Computer Methods and Advances in Geomechanics, 241-250.

25. Smith, T.E., Brandon, T.L., Al-Qadi, I.L., Lacina, B.A., Bhutta, S.A., and Hoffman, S.E., 1995, "Laboratory Behavior of Geogrid and Geotextile Reinforced Flexible Pavements", Final Report, Virginia Polytechnic Institute and State University, Blacksburg, VA.

26. Nishizawa, T., Matuno, S., and Komura, M., 1984, "Analysis of Interlocking Block Pavements by Finite Method", Second International Conference on Concrete Block Paving, 80-85.

27. Tian, P., Zaman M.M., and Laguros J.G., 1997, "Influence of Testing Procedure on Resilient Modulus of Aggregate Materials", Computer Methods and Advances in Geomechanics, Rotterdam, 795-800.

28. Timoshenko,S.P., and Goodier,J.N., 1970, Theory of Elasticity, 3rd Edition, McGraw-Hill Book Company.

29. Tottenham, H., and Brebbia,C., 1970, Finite Element Techniques in Structural Mechanics, Stress Analysis Publishers, Southampton, England.

30. Zienkiewicz, O.C., and Taylor, R.L., 1994 ,The Finite Element Method , McGraw-Hill Inc., Great Britain.

Jianbin Yu was born on May 24, 1971 in Yingtan, Jiangxi, P.R.China. After finishing 11 years of elementary and high-school education, he passed the United University Entrance Exams and was enrolled in Tongji University, majoring in Civil Engineering in 1989. He graduated with a Bachelor of Engineering in 1993.

After graduation, he worked in Shenzhen, Guangdong, in The First Construction Company as an assistant engineer and engineer for five years until he got the admission to University of Windsor in August, 1998. He is currently a candidate for the Master's of Applied Science Degree in Civil Engineering at the University of Windsor. He hopes to complete the degree requirement on January, 2000.